Ferdowsi University of Mashhad

Journal of Agricultural Machinery

Iranian Society of Mechanical Engineers (ISME)

Vol. 12 No. 1

2022

ISSN: 2228-6829

Contents

Full Research Papers

Journal of Agricultural Machinery

Vol. 12 **No. 1** **2022**

Published by: Ferdowsi University of Mashhad, (College of Agriculture), Iran

Publisher: Ferdowsi University of Mashhad Press

Address: College of agriculture, Ferdowsi University of Mashhad, Iran

P.O. BOX: 91775-1163

Fax: +98-05138787430

E-Mail: jame@um.ac.ir

Web Site: http://jame.um.ac.ir

Contents

Full Research Papers

Journal of Agricultural Machinery

Homepage: https://jame.um.ac.ir/

Full Research Paper
Vol. 12, No. 1, Spring 2022, p. 1-19

Comparison of Fiber Reinforced Polymer (FRP) Composite Blade with Steel Blade Performance Used in Chisel Plow

M. Rahmatian[1], S. H. Karparvarfard[2*], M. A. Nematollahi[3], A. Sharifi Malvajerdi[4]

1- Graduate Student, Department of Biosystems Engineering, College of Agriculture, Shiraz University, Shiraz, Iran
2- Associate Professor, Department of Biosystems Engineering, College of Agriculture, Shiraz University, Shiraz, Iran
3- Assistant Professor, Department of Biosystems Engineering, College of Agriculture, Shiraz University, Shiraz, Iran
4- Associate Professor, Agricultural Engineering Research Institute, Agricultural Research, Education and Extension Organization (AREEO), Karaj, Iran

Received: 16-07-2019
Revised: 01-12-2019
Accepted: 29-12-2019
Available Online: 28-09-2021

How to cite this article:
Rahmatian, M., S. H. Karparvarfard, M. A. Nematollahi, and A. Sharifi Malvajerdi. 2022. Comparison of Fiber Reinforced Polymer (FRP) Composite Blade with Steel Blade Performance Used in Chisel Plow. Journal of Agricultural Machinery 12 (1): 1-19.
DOI: 10.22067/jam.v12i1.81980

Abstract

All over the world, farmers choose different implements for tillage, which depend on crop type, soil type, the amount of plant residue from the previous crop, etc. Tillage implement selection is also affected by the availability of implements, power consumption, labor costs, and fund. In this research, the draft force, soil disturbance area, soil cone index, and fuel consumption were considered. The effects of rake angle, forward speed, and soil moisture content on the above-mentioned parameters were investigated. In this research, a comparison between the performance of a Fiber Reinforced Polymer (FRP) composite blade and a conventional steel blade was carried out. Tests were based on the split-split plot in a completely randomized design. The factors of soil moisture content, rake angle, and forward speed were included in three levels. Three levels for the soil moisture content (9.3, 13, 16.7 %), rake angle (20°, 30°, 40°), and forward speed (3, 5, 7 $km.h^{-1}$), were considered. The FRP composite blade (on average in the desired range for variables) has reduced the draft force, fuel consumption, and soil cone index, 14.97%, 16.63%, and 35.08%, respectively, than the steel blade. Also, the soil disturbance area created by the FRP composite blade was 4.93% higher than the steel blade. Based on the results of this study, it is clear that the FRP composite blade has better performance rather than the conventional steel blade for the aforementioned test variables. The FRP composite is inexpensive than the steel, this leads to remarkable save money in the production of the FRP composite blade used in the chisel and combined tillage tools that is economical for the farmer and manufacturer.

Keywords: Forward speed, FRP composite blade, Rake angle, Soil moisture content, Steel blade

Introduction

Tillage operation is the most important step in the production of crops and provision of agricultural land that consumes a great amount of power and energy. In the past decades, several tillage tools have been designed to achieve the main purpose of the tillage operation. Although a farmer is free to choose any of the tools, he always attempts to recognize their consumption energy and choose them according to the cultivation conditions (Godwin, 2007). The amount of energy used in tillage is very high compared to the other agricultural operations. Therefore, saving a small portion of consumption energy in agricultural operations will reduce the costs (Sanchez-Giron *et al*., 2005). Due to the problems of conventional tillage, the conservation tillage in the form of minimum and no-tillage was introduced gradually. For this purpose, implements such as chisel and combined tillage tools were developed. The most important part of these tillage tools is their blade, which is typically made from steel. Adjustment of the blade is effective on draft, fuel consumption, and plowing quality. However other factors such as soil moisture content, forward speed, depth of tillage, and blade angles also have significant effects on

(*- Corresponding Auther Email: Karparvr@shirazu.ac.ir)

the plowing quality (Liu and Kushwaha, 2006).

Some researchers investigated the effects of forward speed, rake angle, and soil moisture content on several factors such as draft force (Akbarnia *et al*., 2014; Ibrahmi *et al*., 2015), soil disturbance area (Manuwa, 2009; Jafari *et al*., 2011), fuel consumption (Ranjbarian *et al*., 2017), and cone index (Kumar *et al*., 2012). Khalilian *et al*. (1998) compared the required draft force of the tillage tools including subsoiler, the Para plow, and chisel plow at different tillage depths. They estimated the amount of draft force for the chisel, subsoiler, and Para plows as 2.88, 4.45, and 5 kN, respectively. Rahman and Chen (2001) compared two types of disk tillage tools and sweep plows in terms of soil disturbance area. They considered the applied treatments as the depth of tillage and forward speed and reported that with increasing the tillage depth and forward speed, the amount of soil disturbance area increased in both tillage tools, and the sweep blades showed better performance rather than the disk in soil disturbance. Chaplain *et al*. (2011) showed that the continuity in the no-tillage causes to increase in the bulk density, mechanical strength of the soil, and the soil cone index, which results in reducing water infiltrations and also root reduction in the soil, and increasing soil erosion. The results of some researches on the fuel consumption of the tractor showed that increasing the forward speed and depth of tillage increased the fuel consumption (Al-Jasim, 1993; Ranjbarian *et al*., 2017).

Some other researchers, using other materials in the form of the cover or employing the main materials for making the blade, tried to improve draft force, fuel consumption, etc. (Soni *et al*., 2007; Barzegar-Tabrizi *et al*., 2017). Chen *et al*. (1990) compared the draft force resulting from a plate of moldboard plow made from Teflon material with steel Ck45. The results showed that the draft force decreased by 25%, due to the reduction in friction between Teflon and soil, and stated that friction between Teflon and soil (apparent friction of soil) was 50% less than friction between steel Ck45 and soil. Ren *et al*. (1990) used Teflon as a coating on the surface of a moldboard plow to reduce soil-tool friction and they reported that Teflon coating causes draft force decreases. Salokhe *et al*. (1990) reported that the enamel-coated plows reduced draft force by up to 14% and 16% at 3.6 and 4 $km.h^{-1}$, respectively. Soni *et al*. (2007) constructed the moldboard plow which was covered with rows of ultra-high molecular weight polyethylene (UHMW-PE), as the material with low viscosity and friction, and its draft force was compared with steel moldboard plow in the adhesive soil. The results indicated that the draft force of the moldboard plow with a UHMWPE coating was 36% less than that of the moldboard plow. Barzegar *et al*. (2016) covered a furrower with ultra-high molecular weight polyethylene (UHMW-PE) and examined on the blade the draft force and adhesive. Their results showed that the UHMW-PE coating reduced the draft force and adhesion.

Recent studies on comparing plow types, changing the blade's material, and finding the best performance in the tillage operations indicated that the researchers are seeking the best performance with the lowest cost and power consumption in the tillage operation. The purpose of this research was to evaluate the performance of the Fiber Reinforced Polymer (FRP) composite blade compared to conventional steel ones. The factors of this research were including draft force, fuel consumption, soil disturbance area, and cone index. Performance comparison such as draft force, soil disturbance area, etc. of the FRP composite blade and conventional steel one (considering the effect of the blade properties, such as weight, adhesion, etc., but without considering the abrasive wear blade) was carried out in the field. The purpose of this research is to present the FRP composite blade and compare it to the steel blade in terms of impact on the mentioned factors.

Materials and Methods

Tillage site

Field experiments were conducted in farm No. 10 of Agriculture school ($29^{\circ}43'41''N$ $52^{\circ}34'51''E$) of Shiraz University, located in Bajgah zone of Fars province, Iran. The soil texture at the experimental site was clay loam with 38% clay, 30% sand, and 32% silt. To do experiments, a total of 27 plots were selected at a predetermined size (30 × 15 m) in the field. Soil moisture content was measured at 10 random locations of each plot prior to the tests. Initial soil moisture content was 7.2 ± 1.3 (d.b %). Also, to measure the soil bulk density, a standard cylinder with a diameter of 5 cm and a height of 10 cm was used, and the bulk density of 1.8 ± 0.4 ($g.cm^{-3}$) was obtained.

Tractor and tillage implement specifications

In this research, a 4WD tractor (model: ITM-399) was used that produced in the Iran Tractor Manufacturing Company. The plow used in this research was the mounted type chisel plow, constructed by Oztoprac Company in Turkey. The plow had a shank and two gauge wheels on both sides. Also, a mechanism was installed on it for adjusting the rake angle (Fig.1).

Fig.1. Mechanism for adjusting the rake angle

Blades

In this research, two chisel blades made of steel (controlling factor) (Fig.2C) and FRP composite (Fig.2B) were compared. The reason to use the FRP composite instead of steel in the chisel blades is due to its similarity or superiority at some mechanical factors over steel (Zhou *et al*., 2019). FRP materials are more resistant than steel in terms of the tensile strength (Jauharia *et al*., 2016). Also, the specific weight of the FRP composite is less than that of the steel (Biscaia and Chastre, 2018), such as the specific weight of FRP composites is one-third that of steel. The ultimate tensile strength for steel and FRP composite is 390 and 1200 MPa, respectively. Also, the young's modulus for the steel and FRP composite is 200 and 55 GPa, respectively (Mazaheri *et al*., 2015). In FRP materials, the volume fraction, size, and cross-sectional area of the FRP fibers used essentially affect their resistivity (Biscaia and Chastre, 2018). FRP composite blade used in this study, was prepared from FRP composite pipes manufactured by Farassan Company (Fars province, Iran). The FRP composite blade was cut off by using a laser cutting technique, according to steel blade pattern, with the same curvature and width (5 cm) (Figures 2B and 2C). The FRP composite toughness is less than steel (Mazaheri *et al*., 2015), therefore, to strengthen the composite blade against impact and better soil cutting, a steel plate (thickness of 8 mm and length of 250 mm) was installed as a base under the FRP composite blade (Fig.2A). For comparison of two blades with the same conditions, the surface area of the FRP composite blade with its support was the same as the surface area of the steel blade.

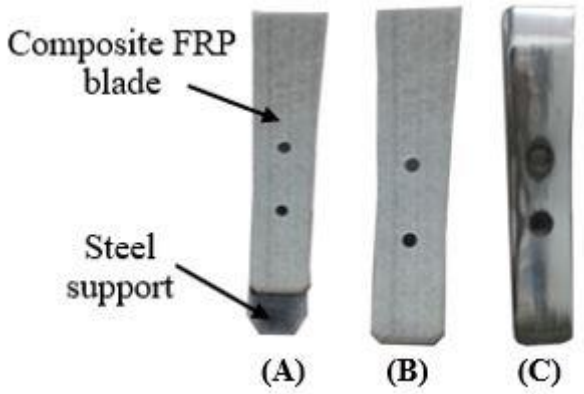

Fig.2. Blades used in this research, (A)- FRP composite with steel support installed below, (B)- FRP composite blade, and (C)- Steel blade (control)

To measure the friction between blades and soil, the adhesion index and external friction angle were used. For this purpose, in this study, a device similar to the devices of Gill and Van Den Berg (1968) and Kepner *et al.* (1972) was used to measure the adhesion and angle of external friction. To measure cohesion, the shear and vertical stresses of the soil at the desired moisture contents were measured by using a direct shear test machine manufactured by the Azmoon Company, Iran. Then, by using the Mohr-Coulomb theory, the cohesion, adhesion, and external friction angle for FRP composite and steel blades were obtained (Table 1). The blades' weight, shank weight, and total weight of the plow were affected the draft force and fuel consumption of the tractor (Karparvarfard and Rahmanian-Koushkaki, 2015). Therefore, the weight of the blades in this research was measured. For this purpose, weights were obtained by using a digital scale (model: MDS15000AP) with the accuracy of ±2g, manufactured by Mahak Company, Iran. Net weight of the steel and the FRP composite blades, net weight of the support, total weight of the FRP composite blade, and its support were obtained 1.355, 0.230, 0.830 and 1.065 kg, respectively.

Table 1- Mechanical and physical properties of farm soil

Moisture content (%)	Soil cohesion (kPa)	Steel chisel blade		FRP composite chisel blade	
		Soil adhesion (kPa)	Angle of external friction (°)	Soil adhesion (kPa)	Angle of external friction (°)
9.3	2.23	1.01	24.20	0.78	23.10
13	3.26	1.40	22.90	1.09	20.60
16.7	4.37	2.14	20.40	1.89	18.20

Field tests

The experimental variables in this research were forward speed (3, 5, and 7 $km.h^{-1}$), rake angle (20°, 30°, and 40°), and soil moisture content (9.3, 13, and 16.7%). The depth of tillage in all experiments was 25 cm. Tests were based on the split-split plot in a completely randomized design. To obtain the tillage depth of 25 cm, several trials were performed by using the desired plow. Several times, for measure tillage depth by using a laser ruler, from the plowed furrow floor to the surface soil was measured. This work was done to fine-tune the tillage depth of the plow in the tillage operation. After reaching a tillage depth of 25 cm, the depth of tillage was fixed using gauge wheels on both sides of the chisel plow.

To obtain the desired moisture content in the field, the whole farm was irrigated using a flooding irrigation system. Then, on a daily basis, soil moisture was measured, and by observing the desired moisture content (from the highest moisture to the lowest moisture),

experiments related to those desired moisture content were performed.

Draft force and fuel consumption

A digital system was employed to measure the draft force and the fuel consumption of the tractor (Rahmanian-Koushkaki *et al*., 2015). This digital system had 11 ports. Two encoder shafts, two fuel transducers, and one load cell were used and connected to it to measure the draft force and fuel consumption (Fig.3). By using the RS232 cable the data was transformed to a Laptop and displayed and saved (Fig.3).

Draft force is the force applied from the soil on the blade and shank of the plow. The RNAM test code was used to measure the reaction force from soil to blade (RNAM Standard, 1995). For this purpose, a traction dynamometer (S type) was used (Table 2). Actual forward speed was measured using two shaft encoders (Fig.3). They were mounted on the center of the fifth wheel and right rear wheel of the tractor for measuring the actual and theoretical forward speed, respectively (Karparvarfard and Rahmanian-Koushkaki, 2015).

Two turbine flow transducers were also used to measure fuel consumption (Table 2). One of them was installed between fuel filters and injector pump of the tractor and the other between the injectors and the fuel tank were placed (Fig.3) (Shafaei *et al*., 2018). The difference between values measured by two turbine flow transducers indicates the actual fuel consumption.

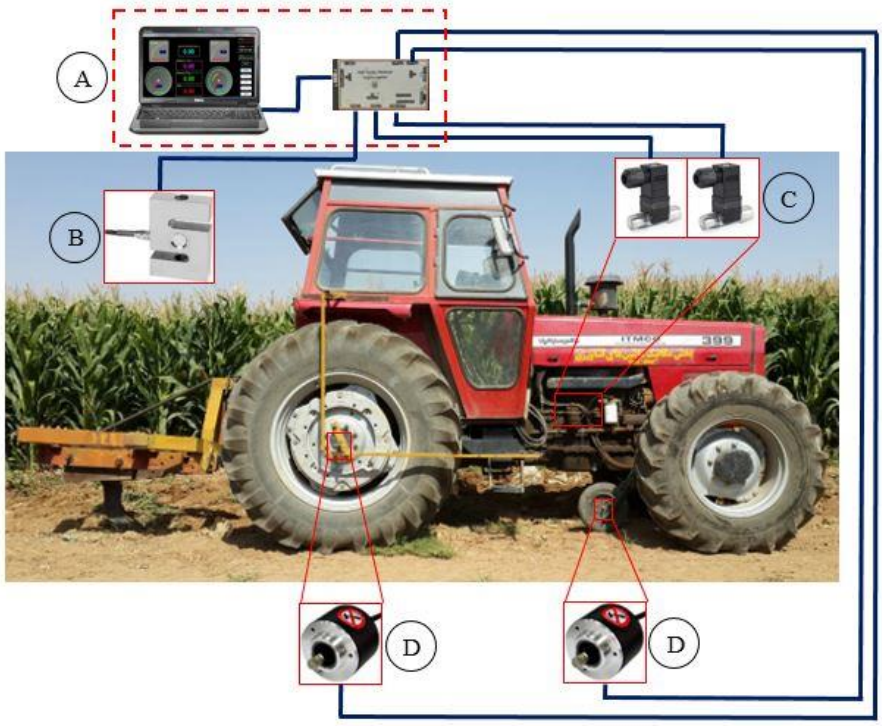

Fig.3. (A) Package of the laptop and data acquisition; (B) Load cell; (C) Turbine flow transducer; (D) Rotary shaft encoder. (Dark blue line is the connection wire).

Table 2- Specification of equipment used

T. No.	Name of the transducer	Specification	Manufacturer
1	Vision-1000, Turbine flow transducer (2 Nos.)	0.1-2.5 $l.min^{-1}$ (22,000 $pulse.l^{-1}$), ±3%	Remag, Switzerland
2	E50S8-500-3-N-24, Shaft encoder (2 Nos.)	500 $pulse.revolution^{-1}$, ±5%	Autonics, South Korea
3	DEE-5t, Traction dynamometer	S type, range 0-50 kN, precision grade: C_3	Keli, China

Soil disturbance area and cone index

For measuring the soil disturbance area in each plot, a transverse cut equal to the size of the soil disturbance, was created in the soil. After drawing out the soil, the profilometer was placed on the soil surface. The distance between the profilometer rods was 2 cm. Thus, several points of soil disturbance area were obtained by profilometer (Conte *et al*., 2011; Hang *et al*., 2017). Then, by using these points and Simpson's rule (Eq. 1), the soil disturbance area in each plot was computed.

$$\int_a^b f(x)dx \approx \frac{h}{3}\left[f(x_0) + 2\sum_{j=1}^{N/2-1} f(x_{2j}) + 4\sum_{j=1}^{N/2} f(x_{2j-1})) + f(x_N) \right] \quad (1)$$

Where a and b are the minimum and maximum values among the points obtained by the profilometer, respectively. N is the number of used data points and h is $(b-a)/2N$.

Cone index was used to measure the amount of soil softness. The soil cone index was measured according to the ASABE standard (ASABE, 2006a) and by using the penetrometer (SP-1000) manufactured by Findly Irvine, Scotland. For this purpose, the cone index was randomly measured at several points in the field before doing the experiments. Also, after each experiment, the cone index was measured with 5 replications in each plot.

Results and Discussions

Draft force and fuel consumption

The draft force value for the steel and FRP composite blades at different levels of soil moisture content, rake angle, and forward speed are shown in Figures 4, 5, and 6. Based on these results, the amount of draft force of the FRP composite blade is less than that of the steel one at different levels of soil moisture content, rake angle, and forward speed. The reduction of the draft force of the FRP composite blade compared to the steel blade in the moisture content of 9.3, 13, and 16.7% were obtained at 11.94% (0.56 kN), 23.40% (1.43 kN), and 11.67% (0.77 kN), respectively (Fig.4). This reduction was also reported at the rake angle of 20°, 30°, and 40° as 10.67% (0.57 kN), 18.50% (1.11 kN), and 14.00% (0.87 kN), respectively (Fig.5), and the reduction of the draft force at the forward speed of 3, 5 and 7 km.h^{-1} were 16.64% (0.91 kN), 10.70% (0.59 kN) and 17.24% (1.16 kN), respectively (Fig.6). According to Table 1, the adhesion value of the FRP composite blade is lower than the adhesion of the steel blade. Therefore, the soil movement on the FRP composite in different levels of the rake angle, forward speed, and moisture content has been flowing and consequently, the required draft force was reduced (Raper and Sharma, 2004; Sanchez-Giron *et al*., 2005). Also, the weight of the plow can be a factor in decrease and increase the draft force and fuel consumption (Karparvarfard and Rahmanian-Koushkaki, 2015). Due to the less adhesion (Table 1) and also the lower weight of the FRP composite blade than the steel one, the draft force of the FRP composite blade in different levels of moisture content, rake angle, and forward speed was less than that of the steel blade.

In Fig.4, with increasing the soil moisture content from 9.3 to 16.7%, the draft force for both FRP composite and steel blades was increased. With increasing moisture content, the cohesion and adhesion (Table 1), the soil bulk density also increases (Raper and Sharma, 2004; Hemmat *et al*., 2007; Chaplain *et al*., 2011). Consequently, with increasing the cohesion and soil bulk density, more draft force is needed to overcome the cohesion between the soil particles, which finally cause to increase the draft force (Qian and Zhang, 1984; Natsis *et al*., 1999; Chaplain *et al*., 2011; Manuwa, 2012). Also, with increasing adhesion between blade and soil, the soil movement speed on the blade is reduced and causes to increase the soil volume in the front of the blade, which requires more force for the displacement of this soil volume that this increases the draft force (Raper and Sharma, 2004; Sanchez-Giron *et al*., 2005).

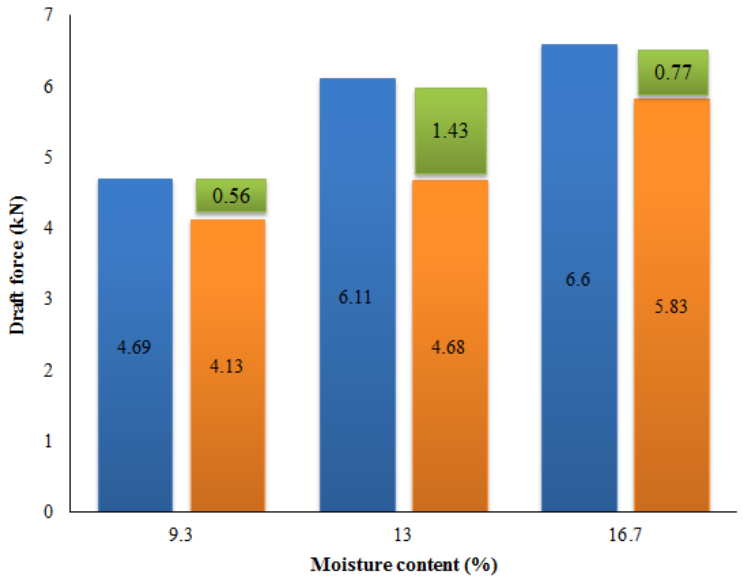

Fig.4. Comparison between the draft force of steel blade and FRP composite blade at different moisture content levels (blue rectangle: steel blade; orange rectangle: FRP composite blade; green rectangle: difference between steel blade and FRP composite blade)

In Fig.5, by increasing the rake angle, the draft force of two FRP composite and steel blades was increased. By increasing the rake angle, the projected area of the blade increases for contact with intact soil (Aluko and Seig, 2000). Therefore, by increasing the blade contact surface at the initial impact to the intact soil, more force is applied to the blade from the soil, and draft force increases. Thus, with increasing rake angle, the draft force increases (Aluko and Seig, 2000; Godwin, 2007).

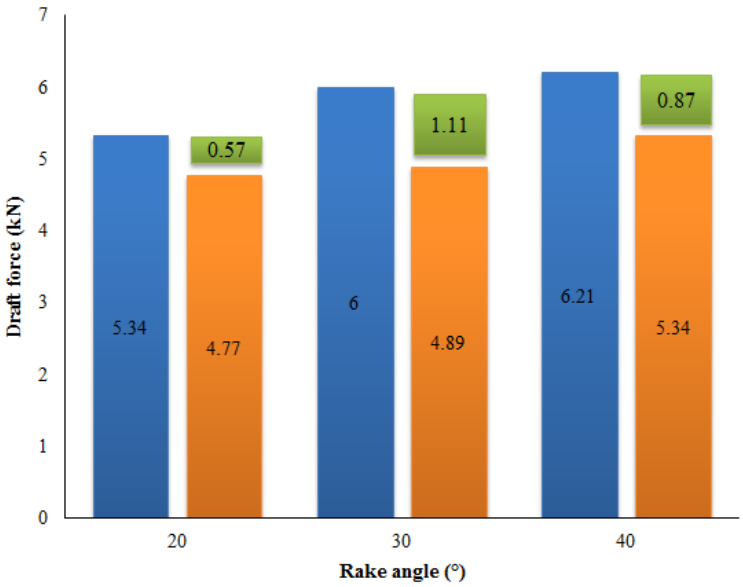

Fig.5. Comparison between the draft force of steel blade and FRP composite blade at different rake angles (blue rectangle: steel blade; orange rectangle: FRP composite blade; green rectangle: difference between steel blade and FRP composite blade)

In Fig.6, it is revealed that with increasing the forward speed, the draft force of the FRP composite and steel blades increased. As the forward speed increases, the blade movement acceleration increases in the soil. According to Newton's second law, with increasing the acceleration of the blade movement in the soil, the force applied to the soil particles increases, and consequently, the soil particles applied more reaction force to the blade, and the draft force increases. Therefore, with increasing forward speed, the draft force increases (Akbarnia *et al*., 2014; Ibrahmi *et al*., 2015).

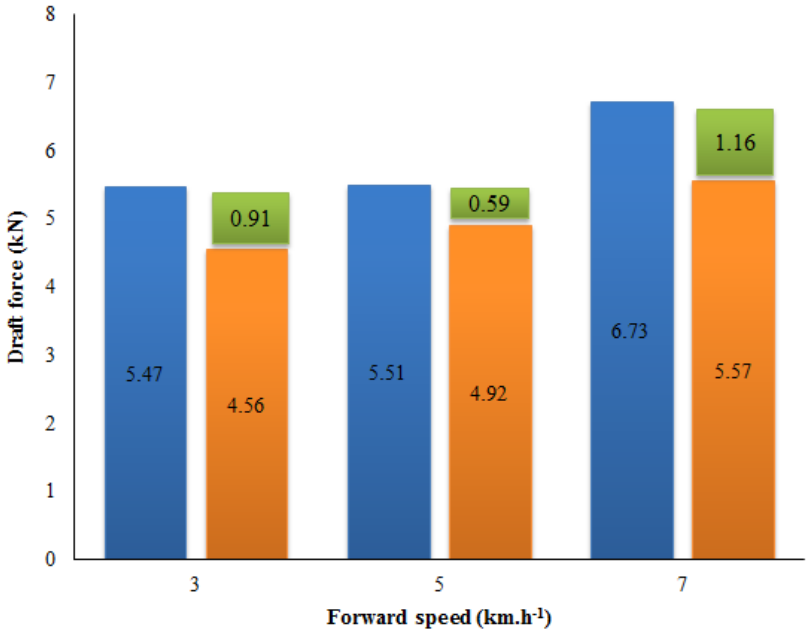

Fig.6. Comparison between the draft force of steel blade and FRP composite blade at different forward speeds (blue rectangle: steel blade; orange rectangle: FRP composite blade; green rectangle: difference between steel blade and FRP composite blade)

Figures 7, 8, and 9, show fuel consumption values of FRP composite and steel blades at different levels of moisture content, rake angle, and forward speed. These figures indicated that the fuel consumption of the FRP composite blade is reduced than the steel blade. Since the fuel consumption is directly related to draft force (Shafaei *et al*., 2017; Shafaei *et al*., 2018), with increasing draft force, the fuel consumption increases. Due to the less draft force of the FRP composite blade than the steel blade at different levels of moisture content, rake angle, and forward speed (Figures 4, 5, and 6), the fuel consumption of the FRP composite blade was lower than that of the steel blade.

The reduction of the fuel consumption related to the FRP composite blade compared to the steel blade in the moisture content of 9.3, 13, and 16.7% were obtained as 11.36% (0.05 $l.min^{-1}$), 12.77% (0.06 $l.min^{-1}$), and 17.65% (0.09 $l.min^{-1}$), respectively (Fig.7). This reduction was also reported at the rake angles of 20°, 30°, and 40° were obtained as 23.08% (0.12 $l.min^{-1}$), 20.75% (0.11 $l.min^{-1}$), and 21.82% (0.12 $l.min^{-1}$), respectively (Fig.8) and the reduction of the fuel consumption at the forward speed of 3, 5, and 7 $km.h^{-1}$ were obtained as 16.67% (0.07 $l.min^{-1}$), 16.00% (0.08 $l.min^{-1}$), and 9.62% (0.05 $l.min^{-1}$), respectively (Fig.9).

Figures 7, 8, and 9 show that fuel consumption is increased with increasing the moisture content, rake angle, and forward speed. With increasing draft force at different levels of moisture content, rake angle, and forward speed (Figures 4, 5, and 6), the tractor should consume more power to move the

blade in the soil and overcome the draft force. Increasing the power consumption by the tractor leads to an increase the fuel consumption. As a result, with increasing moisture content, rake angle, and forward speed, the fuel consumption also increases (Zhang *et al*., 2016; Shafaei *et al*., 2018).

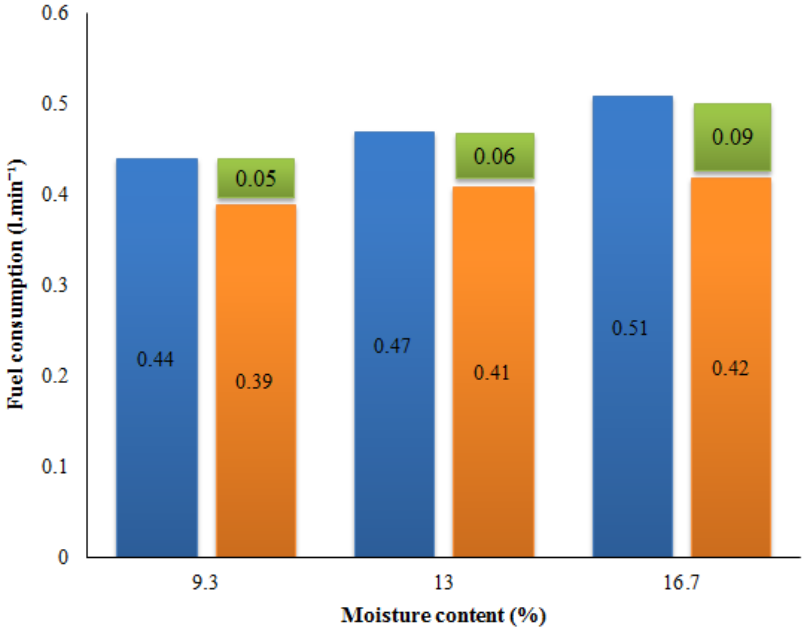

Fig.7. Comparison between the fuel consumption of steel blade and FRP composite blade at different moisture content levels (blue rectangle: steel blade; orange rectangle: FRP composite blade; green rectangle: difference between steel blade and FRP composite blade)

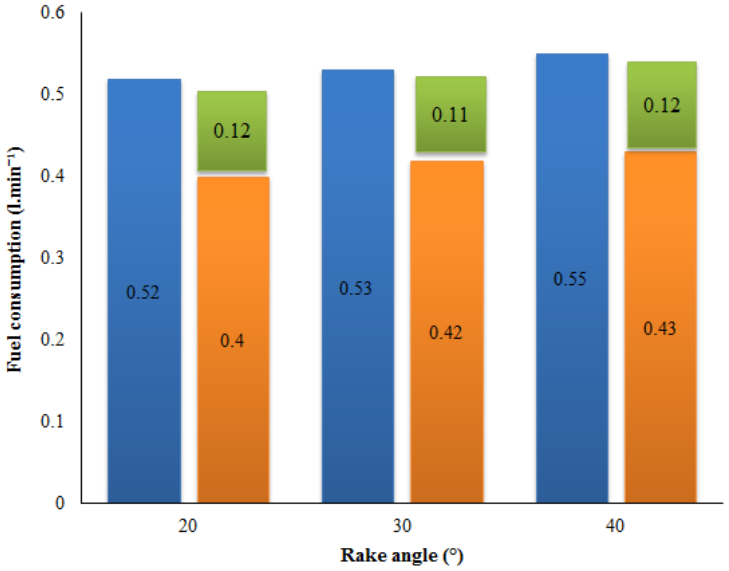

Fig.8. Comparison between the fuel consumption of steel blade and FRP composite blade at different rake angles (blue rectangle: steel blade; orange rectangle: FRP composite blade; green rectangle: difference between steel blade and FRP composite blade)

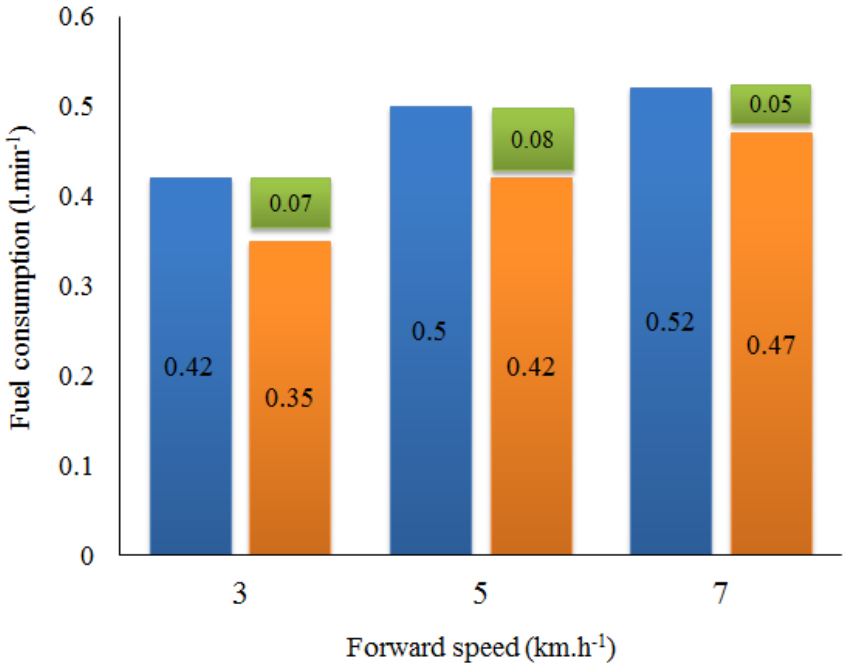

Fig.9. Comparison between the fuel consumption of steel blade and FRP composite blade at different forward speeds (blue rectangle: steel blade; orange rectangle: FRP composite blade; green rectangle: difference between steel blade and FRP composite blade)

Soil disturbance area and cone index

The soil disturbance area shows the soil failure area (Solhjou *et al*., 2014; Hang *et al*., 2017). Due to the less adhesion of the FRP composite blade than the steel blade (Table 1), the soil particles can move easily on the blade and leads to more displacement of soil particles. With these explanations and according to figures 10, 12, and 13, it can be concluded that the soil disturbance area created by the FRP composite blade is more than the steel blade.

The soil disturbance area of the FRP composite blade than the steel blade in the moisture content of 9.3, 13, and 16.7% were increased which obtained as 4.52% (23.17 cm^2), 5.16% (25.93 cm^2), and 5.08% (24.74 cm^2), respectively (Fig.10). Also, this increase was reported at the rake angle of 20°, 30°, and 40° as 4.39% (21.67 cm^2), 5.96% (30.37 cm^2), and 6.22% (32.24 cm^2), respectively (Fig.12). The increase of soil disturbance area of the FRP composite rather than steel blade at the forward speed of 3, 5, and 7 $km.h^{-1}$ were obtained as 3.68% (18.05 cm^2), 3.66% (18.19 cm^2), and 5.71% (28.99 cm^2), respectively (Fig.13).

According to Table 1, with increasing the soil moisture content, cohesion value increases. The high value of soil cohesion leads to the formation of a strong bond among soil particles. Also, by increasing soil moisture content, the soil adhesion was increased (Table 1), which caused slower movement of the soil on the blade. With these explanations, it can be concluded that with increasing the soil moisture content, soil particles movement has been decreased and the soil disturbance area also decreased (Fig.10) (Rahmatian *et al*., 2018).

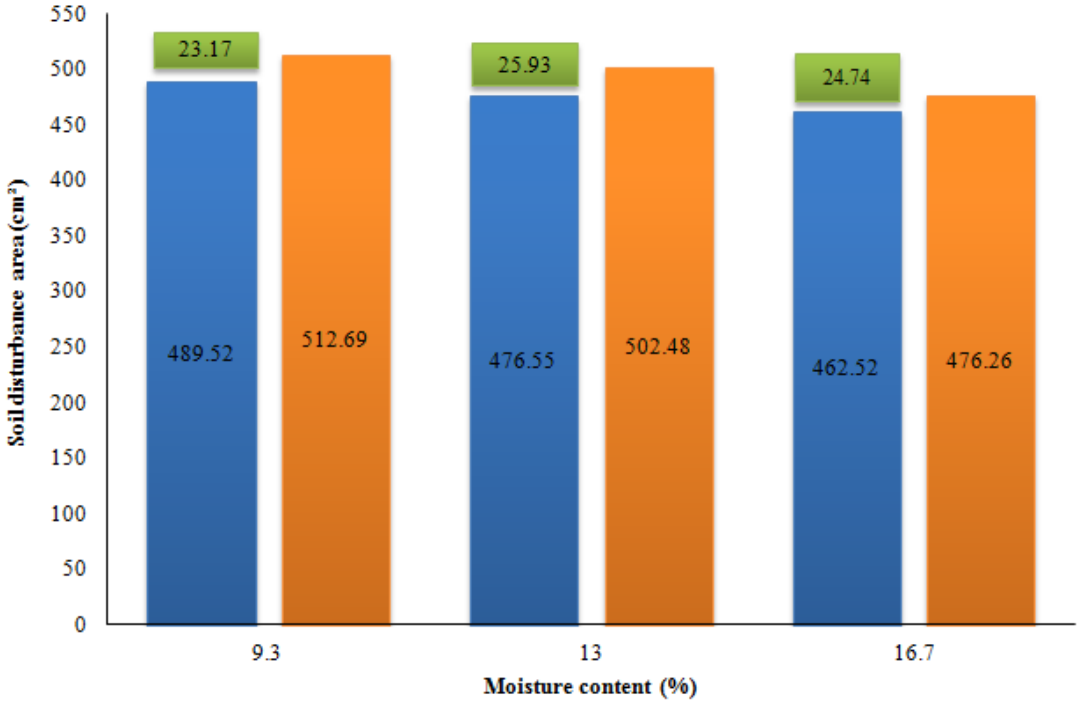

Fig.10. Comparison between the soil disturbance area of steel blade and FRP composite blade at different moisture content levels (blue rectangle: steel blade; orange rectangle: FRP composite blade; green rectangle: difference between steel blade and FRP composite blade)

Fig. 2, shows that the soil disturbance area increased by increasing the rake angle. By increasing the rake angle blade, the projected area of the blade on the intact soil has been increased and at one time, the more surface of the blade hits with the soil and leads to displacement of more soil particles in the soil (Fig.11). For this reason, with increasing the rake angle blade, the soil disturbance area increases (Jafari *et al*., 2011).

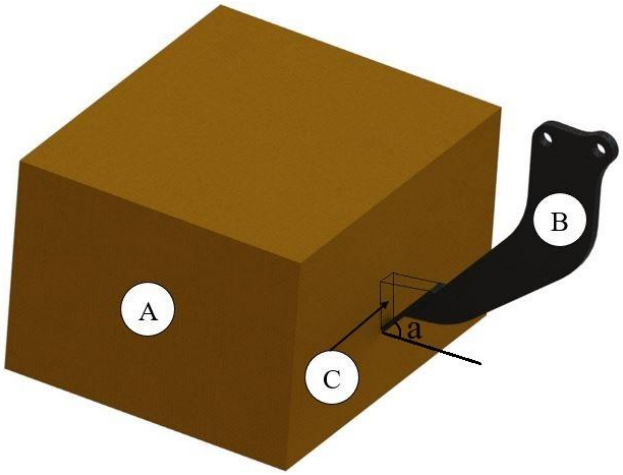

Fig.11. Schematic project blade on the soil: (A) soil, (B) tillage tool, (C) project blade on the soil, and (a) rake angle

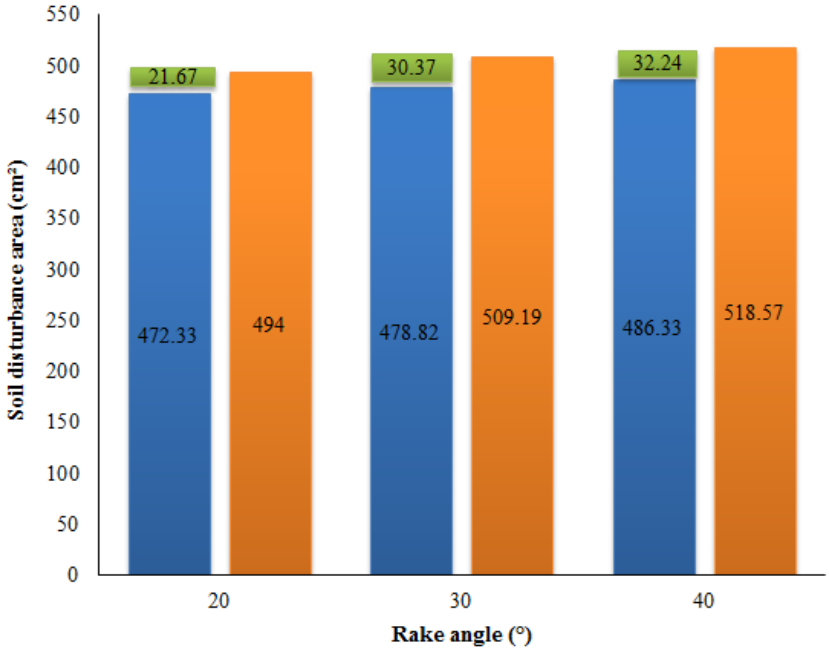

Fig.12. Comparison between the soil disturbance area of steel blade and FRP composite blade at different rake angles (blue rectangle: steel blade; orange rectangle: FRP composite blade; green rectangle: difference between steel blade and FRP composite blade)

Fig.13, shows the effect of the forward speed on the soil disturbance area. According to Fig.13, with increasing the forward speed, the soil disturbance area has been increased (Manuwa, 2009; Jafari *et al.*, 2011). With increasing forward speed, the displacement of soil particles increases, and consequently, the soil disturbance area increases.

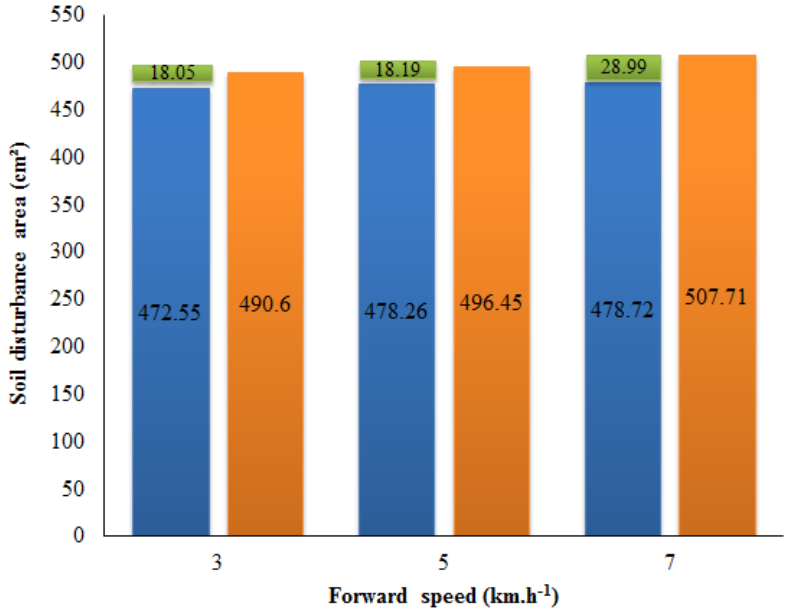

Fig.13. Comparison between the soil disturbance area of steel blade and FRP composite blade at different forward speeds (blue rectangle: steel blade; orange rectangle: FRP composite blade; green rectangle: difference between steel blade and FRP composite blade)

The cone index of the soil is an indicator for measurement soil softening for water and root penetration in soil (Goodin and Priddy, 2016; Pillinger *et al*., 2018). By increasing the soil disturbance area, the soil is softened and the penetration becomes easier. For this reason, the soil cone index decreased (Figures 14, 15, and 16) with increasing soil disturbance area at different levels of moisture content, rake angle and forward speed in this study (Figures 10, 12, and 13) (Tagar *et al*., 2014; Goodin and Priddy, 2016). The reduction amount of soil cone index of the FRP composite blade than the steel blade in the moisture content of 9.3, 13, and 16.7% were obtained 37.12% (1.21 MPa), 34.29% (1.20 MPa), and 30.23% (1.20 MPa), respectively (Fig.14). This reduction was also found at the rake angle of 20°, 30°, and 40° as 31.58% (1.26 MPa), 33.51% (1.24 MPa), and 38.94% (1.18 MPa), respectively (Fig.15) and at the forward speed of 3, 5, and 7 km.h^{-1} were obtained 26.55% (1.24 MPa), 41.46% (1.31 MPa), and 42.07% (1.22 MPa), respectively (Fig.16).

In Fig.14, it has been shown that with increasing soil moisture content, the value of the cone index increases (Patel *et al*., 2013; Lin *et al*., 2014). Due to the increase of moisture content, the cohesion between soil particles is increased (Table 1). Therefore, the soil disturbance area has been decreased (Fig.10), which causes less soil softening, and the soil cone index increases. In figures 13 and 14, with the increase of the rake angle and forward speed, the soil cone index decreased (Tagar *et al*., 2014) that this reason is due to the reduction of soil disturbance area when increasing the rake angle and the forward speed (Figures 12 and 13).

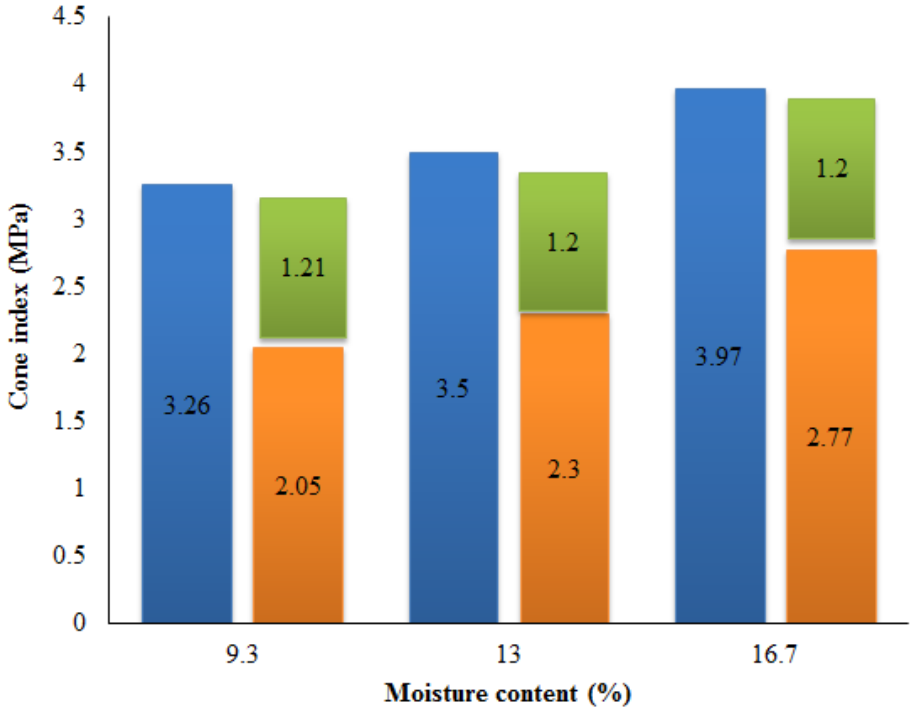

Fig.14. Comparison between the cone index of steel blade and FRP composite blade at different moisture content levels (blue rectangle: steel blade; orange rectangle: FRP composite blade; green rectangle: difference between steel blade and FRP composite blade)

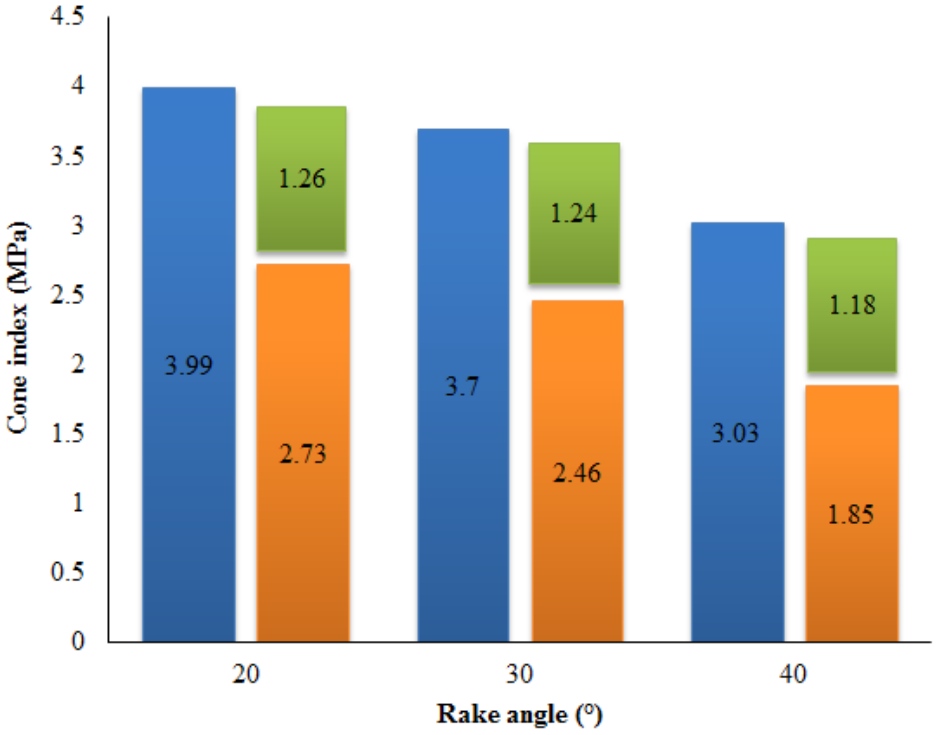

Fig.15. Comparison between the cone index of steel blade and FRP composite blade at different rake angles (blue rectangle: steel blade; orange rectangle: FRP composite blade; green rectangle: difference between steel blade and FRP composite blade)

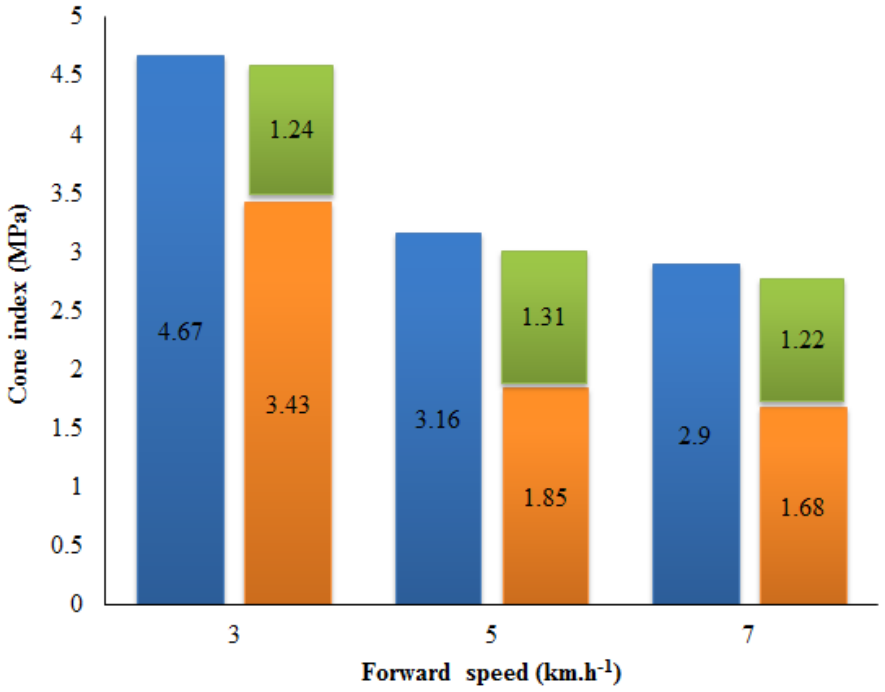

Fig.16. Comparison between the cone index of steel blade and FRP composite blade at different forward speeds (blue rectangle: steel blade; orange rectangle: FRP composite blade; green rectangle: difference between steel blade and FRP composite blade)

Economic comparison

Economic issues, one of the important stages in the engineering design that must be considered (Stanic *et al*., 2016). According to the prices presented by the New York Stock Exchange (NYSE) for steel and FRP composites in 2018 and 2019, it is observed that FRP composites have lower prices on the world market than steel (Fig.17). Also, according to section blades, the FRP composite specific weight is less than that of the steel. Therefore, more blades can be produced with larger volumes of FRP composites per kilogram than steel. According to this information, the use of FRP composite instead of steel for making the chisel blade in terms of economical is affordable. The high production of FRP composite blades with lower cost than steel blades leading to reduce the cost of blade manufacturers and also increases profitability. Of course, due to fluctuations in the world market for gold and oil had a great impact on the price of steel and FRP composite, which in 2018 and 2019 cause to rise or fall in the price of steel and FRP composites in dollar terms (Fig.17), but the price of FRP composite is still lower than steel prices.

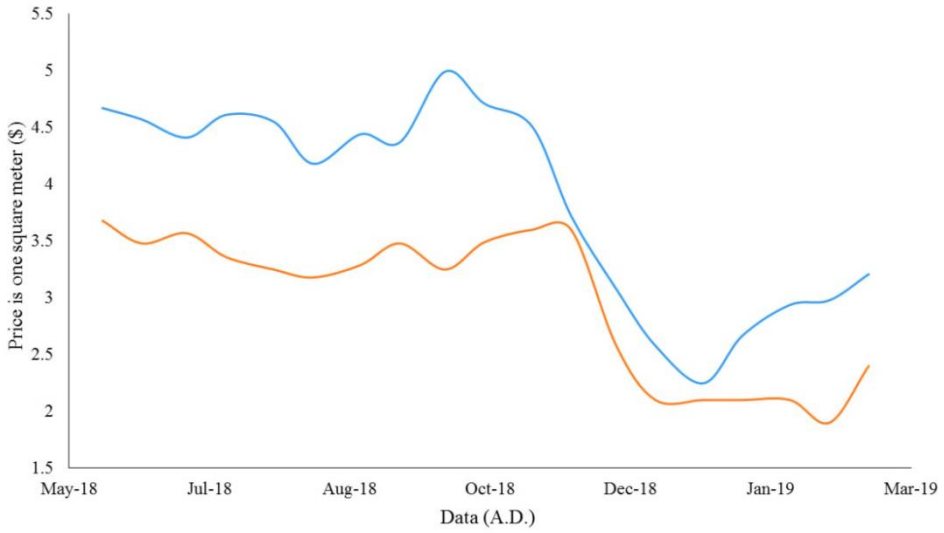

Fig.17. Price comparison in dollar terms between steel and FRP composite in 2018 and 2019 retrieved from New York Stock Exchange (NYSE) site (blue line: steel price; orange line: FRP composite price)

Conclusion

The obtained results from field tests showed that the FRP composite blade (on average in the desired range for variables) has reduced the draft force, fuel consumption, and soil cone index, 14.97%, 16.63%, and 35.08%, respectively, than the steel blade. The soil disturbance area created by the FRP composite blade was 4.93% higher than the steel blade. According to the comparison of FRP composite blade and steel blade in terms of draft force, fuel consumption, soil disturbance area, and cone index in the experimental field, and economic comparison between these two blades, FRP composite blade operation was better and more suitable. According to the results of this research in terms of tillage and economic, the use of the FRP composite blade is recommended to farmers and blade manufacturing. It is suggested that the FRP composite blade checking at different tillage depths and in the subject of abrasive wear, so that information on the characteristics of the FRP composite blade in the tillage operation to be complete.

References

1. Abbaspour-Gilandeh, Y., R. Alimardani, A. Khalilian, A. R. Keyhani, S. H. Sadati. 2006. Energy requirement of site- specific and conventional tillage as affected by tractor speed and soil parameters. International Journal of Agriculture and Biology 8 (4): 499-503.
2. Akbarnia, A., A. Mohammadi, R. Alimardani, and F. Farhani. 2014. Simulation of draft force of winged share tillage tool using artificial neural network model. Agricultural Engineering International: CIGR Journal 16 (4): 57-65.
3. Alimardani, R., Y. Abbaspour-Gilandeh, A. Khalilian, A. R. Keyhani, S. H. Sadati. 2007. Energy savings with variable-depth tillage "A precision farming practice". American-Eurasian Journal of Agriculture and Environment Science, 2 (4): 442-447.
4. Al-Jasim, A. 1993. The technical and economic indicators for soil harrowing with disk harrows. Mijalat al-3ulu: m al-zira: 3iyyat al-3ira: qiyyat (Iraq).
5. Aluko, O., D. Seig. 2000. An experimental investigation of the characteristics and conditions for brittle fracture in two-dimensional soil cutting. Soil and Tillage Research 57 (3): 143-157.
6. ASABE. 2006a. S313.3FEB04. Soil Cone Penetrometer. Mich: ASABE, St. Joseph.
7. Askari, M., and Y. Abbaspour-Gilandeh. 2019. Assessment of adaptive neuro-fuzzy inference system and response surface methodology approaches in draft force prediction of subsoiling tines. Soil and Tillage Research 194: 104338.
8. Barzegar, M., S. J. Hashemi, H. Nazokdast, and R. Karimi. 2016. Evaluating the draft force and soil-tool adhesion of a UHMW-PE coated furrower. Soil and Tillage Research 163: 160-167.
9. Barzegar, M., S. J. Hashemi, and R. Karimi. 2017. Analytical and experimental draft force evaluation of plastic coated chisel tines. Journal of Agricultural Machinery 7 (2): 480-490. (In Persian).
10. Biscaia, H. C., and C. Chastre. 2018. Theoretical analysis of fracture in double overlap bonded joints with FRP composites and thin steel plates. Engineering Fracture Mechanics 190: 435-460.
11. Chaplain, V., P. Défossez, G. Richard, D. Tessier, and J. Roger-Estrade. 2011. Contrasted effects of no-till on bulk density of soil and mechanical resistance. Soil and Tillage Research 111 (2): 105-114.
12. Chen, D., L. Ren, A. Li, and J. Hu. 1990. Study on the method of collecting the body surface liquid of earthworms. Transactions of Chinese Society of Agricultural Engineering 6 (2).
13. Conte, O., R. Levien, H. Debiasi, S. Leandro, M. Mazurana, and J. Muller. 2011. Soil disturbance index as an indicator of seed drill efficiency in no-tillage agrosystems. Soil and Tillage Research 114: 37-42.
14. Gill, W. R., G. E. Vanden-Berg. 1968. Assessment of the dynamic properties of soils. Agriculture handbook. No. 316. U. S. Government Printing Office. Washington, D. C.
15. Godwin, R. 2007. A review of the effect of implement geometry on soil failure and implement forces. Soil and Tillage Research 97 (2): 331-340.
16. Goodin, C., and J. D. Priddy. 2016. Comparison of SPH simulations and cone index tests for cohesive soils. Journal of Terramechanics 66: 49-57.
17. Hang, C., Y. Huang, and R. Zhu. 2017. Analysis of the movement behaviour of soil between subsoilers based on the discrete element method. Journal of Terramechanics 74: 35-43.
18. Hemmat, A., I. Ahmadi, and A. Masoumi. 2007. Water infiltration and clod size distribution as influenced by ploughshare type, soil water content and ploughing depth. Biosystems Engineering 97 (2): 257-266.
19. Ibrahmi, A., H. Bentaher, E. Hamza, A. Maalej, and A. Mouazen. 2015. Study the effect of tool geometry and operational conditions on mouldboard plough forces and energy requirement:

Part 2. Experimental validation with soil bin test. Computers and Electronics in Agriculture 117: 268-275.
20. Jafari, R., S. H. Karparvarfard, and S. A. Hosseini. 2011. The Effect of Geometry and Motion Characteristics of Narrow Tillage Tool on Soil Disturbance Efficiency. Tarım Makinaları Bilimi Dergisi 7 (3).
21. Jauharia, N., R. Mishrab, and H. Thakur. 2016. Stress analysis in FRP composites. Perspective in Science 8: 1-3.
22. Karparvarfard, S. H., and H. Rahmanian-Koushkaki. 2015. Development of a fuel consumption equation: test case for a tractor chisel-ploughing in a clay loam soil. Biosystems Engineering 130 (1): 23-33.
23. Kepner, R. A., R. Bainer, and E. L. Barger. 1972. Principles of Farm Machinery. 2nd Ed. Avi Pub Co. New York, USA.
24. Khalilian, A., T. Garner, H. Musen, R. Dodd, and S. A. Hale. 1988. Energy for conservation tillage in Coastal Plain soils. Transactions of the ASAE, 31 (5): 1333-1337.
25. Kumar, A., Y. Chen, A. Sadek, and S. Rahman. 2012. Soil cone index in relation to soil texture, moisture content, and bulk density for no-tillage and conventional tillage. Agricultural Engineering International: CIGR Journal 14 (1): 26-37.
26. Lin, J., Y. Sun, P. S. Lammers. 2014. Evaluating model-based relationship of cone index, soil water content and bulk density using dual-sensor penetrometer data. Soil and Tillage Research 138: 9-16.
27. Liu, J., and R. Kushwaha. 2006. Modeling of soil profile produced by a single sweep tool. Agricultural Engineering International: CIGR Journal 8: 1-13.
28. Manuwa, S. 2009. Performance evaluation of tillage tines operating under different depths in a sandy clay loam soil. Soil and Tillage Research 103 (2): 399-405.
29. Manuwa, S. I. 2012. Evaluation of Soil/Material Interface Friction and Adhesion of Akure Sandy Clay Loam Soils in Southwestern Nigeria. Advances in Natural Science 5 (1): 41-46.
30. Mazaheri, H., M. Fazel-Najafabadi, and A. Alaei. 2015. Study of microstructure and tribological behavior of the composite layer produced of silicon carbide particles on a steel ASTM A106 GTAW welding method. Journal of Science and Technology of Composites 2 (1): 65-72. (In Persian).
31. Natsis, A., G. Papadakis and J. Pitsilis. 1999. The influence of soil type, soil water and share sharpness of a mouldboard plough on energy consumption, rate of work and tillage quality. Journal of Agricultural Engineering Research 72: 171-176.
32. Patel, M. A., H. S. Patel, and G. Dadhich. 2013. Prediction of Subgrade Strength Parameters from Dynamic Cone Penetrometer Index, Modified Liquid Limit and Moisture Content. Procedia-Social and Behavioral Sciences 104: 245-254.
33. Pillinger, G., A. Géczy, Z. Hudoba, and P. Kiss. 2018. Determination of soil density by cone index data. Journal of Terramechanics 77: 69-74.
34. Qian, D. H., and J. X. Zhang. 1984. Research on adhesion and friction of soil against metallic materials. Acta Agromech 15 (1): 70-81.
35. Rahman, S., and Y. Chen. 2001. Laboratory investigation of cutting forces and soil disturbance resulting from different manure incorporation tools in a loamy sand soil. Soil and Tillage. Research 58 (1): 19-29.
36. Rahmanian-Koushkaki, H., S. H. Karparvarfard, and A. Mortezaei. 2015. The effect of the operational characteristics of the tractor composite electronic measurement system by the standards of emotion on the performance of chisel plows in a clay loam soil. Agricultural Engineering International: CIGR Journal 17 (1): 44-49.

37. Rahmatian, M., S. H. Karparvarfard, and M. A. Nematollahi. 2018. Prediction for optimizing performance of chisel blade used in combined tillage to obtain suitable effectiveness. Iran Journal Biosystems Engineering 49 (1): 73-82. (In Persian).
38. Ranjbarian, S., M. Askari, and J. Jannatkhah. 2017. Performance of tractor and tillage implements in clay soil. Journal of the Saudi Society of Agricultural Sciences 16: 154-162.
39. Raper, R. L., and A. K. Sharma. 2004. Soil moisture effects on energy requirements and soil disruption of subsoiling a coastal plain soil. Transactions of the ASAE 47 (6).
40. Ren, L., D. Chen, and J. Hu. 1990. Initial analysis on the law of reducing adhesion of soil animals. China Society Agricultural Engineering, 6 (1): 15-21.
41. RNAM standard. 1995. RNAM test codes and procedures for farm machinery/Economic and Social Commission for Asia and the Pacific, Regional Network for Agricultural Machinery. RNAM technical publications: 12. Bangkok, Thailand.
42. Salokhe, V. M., D. Gee-Clough, S. Manzoor, and K. K. Singh. 1990. Improvement of the tractive performance of cage wheel lugs by enamel coating. Journal Agricultural Engineering Research, 45: 209-224.
43. Sanchez-Giron, V., J. Ramírez, J. Litago, and J. Hernanz. 2005. Effect of soil compaction and water content on the resulting forces acting on three seed drill furrow openers. Soil and Tillage Research 81 (1): 25-37.
44. Shafaei, S. M., M. Loghavi, and S. Kamgar. 2017. Appraisal of Takagi-Sugeno-Kang type of adaptive neuro-fuzzy inference system for draft force prediction of chisel plow implement. Computers and Electronics in Agriculture 142 (1): 406-415.
45. Shafaei, S. M., M. Loghavi, and S. Kamgar. 2018. On the neurocomputing based intelligent simulation of tractor fuel efficiency parameters. Information Processing in Agriculture 5 (2): 205-223.
46. Solhjou, A., J. M. Fielke, J. M. A. Desbiolles, and C. Saunders. 2014. Soil translocation by narrow openers with various bent leg geometries. Biosystems Engineering 127: 41-49.
47. Soni, P., V. Salokhe, and H. Nakashima. 2007. Modification of a mouldboard plough surface using arrays of polyethylene protuberances. Journal of Terramechanics 44: 411-422.
48. Stanic, A., B. Hudobivnik, and B. Brank. 2016. Economic-design optimization of cross laminated timber plates with ribs. Composite Structures 154: 527-537.
49. Tagar, A. A., J. Changying, Q. Ding, J. Adamowski, F. A. Chandio, and I. A. Mari. 2014. Soil failure patterns and draft as influenced by consistency limits: An evaluation of the remolded soil cutting test. Soil and Tillage Research 137: 58-66.
50. Zhang, X., C. Wang, Zh. Chen, and Zh. Zeng. 2016. Design and experiment of a bionic vibratory subsoiler for banana fields in southern China. International Journal of Agricultural and Biological Engineering 9 (6): 75-83.
51. Zhou, Y., Y. Zheng, J. Pan, L. Sui, F. Xing, H. Sun, and P. Li. 2019. Experimental investigations on corrosion resistance of innovative steel-FRP composite bars using X-ray microcomputed tomography. Composites Part B: Engineering 161: 272-284.

نشریه ماشین‌های کشاورزی
https://jame.um.ac.ir/

مقاله پژوهشی

جلد ۱۲، شماره ۱، بهار ۱۴۰۱، ص ۱۹-۱

مقایسه عملکرد تیغه کامپوزیت پلیمر تقویت شده با الیاف (FRP) با تیغه فولادی مورد استفاده در گاوآهن قلمی

محمد رحمتیان[۱]، سید حسین کارپرورفرد[۲*]، محمد امین نعمت اللهی[۳]، احمد شریفی مالواجردی[۴]

تاریخ دریافت: ۱۳۹۸/۰۴/۲۵
تاریخ پذیرش: ۱۳۹۸/۱۰/۰۸

چکیده

در سراسر دنیا، کشاورزان ادوات مختلفی را برای خاک‌ورزی انتخاب می‌کنند که این به نوع محصول، نوع خاک، میزان باقی‌مانده گیاه از محصول قبلی و غیره بستگی دارد. انتخاب ابزار خاک‌ورزی نیز تحت تأثیر در دسترس بودن ابزارآلات، توان مصرفی، هزینه‌های کارگری و سرمایه‌های موجود است. در این تحقیق، نیروی کششی، سطح مقطع به‌هم خوردگی خاک، شاخص مخروط خاک و مصرف سوخت در نظر گرفته شد. اثرات زاویه حمله، سرعت پیشروی و رطوبت خاک بر پارامترهای نام برده بررسی شد. در این تحقیق، مقایسه‌ای بین عملکرد تیغه کامپوزیت پلیمر تقویت شده با الیاف (FRP) و تیغه فولادی معمولی انجام شد. آزمایش‌ها بر اساس آزمایش کرت‌های دو بار خرد شده بر پایه‌ی طرح کاملاً تصادفی، انجام شد. عوامل رطوبت خاک، زاویه حمله و سرعت پیشروی در سه سطح گنجانده شد. سه سطح برای رطوبت خاک (۹/۳، ۱۳، ۱۶/۷٪)، زاویه حمله (۲۰، ۳۰، ۴۰ درجه) و سرعت پیشروی (۳، ۵، ۷ کیلومتر در ساعت) در نظر گرفته شد. تیغه کامپوزیت FRP به‌طور متوسط در محدوده مورد نظر برای متغیرها باعث کاهش نیروی کششی، مصرف سوخت و شاخص مخروط خاک به‌ترتیب ۱۴/۹۷٪، ۱۶/۶۳٪ و ۳۵/۰۸٪ نسبت به تیغه فولادی شده است. همچنین، سطح به‌هم خوردگی خاک ایجاد شده توسط تیغه کامپوزیت FRP، ۴/۹۳٪ بیشتر از تیغه فولادی بود. با توجه به نتایج این مطالعه، مشخص است که تیغه کامپوزیت FRP عملکرد بهتری نسبت به تیغه فولادی معمولی برای متغیرهای آزمون فوق دارد. با توجه به این‌که کامپوزیت FRP از فولاد ارزان‌تر است، این امر منجر به صرفه‌جویی قابل‌توجهی در تولید تیغه کامپوزیت FRP مورد استفاده در گاوآهن چیزل و ابزارهای خاک‌ورزی مرکب می‌شود که از نظر اقتصادی برای کشاورز و تولیدکننده مقرون به صرفه است.

واژه‌های کلیدی: تیغه کامپوزیت FRP، تیغه فولادی، زاویه حمله، سرعت پیشروی، میزان رطوبت خاک

۱- دانش‌آموخته کارشناسی ارشد، بخش مهندسی بیوسیستم، دانشکده کشاورزی، دانشگاه شیراز، شیراز، ایران
۲- دانشیار بخش مهندسی بیوسیستم، دانشکده کشاورزی، دانشگاه شیراز، شیراز، ایران
۳- استادیار بخش مهندسی بیوسیستم، دانشکده کشاورزی، دانشگاه شیراز، شیراز، ایران
۴- دانشیار مؤسسه تحقیقات فنی و مهندسی کشاورزی، سازمان تحقیقات، آموزش و ترویج کشاورزی، کرج، ایران
(*- نویسنده مسئول: Email: Karparvr@shirazu.ac.ir)

DOI: 10.22067/jam.v12i1.81980

Journal of Agricultural Machinery

Homepage: https://jame.um.ac.ir/

Full Research Paper
Vol. 12, No. 1, Spring 2022, p. 21-32

Workplace and Gravity: Two Mechanized Cow Milking Systems Compared for Human Physiological Strains

A. Hayati[1], A. Marzban[2*], M. A. Asoodar[3]

1- PhD in Agricultural Mechanization, Department of Agricultural Machinery and Mechanization Engineering, Agricultural Sciences and Natural Resources University of Khuzestan, Mollasani, Khuzestan, Iran
2- Associate Professor, Department of Agricultural Machinery and Mechanization Engineering, Agricultural Sciences and Natural Resources University of Khuzestan, Mollasani, Khuzestan, Iran
3- Professor, Department of Agricultural Machinery and Mechanization Engineering, Agricultural Sciences and Natural Resources University of Khuzestan, Mollasani, Khuzestan, Iran

Received: 11-05-2020
Revised: 03-11-2020
Accepted: 16-12-2020
Available Online: 28-09-2021

How to cite this article:
Hayati, A., A. Marzban, and M. A. Asoodar. 2022. Workplace and Gravity: Two Mechanized Cow Milking Systems Compared for Human Physiological Strains. Journal of Agricultural Machinery 12 (1): 21-32.
DOI: 10.22067/jam.2020.58607.0

Abstract

Despite the development of dairy farm mechanization, milking operations are still associated with heavy workloads which result in human physiological strains. This study investigated the role of gravity force in the linkage between load carriage and workers' physiological strains in milking work tasks of two major cow milking systems (milking in stanchion barns and tandem parlors). These two milking methods similarly included washing the teats, attaching the cluster, and detaching the cluster. Human energy expenditure (EE) was calculated and load carriage direction in comparison with gravity (LCG) was tracked among twenty-four male workers. The highest heart rate (107 beats min^{-1}) and EE (35.5 kJ min^{-1}) were reported for attaching the cluster in the tandem parlor milking method. Tandem parlor milking caused higher human physiological strains and higher proportions of converse LCG compared with stanchion barn milking. By developing dairy farm mechanization from stanchion barn to tandem parlor, cow milking workers are induced to apply higher forces including converse LCG causing higher human physiological strains. Mechanization of dairy farms should be developed not only for improving the rate of work and performance but also for making conditions toward a reduction in the use of human physical forces.

Keywords: Energy expenditure, Load carriage, Stanchion barn, Tandem parlor

Introduction

Agricultural mechanization has been a key factor in improvement of performance and work speed in recent decades (Hasantabar *et al*., 2019). Meanwhile, occupational health issues have not been considered as wide as work speed and performance, and labor-intensive activities and ergonomic challenges are still prevalent among agricultural subsectors (Javidi Gharacheh and Khojastehpour, 2016; Gholami *et al*., 2017; Hayati *et al*., 201 8a). Even, in some cases, farm workers suffer from ergonomic problems although they use farm machinery because these machines do not match properly with their operators' anthropometric dimensions (Rostami *et al*., 2015). Dairy farm is one of the agricultural subsectors in which the workers are exposed to hazardous situations concerning occupational risk factors (Jakob and Rosecrance, 2018).

Dairy production was one of the first livestock operations that has been mechanized (Puckett, 1980). However, the stanchion milking method as a traditional one, in which the cows are tied up, is still a common cow milking method (Hayati *et al.*, 2015a; Hayati *et al.*, 2018b). The dairy farm production

(*- Corresponding Author Email: afshinmarzban@asnrukh.ac.ir)

system, in both traditional and mechanized systems, involves many of the work tasks associated with risk factors such as repetitive and forceful movements, awkward postures and load carriage (Nemeth *et al*., 1990; Ahonen *et al*., 1990; Hayati *et al*., 2015b). Employees within dairy farm activities, regularly work with heavy loads. The continuous load carriage is accounted for as a reason for low back pain and joint degeneration and elevating the risk of muscle fatigue and injury, and the physiological strains of activities will be higher when carrying the load (Taylor *et al*., 2016).

Physiological-based studies addressed the ergonomic problems in milking systems and partly investigated the workplace design and equipment as the effective factors in the milking operations. For example, the effects of working height, and vertical and horizontal distances between the worker and the cow on muscular and energy loads (Vos, 1974; Nemeth *et al*., 1990) and a decline in cardiorespiratory loads by installing automatic milking units (Perkiö-Mäkelä and Hentilä, 2005) were introduced as physiological issues related to the milking operation workplace. However, the role of gravity through the variations of human physiological strains in dairy farms has still not been investigated.

Gravity and human physiological strains were studied in some areas. Studies about relationships among equipment design, gravity, and physiological strains suggested that loads carried close to the body's center of gravity exert the least physiological strain (Taylor *et al*., 2016). Physiological strains applied to the climbing workers of traditional date fruit harvesting were affected when changing the approximate angle between their moving direction and gravity force (Marzban and Hayati, 2018). These were some studies about the linkage between load carriage and physiological strain in various areas, which could be considered in the dairy farm area. Lack of such studies in the dairy farm area encouraged us to investigate the role of gravity in the linkage between load carriage and workers' physiological strains in cow milking work tasks.

Materials and Methods

Milking methods and work tasks

Milking in a stanchion barn (a type of tethering system) and milking in a tandem parlor (a type of loose-housing system), as two major methods, were considered in the present study (Fig.1). Tandem parlor milking is more mechanized than the stanchion one. Work tasks of stanchion and tandem milking systems were similarly "washing the teats", "attaching the cluster" and "detaching the cluster".

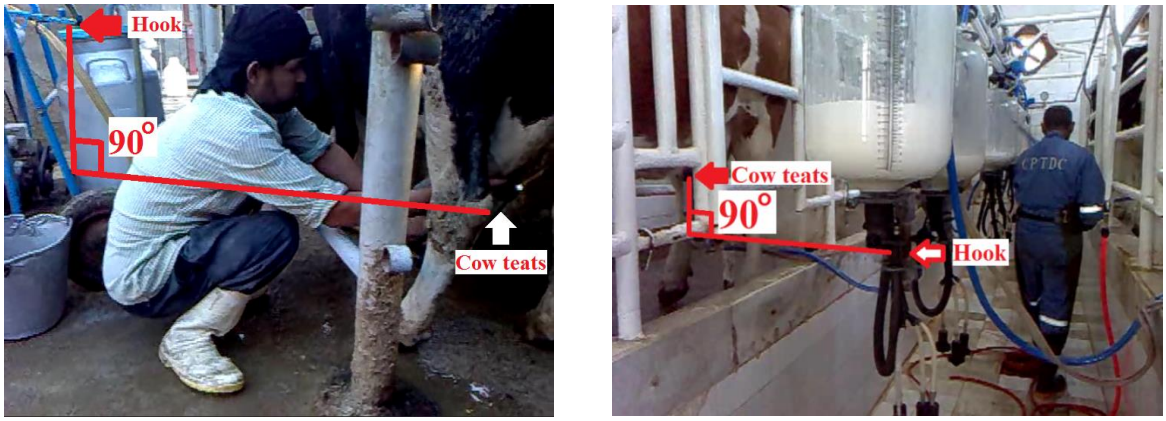

Fig.1. A stanchion barn (a) and a tandem parlor (b)

Workers were instructed to perform given job tasks at the normal routine times. After familiarizing the worker with their instruction, work tasks' cycle times were recorded using a stopwatch. Average cycle times in stanchion and tandem milking systems were 15.5 s and

9.75 s, respectively, for washing the teats, 15.25 s and 9.5 s for attaching the cluster, and 7 s and 4.75 s for detaching the cluster.

In washing the teats in the stanchion milking method, the worker takes a little water from a bucket full of water by a bowl and strews it on the teats in a squatting posture, and washes the teats associated with massaging the teats by the right hand. This work task is performed in the tandem method with the following manner: worker holds the water's hose by the left hand in a standing posture as the cow is at a higher level than the worker and washes the teats associated with massaging the teats by the right hand. In attaching the cluster in both methods, the worker takes the cluster from its hook, carries, and installs it on the teats. Detaching the cluster was performed as follows: the cluster is uninstalled from teats, carried, and put on its hook. Attaching and detaching the cluster were carried out with walking and standing postures in the tandem parlor and with stooping and squatting postures in the stanchion barn.

A cluster, in both milking methods, weighed about 2.6 kg, which consisted of a claw piece and four liners, shells, short milk tubes, and short pulsation tubes. The mass of a part of a long milk tube, a part of a long pulsation tube, water's bowl, and hose borne by hands was considered negligible.

Participants

Twelve male workers in stanchion barn and twelve male workers in tandem parlor whose job is milking, participated in this study (Table 1). They had no musculoskeletal symptoms, no medication, and at least two years' job experience. They were right-handed and had full consent to take part in this study. Three workers of stanchion barns and three workers of tandem parlors were overweight and the rest of them were in the normal range based on body mass index (Pizzol *et al*., 2020).

Table 1- Background of workers recruited in this study

Variable	Stanchion barn	Tandem parlor
No.	12	12
Gender	Male	Male
Age (year)	32.3 (±4.5)	37 (±3.6)
Height (m)	1.71 (±0.06)	1.78 (±0.05)
Mass (kg)	69 (±3.5)	78.7 (±2.3)
Body mass index (kg m^{-2})*	23.7 (±2.1)	24.6 (±2.3)

Body mass index=Mass/$(Height)^2$ (Pizzol *et al.*, 2020).

Physiological strains

Heart rate, heart rate range (HRR), rate of perceived exertion (RPE), and human energy expenditure in physical activity (EE) were used to evaluate physiological strains (Table 2). Heart rate was measured by a Beurer PM 45 heart rate monitor (Beurer, Germany). The signals were transferred from the Beurer transmitter, put on the chest, to the heart rate monitor, put on the wrist. Data were recorded in temperatures between 36°C and 41°C. Physiological indexes were measured (or calculated) eight times for each participant in each work task. Means of physiological indexes were entered in statistical analysis.

Tracking the direction of load carriage in comparison with gravity

Work tasks were videotaped by a camera to track the load carriage direction in comparison with the force of gravity (LCG). LCG was classified into three major categories as follows: similar LCG: load carriage and force of gravity are in a similar direction (SLCG); converse LCG: load carriage and force of gravity are in the converse directions (CLCG); and orthogonal LCG: load carriage, in comparison with the force of gravity, is in an orthogonal direction (OLCG) (Fig.2). Each second was divided into four parts to increase the precision of video analysis. A skilled observer analyzed the videos. Data were collected with visual observation. Observational methods are reliable and valid for identifying potentially hazardous occupational jobs (Lowe *et al*., 2019). The average height level difference between hook and cow teats (Fig.1) in stanchion barns and tandem parlor was approximately measured as

0.36 m and 0.25 m, respectively. Videos were recorded for each participant with three repetitions and means of LCG values were represented. Means of LCG values were considered for statistical analysis.

Table 2- Indexes used to evaluate the physiological strains

Index*	Formula/Instruction
HR (heart rate at work)	Measured during different operations based on beats per minute (bpm)
HRR (heart rate range)	$(HR_{work}-HR_{rest})/(HR_{max}-HR_{rest})\times100$
HR_{rest} (heart rate at rest)	Measured after a 5-minute seated rest period
HR_{max}(maximal heart rate)	205.8-0.685×Age
RPE (rate of perceived exertion)	Borg RPE 20 scale, ranging from six to 20 where six means "no exertion at all" and 20 means "maximal exertion". Participant marks a point on a 14-cm bar with two anchors (no exertion (0) and maximal exertion (20)). By measuring the distance between no exertion and that point the rate of perceived exertion is shown.
EE (the energy expenditure in physical activity)	-55.0969+0.6309×HR+0.1988×Mass+0.2017×Age

* References used: HRR (Claessen *et al*., 2019), HR_{rest} (Montes *et al*., 2019), HR_{max} (Póvoas *et al., 2020), RPE* (Garzon and Comtois, 2020), EE (Chang *et al*., 2020).

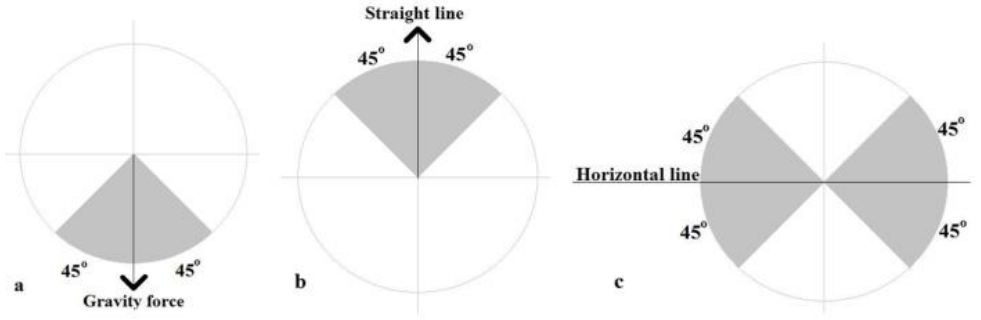

Fig.2. Load carriage directions (ranges shown with grey color) in comparison with the gravity (a: similar LCG; b: converse LCG; c: orthogonal LCG)

Statistical analysis

The data handling was carried out using IBM SPSS Statistics 24 (IBM Corporation, US). Before doing statistical analysis, the normality of the data was checked and confirmed. ANOVA, Duncan's test, and independent samples t-test were used to compare the group mean related to the physiological indexes. Overall and partial proportions of SLCG, CLCG, and OLCG in each work task in each milking method were compared with their corresponding value in the other work tasks of that milking method using ANOVA and Duncan's test and were compared with their corresponding value in the corresponding work task of other milking method using independent samples t-test. A value of $p<0.05$ (two-tailed) was regarded as statistically significant. A completely randomized design (CRD) was used to examine the groups with twelve repetitions (equal to the number of participants in each milking method) for each treatment. Treatments were the work tasks in ANOVA and were the milking methods in independent samples t-test. In the case of three categories of LCG, only where it was a necessity to reinforce the "results and discussion" section, categories with significant differences were mentioned and used. Regression analysis was conducted to validate the RPE-HR relationship and to investigate the predictor factors on EE. Values of milking methods were considered as a dichotomy (tandem method=1 and stanchion milking=0) in EE regression. Values of the

LCG have been presented as means based on the percent of the work task's cycle time.

Procedure

After evaluating physiological strains and tracking LCG, the role of gravity in the linkage between load carriage and workers' physiological strains in milking work tasks was descriptively discussed. Through conducting this study, validation of Borg scale based on heart rate, and linkage between milking methods and some physiological indexes were investigated.

Results and Discussion

Physiological strains

Table 3 and Table 4 show the results of ANOVA and comparison of means in terms of physiological strains. A significant difference was between the stanchion and tandem milking methods concerning each of work tasks and physiological indexes (HR, HRR, RPE, and EE). Significant differences were observed among work tasks of each milking method in the case of physiological indexes except for comparisons between washing the teats and detaching the cluster regarding HR, HRR, and EE in the stanchion method.

The heart rate is one of the important factors for workload indication (Manjarres *et al*., 2020). According to categorizing the workloads from "light work" to "extremely heavy work" based on heart rate (Astrand and Rodahl, 1986), both stanchion and tandem milking methods were classified in "moderate work". This result also supports those of other researchers (Perkiö-Mäkelä and Hentilä, 2005) who reported that the milking operation is a "moderate job" in a dairy farm. The present study introduced the tandem parlor to be higher than the stanchion barn regarding HR.

Table 3- Results of ANOVA among work tasks of milking methods with reference to HR, HRR, and EE

Variable		Source of variance	Degree of freedom	MS	F
HR	Stanchion barn	Treatment	2	51.63	15.98**
		Error	33	3.23	
	Tandem parlor	Treatment	2	480.13	154.18**
		Error	33	3.114	
HRR	Stanchion barn	Treatment	2	37.68	17.22**
		Error	33	2.19	
	Tandem parlor	Treatment	2	369.88	209.76**
		Error	33	1.76	
EE	Stanchion barn	Treatment	2	23.38	26.19**
		Error	33		
	Tandem parlor	Treatment	2	190.65	285.42**
		Error	33	0.67	

Note: ** refer to significant differences at level 0.01.

Table 4- Physiological strains in milking methods

Variables		Washing the teats	Attaching the cluster	Detaching the cluster	Average*
HR (bpm)	Stanchion barn	90.7 (±1.2)	94.6 (±1.5)	91.3 (±2.5)	92.5 (±1.6)
	Tandem parlor	100.7 (±1.2)	107.0 (±1.5)	94.3 (±2.5)	101.9 (±1.6)
HRR (%)	Stanchion barn	23.0 (±2.2)	26.2 (±0.5)	23.2 (±1.2)	24.4 (±1.4)
	Tandem parlor	31.6 (±2.2)	36.4 (±0.5)	25.6 (±1.2)	32.2 (±1.4)
RPE	Stanchion barn				10.5 (±0.8)
	Tandem parlor				11.5 (±0.6)
EE (kJ min^{-1})	Stanchion barn	22.3 (±0.9)	24.9 (±0.3)	22.6 (±1.4)	23.4 (±1.4)
	Tandem parlor	31.5 (±0.6)	35.5 (±1.2)	27.5 (±0.6)	32.3 (±1.9)

* Refer to the weighted arithmetic mean of three work tasks according to their cycle times.

This result resembles other studies where HR during the milking in parlors (97 bpm) (Perkiö-Mäkelä and Hentilä, 2005) was higher than HR in tie-stall milking (89 bpm) (Ahonen *et al.*, 1990) for men. Therefore, it can assume that milking in tandem systems is heavier than

milking in stanchion ones for men which was in the inverse of the result revealed by Perkiö-Mäkelä and Hentilä (2005) for women. It may be due to the fact that walking in the tandem milking method constrains worker to have a higher physiological exertion in the present study.

The linear regression analysis to validate RPE-HR linkage in milking operation extracted a significant relationship (p-value <0.00) between HR and RPE as the following equation: RPE=0.095×HR+1.1552 (Adjusted R^2=0.644). This equation showed that by increasing the heart rate at a work, the perceived exertion of the worker to carry out that work increases. The present study was supported by other studies in which the Borg scale was introduced as valid and reliable for identifying the relationship between heart rate and rate of perceived exertion (Cabral *et al*., 2020; Williams, 2017; Penko *et al*., 2017).

Linear regression was also established including EE as the dependent variable, and HR and milking methods as the independent variables (Table 5). HR variations could not explain the EE variation, but milking methods did. The regression showed that the utilization of the tandem milking method, in comparison with the stanchion method, increased the EE by 6.265 units (kJ min^{-1}). The improvement of the mechanization level caused an increase in energy expenditure (Table 5). Indeed, it forced upon the worker to have more walking and standing during work cycle time more than the less mechanized method (stanchion method) which may be rationally accepted as a reason for increased EE. However, it decreased the time taken to perform work tasks. It highlights the addressing worker's health and comfort, besides the worker's rate of work improvement through technology development (Almassi *et al*., 2014).

Table 5- Regression established with the dependent variable of energy expenditure (EE)

Variables	B	Standardized B	t	Sig.
Constant	23.539		21.726	0.000
Heart Rate (HR)	-0.003	-0.020	-0.225	0.823
Milking method	6.265	0.666	7.352	0.000

Model summary: R^2=0.664; Adjusted R^2=0.441; F=27.235; *p-value*: <0.000

In the present study, load (cluster) carried by workers of stanchion and tandem milking methods was approximately 3.5% of their mean body mass. Some studies reported that although HR was not significantly affected by load mass (0%, 20%, 30%, and 40% of body mass), RPE was significantly affected by increasing load mass and distance (Simpson *et al*., 2011). Others reported increased heart rate and RPE with increasing load from 0% to 50% body mass (Gordon, *et al*., 1983). In these studies and similar former studies increased load units were often equal to or over 10% of body mass. It seems partly improbable that a load of 3.5% body mass significantly affects physiological strains in the present study. But, regarding the studied milking methods, load carriages were often performed by hands in milking operations, and among four load carriage methods (rucksack, low back, across the shoulder, and in the hand), maximum physiological strains were found for load carriage by hand, besides earlier fatigue and bending of the body and deformity in posture (Malhotra and Gupta, 1965). Workers of our study may not be exempt from these risk factors. In mentioned studies (Gordon, 1983; Simpson *et al*., 2011), loads were often carried by a body part rather than hands, so the difference in physiological-based results respecting load carriage was acceptable based on the findings of another study (Malhotra and Gupta, 1965). However, it may be an interesting case for further studies to investigate various load carriage methods with various weights in cow milking operations.

The role of gravity in the linkage between load carriage and physiological strains

Table 6 and Table 7 show the results of ANOVA and comparison of means in terms of tracking the LCG. At the detaching cluster, the

proportion of converse position in the tandem parlor (50%) was significantly higher than that in the stanchion barn (11%+12%) ($p<0.00$). In general, findings of applied physiology studies imply that physiological strains to do work including CLCG are higher compared with those including OLCG. Also, physiological strains to do work including OLCG are higher compared with those including SLCG (Brubaker *et al*., 1986; Minetti *et al*., 2002; Abe *et al*., 2008). Based on this rule, we discussed the workers' physiological strains as follows:

Table 6- Results of ANOVA among work tasks of milking methods with reference to LCG classification

Variable		Source of variance	Degree of freedom	MS	F
SLCG	Stanchion barn	Treatment	2	775.4	1715.3**
		Error	33	0.5	
	Tandem parlor	Treatment	2	4853.4	11719.3**
		Error	33	0.4	
CLCG	Stanchion barn	Treatment	2	20642.7	21857.0**
		Error	33	0.9	
	Tandem parlor	Treatment	2	16151.0	5580.9**
		Error	33	2.9	
OLCG	Stanchion barn	Treatment	2	29683.7	21808.4**
		Error	33	1.4	
	Tandem parlor	Treatment	2	21732.2	14685.9**
		Error	33	1.480	

Note: ** refer to significant differences at level of 0.01.

Table 7- Proportions (%) of the direction of load carriage in comparison with the force of gravity based on work tasks' cycle times*

		Work tasks								
		Washing the teats		Attaching the cluster			Detaching the cluster			
Stanchion barn	Proportion	100%		16%	3%	81%	11%	6%	71%	12%
	Direction of load carriage in the order of appearance	→		↓	→	↑	↑	↓	→	↑
Tandem parlor	Proportion	11%	89%	16%	19%	65%	50%		35%	15%
	Directionof load carriage in the order of appearance	↑	→	→	↑	↑	↑		↓	→

*Legend: ↓, ↑ and → refer to similar, converse, and orthogonal LCGs (SLCG, CLCG, and OLCG) respectively.

In both milking methods, physiological strains (except RPE) for attaching the cluster were found to be higher than detaching the cluster. Based on the aforementioned studies, the increase in these indexes may be partly affected by the gravity effects (the mass of clusters). In attaching the cluster, the worker expended a considerable physiological effort to maintain the cluster at a constant height by applying the force converse of gravity with one hand. Simultaneously, the other hand was occupied to install the cluster's liners on the teats. This occupied a major proportion of cycle time in attaching the cluster in stanchion barns (81%) and tandem parlor (65%) (Table 7). In both methods, during detaching the

cluster, the worker maintained the cluster with one hand and uninstalled the liners with another hand. This also induced applying the force converse of gravity to maintain the cluster. According to Table 7, proportions shown for uninstalling liners were lower than those of installing the liners in both stanchion barns (81%>11%) and tandem parlor (65%>50%). It could be the main reason for the increase in physiological strains in attaching the cluster compared with detaching the cluster in both methods.

The comparison between milking methods could address the effect of the workplace. The workplace design of the tandem parlor had major differences from that of the stanchion barn. The height level of the cluster hook was lower than cow teats in the tandem parlors, whereas, the inverse of this condition was established in the stanchion barn (Fig.1). Therefore, the workplace design of the tandem parlor induced the worker to carry the cluster from its hook (16%) and lift it to a higher level (cow teats) by applying a force converse of gravity (19%). But in stanchion barn worker carried it while changing his posture from stooping to squatting (declining work height, 16%) and moved it toward cow teats at the same height level (3%). These, in addition to installing cluster's liners (81% and 65% in stanchion barn and tandem parlor respectively), implied that during attaching the cluster, workers bore higher physiological strains in tandem parlor compared with stanchion barn.

Although, detaching the cluster was partly performed in an inverse order compared with attaching the cluster, LCGs of this operation were not in the inverse order of that of attaching the cluster. In the stanchion barn, in the work task of detaching the cluster, as shown in Table 7, the worker uninstalled the cluster's liners (11%), brought it down in a similar direction with gravity (6%), carried it toward milking machine (71%) and changed squatting posture to stooping posture to bring the cluster to the height level of the hook (12%). Uninstalling the cluster's liners in the tandem parlor (50%) induced to apply a more converse LCG (50%>11%+12). Then, the worker carried the cluster downward (35%) and toward hook (15%) in the tandem parlor. Results implied that perhaps the most important reason for the increase in physiological strains in tandem parlor compared with stanchion barn during detaching the cluster is more clearly expressed by considering the CLCG in the tandem parlor (50%) and stanchion barn (11%+12%=23%).

The present study showed "it is discussable that some factors, which have not been addressed yet, may affect physiological strains in dairy farms such as the force of gravity". Our study did not decide to generalize the effect of gravity as the absolute factor affecting physiological strains in all cases. Some other factors may also affect the physiological strains in dairy farm activities. For example, working posture is an important factor in the variation in physiological strains. In this case, former researchers reported that more walking was an explanation for increasing HR from women to men during milking (Perkiö-Mäkelä and Hentilä, 2005). The work habits of the worker may also contribute to the physiological strains in dairy farm activities, as a strong matter in ergonomic issues, which is not easily changed (Nevala-Puranen, 1995). Besides, the impact of any load is not just a function of its mass, but its dimensions and distribution around the body which could affect the body's center of gravity and finally affect physiological strains (Taylor *et al.*, 2016). Overall, it could be said that probably several factors (e.g. gravity, working postures, and body's center of gravity) could simultaneously affect the human physiological strains in milking work tasks in dairy farms. Further studies would be undertaken to illuminate these cases.

Limitations

This study was undertaken by employing the male gender only. If women took part in this study, findings could be more generalizable.

Conclusion

The present study showed that by developing dairy farm mechanization from

stanchion barn to tandem parlor, during cow milking, workers are induced to apply higher forces converse of gravity which causes higher human physiological strains as one of the occupational health challenges. It had been shown that the force of gravity affects human physiological strains. Simultaneously, other factors may also affect human physiological strains. Therefore, the mechanization of dairy farms should be developed not only for improving the rate of work and performance but also for making conditions toward a reduction in the use of human physical forces.

Acknowledgment

This work was supported by the Research Deputy of Agricultural Sciences and Natural Resources University of Khuzestan. The authors hereby thank the volunteer workers who made this study possible and Mr. Eng. Raoufikia for his assistance in data collection.

References

1. Abe, D., S. Muraki, and A. Yasukouchi. 2008. Ergonomic effects of load carriage on energy cost of gradient walking. Applied Ergonomics 39: 144-149. https://doi.org/10.1016/j.apergo.2007.06.001.
2. Ahonen, E., J. M. Venäläinen, U. Könönen, and T. Klenk. 1990. The physical strain of dairy farming. Ergonomics 33: 1549-1555. https://doi.org/10.1080/00140139008925353.
3. Almassi, M., S. Kiani, and N. Loveimi. 2014. Principles of agricultural mechanization. Gofteman-e-Andishe-e-Mo'aser, Tehran, Iran. (In Persian).
4. Astrand, P. O., and K. Rodahl. 1986. Textbook of work physiology: physiological bases of exercise, 3rd ed. McGraw-Hill Book Company, New York.
5. Brubaker, C. E., C. A. McLaurin, and, I. S. McClay. 1986. Effects of side slope on wheelchair performance. Journal of Rehabilitation Research and Development 23: 55-58.
6. Cabral, L. L., F. Y. Nakamura, J. M. Stefanello, L. C. Pessoa, B. P. Smirmaul, and G. Pereira. 2020. Initial Validity and Reliability of the Portuguese Borg Rating of Perceived Exertion 6-20 Scale. Measurement in Physical Education and Exercise Science 24: 103-114. https://doi.org/10.1080/1091367X.2019.1710709.
7. Chang, Y. K., B. L. Alderman, C. H. Chu, T. M. Hung, and J. H. Liu. 2020. Conducting exercise trials for obese adolescents within the effectiveness setting: A response with commentary to Ejima *et al*. (2019). Psychology of Sport and Exercise 46: 101605. https://doi.org/10.1016/j.psychsport.2019.101605.
8. Claessen, G., A. La Gerche, A. Van De Bruaene, M. Claeys, R. Willems, S. Dymarkowski, J. Bogaert, P. Claus, W. Budts, H. Heidbuchel, and M. Gewillig. 2019. Heart rate reserve in fontan patients: chrono tropic incompetence or hemodynamic limitation? Journal of the American Heart Association 8: e012008. DOI: 10.1161/JAHA.119.012008.
9. Garzon, M., and A. S. Comtois. 2020. Discussion of "Concurrent and Construct Validation of a Scale for Rating Perceived Exertion in Aquatic Cycling for Young Men". Journal of Sports Science & Medicine 19: 231-234.
10. Gholami, H., D. Kalantari, and M. Rajabi Vandechali. 2017. Ergonomic Evaluation of Vibrations of a Rototiller with New Blade. Journal of Agricultural Machinery 7: 491-502. DOI: 10.22067/jam.v7i2.56061. (In Persian).
11. Gordon, M. J., B. R. Goslin, T. Graham, and J. Hoare. 1983. Comparison between load carriage and grade walking on a treadmill. Ergonomics 26: 289-298. DOI: 10.1080/00140138308963342.
12. Hasantabar, S., S. R. M. Seyedi, and D. Kalantari. 2019. Construction of a seed pod husker and evaluating with soybean in laboratory scale. Journal of Agricultural Machinery 9: 15-29. DOI: 10.22067/jam.v9i1.66218. (In Persian).

13. Hayati, A., A. Marzban, and M. Leylizadeh. 2018a. Discovering the physical onerous activities in manual sesame grain harvest using postural analysis. Agricultural Engineering International: CIGR Journal 20: 126-131.
14. Hayati, A., A., Marzban, and M. A. Asoodar. 2015a. Ergonomic assessment of hand cow milking operations in Khuzestan province of Iran. Agricultural Engineering International: CIGR Journal 17: 140-145.
15. Hayati, A., A., Marzban, and M. A. Asoodar. 2015b. Ergonomic evaluation of hand and mechanized milking in dairy farms. Iranian Journal of Ergonomics 3: 65-75. (In Persian).
16. Hayati, A., A., Marzban, and M. A. Asoodar. 2018b. Evaluation of performance and cost of hand and mechanized cow milking methods. Iranian Journal of Biosystems Engineering 49: 27-34. DOI: 10.22059/ijbse.2017.138776.664695. (In Persian).
17. Jakob, M. C., and J. Rosecrance, 2018. International perspectives on health and safety among dairy workers: challenges, solutions and the future. Frontiers in Public Health, London.
18. Javidi Gharacheh, M., and M. Khojastehpour. 2016. Ergonomic evaluation of tea farmers in north of Iran during plucking using body modeling. Journal of Agricultural Machinery 6: 488-498. (In Persian).
19. Lowe, B. D., P. G. Dempsey, and E. M. Jones. 2019. Ergonomics assessment methods used by ergonomics professionals. Applied Ergonomics 81, 102882. https://doi.org/10.1016/j.apergo.2019.102882.
20. Malhotra, M. S., and J. S. Gupta. 1965. Carrying of school bags by children. Ergonomics 8: 55-60. https://doi.org/10.1080/00140136508930774.
21. Manjarres, J., P. Narvaez, K. Gasser, W. Percybrooks, and M. Pardo. 2020. Physical workload tracking using human activity recognition with wearable devices. Sensors 20: 39. https://doi.org/10.3390/s20010039.
22. Marzban, A., and A. Hayati. 2018. Ergonomic evaluation of traditional date fruit harvesting. Iranian Journal of Ergonomics 6: 11-20. DOI: 10.30699/jergon.6.3.2. (In Persian).
23. Minetti, A. E., C. Moia, G. S. Roi, D. Susta, and G. Ferretti, 2002. Energy cost of walking and running at extreme uphill and downhill slopes. Journal of Applied Physiology 93: 1039-1046. https://doi.org/10.1152/japplphysiol.01177.2001.
24. Montes, J., and J. W. Navalta. 2019. Reliability of the Polar T31 Uncoded Heart Rate Monitor in Free Motion and Treadmill Activities. International Journal of Exercise Science 12: 69-76.
25. Nemeth, G., U. P. Arborelius, O. K. Svensson, and R. Nisell, 1990. The load on the low back and hips and muscular activity during machine milking. International Journal of Industrial Ergonomics 5: 115-123. https://doi.org/10.1016/0169-8141(90)90002-J.
26. Nevala-Puranen, N. 1995. Reduction of farmers' postural load during occupationally oriented medical rehabilitation. Applied Ergonomics 26: 411-415. https://doi.org/10.1016/0003-6870(95)00027-5.
27. Penko, A. L., J. E. Barkley, M. M. Koop, and J. L. Alberts. 2017. Borg scale is valid for ratings of perceived exertion for individuals with Parkinson's disease. International Journal of Exercise Science 10: 76.
28. Perkiö-Mäkelä, M., and H. Hentilä. 2005. Physical work strain of dairy farming in loose housing barns. International Journal of Industrial Ergonomics 35: 57-65. https://doi.org/10.1016/j.ergon.2004.08.004.
29. Pizzol, D., L. Smith, L. Fontana, M. G. Caruso, A. Bertoldo, J. Demurtas, D. McDermott, A. Garolla, I. Grabovac, and N. Veronese. 2020. Associations between body mass index, waist circumference and erectile dysfunction: a systematic review and META-analysis. Reviews in Endocrine and Metabolic Disorders. https://doi.org/10.1007/s11154-020-09541-0.

30. Póvoas, S., P. Krustrup, and C. Castagna. 2020. Estimation of maximal heart rate in recreational football: a field study. European Journal of Applied Physiology 120: 925-933. https://doi.org/10.1007/s00421-020-04334-4.
31. Puckett, H. B. 1980. Mechanization of livestock production in the United States. BSAP Occasional Publication 2: 191-204. https://doi.org/10.1017/S0263967X00000380.
32. Rostami, M. A., A. Gavadi, M. Heidari Soltanabadi, A. Mehdinia, and M. Shaker. 2015. Ergonomic assessment of some commonly used tractors in Iran. Journal of Agricultural Machinery 5: 456-467. (In Persian).
33. Simpson, K. M., B. J. Munro, and J. R. Steele. 2011. Effect of load mass on posture, heart rate and subjective responses of recreational female hikers to prolonged load carriage. Applied Ergonomics 42: 403-410. https://doi.org/10.1016/j.apergo.2010.08.018.
34. Taylor, N. A., G. E. Peoples, and S. R. Petersen. 2016. Load carriage, human performance, and employment standards. Applied Physiology, Nutrition, and Metabolism 41: S131-S147. dx.doi.org/10.1139/apnm-2015-0486.
35. Vos, H. W. 1974. Some ergonomic aspects of parlour milking. Canadian Agricultural Engineering 16: 45-48. https://doi.org/10.3168/jds.2014-8535.
36. Williams, N. 2017. The Borg rating of perceived exertion (RPE) scale. Occupational Medicine 67: 404-405. https://doi.org/10.1093/occmed/kqx063.

نشریه ماشین‌های کشاورزی
https://jame.um.ac.ir/

مقاله پژوهشی

جلد ۱۲، شماره ۱، بهار ۱۴۰۱، ص ۳۲-۲۱

مقایسه فشارهای فیزیولوژیکی انسانی در دو روش مکانیزه شیردوشی گاو شیری با تأکید بر محیط کار و گرانش زمین

عبدالله حیاتی[۱]، افشین مرزبان[۲*]، محمدامین آسودار[۳]

تاریخ دریافت: ۱۳۹۹/۰۲/۲۲
تاریخ پذیرش: ۱۳۹۹/۰۹/۲۶

چکیده

با وجود توسعه مکانیزاسیون دامداری‌های گاو شیری، هنوز هم فعالیت‌های شیردوشی همراه با فشارهای کاری سنگین می‌باشد که باعث بروز فشارهای فیزیولوژیکی روی نیروی کار می‌شود. در این مطالعه نقش نیروی گرانش در ارتباط بین حمل بار و فشارهای فیزیولوژیکی در وظایف کاری دو سیستم عمده شیردوشی گاو شیری شامل شیردوشی در جایگاه‌های استانشیون و سالن‌های تاندم مورد بررسی قرار گرفت. این دو روش به‌طور مشابه شامل سه وظیفه کاری شستن پستان‌های گاو، وصل کردن خرچنگی شیردوش و جداکردن آن بود. انرژی مصرفی انسانی برآورد شد و راستای حمل بار در مقایسه با نیروی گرانش مورد ملاحظه قرار گرفت. بیست و چهار کارگر در این مطالعه شرکت کردند. بالاترین ضربان قلب (۱۰۷ ضربه بر دقیقه) و بالاترین میزان مصرف انرژی انسانی (۳۳/۵ کیلوژول بر دقیقه) برای وظیفه کاری وصل کردن خرچنگی شیردوش در روش شیردوشی در سالن‌های تاندم گزارش شد. در کل، این روش در مقایسه با روش شیردوشی استانشیون باعث اعمال فشارهای فیزیولوژیکی بالاتری شد و نسبت بالاتری از حمل بارهایی که در این روش استفاده شد در خلاف جهت گرانش بود. با توسعه مکانیزاسیون دامداری‌های گاو شیری از ایستگاه‌های استانشیون به سمت سالن‌های تاندم، کارگران شیردوشی به سمت اعمال نیروهای بیشتری در خلاف جهت نیروی گرانشی سوق داده می‌شوند که این باعث بالا رفتن فشارهای فیزیولوژی وارد بر کارگر می‌شود. در توسعه مکانیزاسیون دامداری‌های گاو شیری نه تنها می‌بایست بهبود سرعت کار و عملکرد را مد نظر قرار داد بلکه باید شرایط را به گونه‌ای فراهم کرد که باعث کمتر شدن استفاده از توان فیزیکی نیروی کار شود.

واژه‌های کلیدی: انرژی مصرفی، حمل بار، شیردوشی استانشیون، شیردوشی سالنی تاندم

۱- دکتری مکانیزاسیون کشاورزی، دانشگاه علوم کشاورزی و منابع طبیعی خوزستان، ملاثانی، خوزستان، ایران
۲- دانشیار گروه مهندسی ماشین‌های کشاورزی و مکانیزاسیون، دانشگاه علوم کشاورزی و منابع طبیعی خوزستان، ملاثانی، خوزستان، ایران
۳- استاد گروه مهندسی ماشین‌های کشاورزی و مکانیزاسیون، دانشگاه علوم کشاورزی و منابع طبیعی خوزستان، ملاثانی، خوزستان، ایران
(*- نویسنده مسئول: Email: afshinmarzban@asnrukh.ac.ir)

DOI: 10.22067/jam.2020.58607.0

Journal of Agricultural Machinery

Homepage: https://jame.um.ac.ir/

Full Research Paper
Vol. 12, No. 1, Spring 2022, p. 33-41

Vibration Mode for Effective Mechanical Harvesting of Shengy Olive

H. Golpira[1*], M. Loghavi[2]

1- Assistant Professor, Department of Biosystems Engineering, University of Kurdistan, Sanandaj, Iran
2- Professor, Department of Biosystems Engineering, University of Shiraz, Shiraz, Iran

Received: 28-06-2020
Revised: 08-04-2021
Accepted: 07-06-2021
Available Online: 28-09-2021

How to cite this article:
Golpira, H., and M. Loghavi. 2022. Vibration Mode for Effective Mechanical Harvesting of Shengy Olive. Journal of Agricultural Machinery 12 (1): 33-41.
DOI: 10.22067/jam.2021.58671.0

Abstract

The main aim of this study was to optimize the design parameters of the fruit shakers for efficient harvesting of Shengy olive. A single-degree-of-freedom spring-mass model was established to determine the natural frequency and damping coefficient of the limb. A tractor-mounted shaker that transmits vibration to limbs and fruits via a reciprocating mechanism was fabricated for field evaluation of the forced vibration modes. A 3×4 factorial experiment with a completely randomized design was conducted to investigate the effects of shaking amplitudes and frequencies on fruit removal. The shaking mode with a frequency of 10 Hz and amplitude of 80 mm transmitted the average power of 92 W to remove 95% of fruits in the field trial. This oscillation characteristic should be used to redesign the fruit shakers to pass human safety standards and efficient harvesting.

Keywords: Fruit harvester, Forced vibration, Limb shaker, Mathematical modeling, Natural frequency

Introduction

Fruit shakers shake the trunk or branches or have contact heads with rods that extend into the canopy (Giametta and Bernardi, 2010; Lavee, 2010; Ravetti and Robb, 2010; Sarri and Vieri, 2010; Tous *et al.*, 2010; Vieri and Sarri, 2010; Sola-Guirado *et al.*, 2014; Moreno *et al.*, 2015; Sola-Guirado *et al.*, 2016; Zhang *et al.*, 2016; Sola-Guirado *et al.*, 2018; Peça *et al.*, 2019). Frequency and amplitude are among the principal operating parameters of the shakers concerning humans, trees, and fruit (El Attar *et al.*, 2004; Blanco-Roldán *et al.*, 2009; Zhou *et al.*, 2013; He *et al.*, 2017a). Due to the damage of high frequency on humans, the manufacturers must declare the acceleration value in the machine instruction manual (Saraçoğlu *et al.*, 2011; Deboli *et al.*, 2014a). However, manufacturers of shakers do not often know which variety of their machines will be used on; therefore, they design shakers with fixed acceleration and frequency values leaving the operators the responsibility of choosing the suitable shaking mode (Costa *et al.*, 2013).

Modal testing is one of the best tools for the dynamic characterization of the fruit shakers (Crooke and Rand, 1969; Tsatsarelis, 1987; Amirante *et al.*, 2007; García *et al.*, 2007; Castro-García *et al.*, 2008; Torregrosa *et al.*, 2014). Recording accelerations of fruits or limbs in response to applied vibration modes by accelerometers (Torregrosa *et al.*, 2009; Du *et al.*, 2012; Bentaher *et al.*, 2013) and modeling of the vibration system by a mass-spring model (Gupta *et al.*, 2015; Du *et al.*, 2020; Chen *et al.*, 2021) were tried for analyzing vibration mode and redesigning of mechanical fruit shakers. Natural frequency, damping ratio, and transmitted power are the important oscillation factors for the redesign of the mechanical fruit harvesters.

The main objective of this study is to identify an effective oscillating mode of the Shengy olive limbs useful for the redesign of mechanical harvesters. Mathematical modeling of the single-degree-of-freedom system

(*- Corresponding Author Email: h.golpira@uok.ac.ir)

provides the vibration mode for olive shakers concerning fruit removal efficiency and human safety standard levels.

Materials and Methods

Mathematical modeling

Figure 1 shows a model of the limb which consists of a mass m, a spring with constant k, and a damper with a coefficient of viscous damping c.

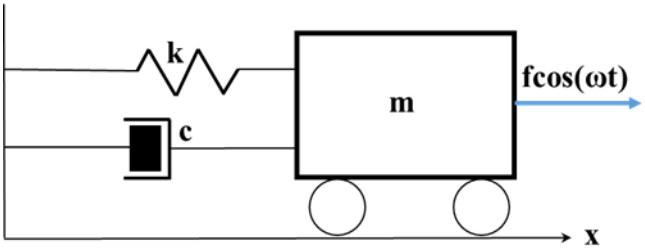

Fig.1. Schematic diagram of the olive fruit limb model represented by a spring (*k*), a damper (*c*), and a mass (*m*) with a driving force (*f*) acting in direction of (*x*).

A limb consists of the limb, fruits, and leaves. The sinusoidal force applied on the spring-mass system of the limb by the shaker produces acceleration which depends on the spring rate and damper constant. Newton's Second Law for representing the limb behavior in response to an external harmonic force gives the equation of motion.

$$m\ddot{x}(t) + c\dot{x}(t) + kx(t) = f\,cos(\omega t) \quad (1)$$

$$x(t) = (\frac{S}{2})\,cos(\omega t - \alpha) \quad (2)$$

$$\dot{x}(t) = (-\frac{S}{2})\,\omega sin(\omega t - \alpha) \quad (3)$$

$$\ddot{x}(t) = (-\frac{S}{2})\omega^2\,cos(\omega t - \alpha) \quad (4)$$

where *m*, *f*, *c*, *k*, *ω*, *S*, and *α* are the mass (kg), the applied force (N), the damping coefficient (kg s^{-1}), the spring rate (N m^{-1}), the circular frequency of the system (Rad s^{-1}), the amplitude (m), and the phase angle (Rad), respectively. The displacement of mass *M* at time *t* is x(t).

Replacing of (2) through (4) in (1) yields.

$$(\frac{S}{2})[(-m\omega^2 + k)\,cos(\omega t - \alpha) - c\omega\,sin(\omega t - \alpha)] = \underbrace{f\,cos\,\omega\,t}_{\boldsymbol{F}(t)} \quad (5)$$

and by setting *t* = 0, one could re-write (5) as:

$$(\frac{S}{2})[(-m\omega^2 + k)\,cos(\alpha) + c\omega\,sin(\alpha)] = \boldsymbol{F} \quad (6)$$

The amplitude of the force vector **F** in (6) defines as:

$$(\frac{S}{2})[(-m\omega^2 + k)^2 + c^2\omega^2]^{\frac{1}{2}} = |\boldsymbol{F}| \quad (7)$$

Using the notation of **F** in (5), the power *P* can be calculated by:

$$P(t) = \underbrace{\boldsymbol{F}(t)}_{|\boldsymbol{F}|\,cos\,\omega t} \times \boldsymbol{V}(t) \quad (8)$$

Replacing (7) in (8) using the definition of (3) yields.

$$\left(-\frac{S^2}{4}\right)\omega[(k - m\omega^2)^2 + c^2\omega^2]^{\frac{1}{2}}\,cos\,\omega\,t\,sin(\omega t - \alpha) \quad (9)$$

By setting the derivative of (9), in respect to *t*, to zero, the maximum required power could be represented by:

$$\frac{dP}{dt} = \left(-\frac{S^2}{4}\right)\omega[(k - m\omega^2)^2 + c^2\omega^2]^{\frac{1}{2}}[-sin\,\omega\,t\,sin(\omega t - \alpha) + cos\,\omega\,t\,cos(\omega t - \alpha)] = 0 \quad (10)$$

Which implies:

$$cos\,\omega\,t\,cos(\omega t - \alpha) - sin\,\omega\,t\,sin(\omega t - \alpha) = 0 \rightarrow t = \frac{\frac{\pi}{4} + \frac{\alpha}{2}}{\omega} \quad (11)$$

By replacing (11) in (9), one could write the maximum power in the final form of:

$$P_{max} = \left(\frac{S^2}{8}\right)\omega[(k - m\omega^2)^2 + c^2\omega^2]^{\frac{1}{2}}(1 - sin\,\alpha) \quad (12)$$

Furthermore, the average power can be calculated as:

$$P_{av} = \sum\left(\frac{p.\Delta t}{T_f}\right) = \frac{1}{T_f}\int_0^T p.\,dt \quad (13)$$

and by replacing (9) in (13), one has that:

$$P_{av} = \left(\frac{S^2}{4}\right)\omega[(k - m\omega^2)^2 + c^2\omega^2]^{\frac{1}{2}} sin\,\alpha \quad (14)$$

In which the phase angle (α) can be calculated by (Dimarogonas, 1976; Blevins, 2015):

$$\alpha = \tan^{-1}\frac{2\zeta\left(\frac{\omega}{\omega_n}\right)}{1-\zeta\left(\frac{\omega}{\omega_n}\right)^2} \quad (15)$$

Where,

$$\omega_n = \left(\frac{k}{m} - \frac{c^2}{4m^2}\right)^{\frac{1}{2}} \quad (16)$$

and

$$\zeta = \frac{c}{2m\omega_n} \quad (17)$$

By replacing (16) in (17), one could define the natural frequency, ω_n, as:

$$\omega_n^2 = \frac{k}{m}\frac{1}{(1+\zeta^2)} \quad (18)$$

In (15) ω, and ζ are the circular frequency of the system (Rad s^{-1}), and the damping ratio of the limb, respectively.

Experimental area and layout

A limb shaker was designed and fabricated to oscillate the limbs with different vibration modes (Fig.2a). The tractor-mounted fruit harvester received its power from the power take-off (PTO) shaft and transmitted it to the tree limb through a boom and a special clamping device (Fig.2b). A V-belt drive system changed the initial 540 revolutions per minute (rpm), supplied by the standard tractor PTO shaft, to 200-1200 rpm and corresponding frequency ranging from 3.2 to 20 Hz. Five levels of shaking amplitude (4, 6, 8, 10, 12 cm) were provided by a slider-crank mechanism, where rotating motion was converted to a reciprocating motion. The clamping device is a quick fastening type equipped with a soft pad as an intermediate media for the protection of the bark. The machine's overall dimensions are 140×80×100 cm. The machine seats on the ground utilizing a hydraulic system of the tractor.

a b

Fig.2. a) Fabricated limb shaker during evaluation in the orchard, b) clamping device with soft pad attached to limb for vibration cushioning.

The experiments were performed in the Bash Garden in Shiraz (29° N latitude and 52° E longitude), Iran. A 3×4 factorial experiment with a completely randomized design with three replications was conducted to investigate the effect of shaking amplitude and frequency on fruit detachment of green (unripe) Shengy olives. Three levels of oscillating frequency (10, 14, and 20 Hz) and four levels of shaking amplitude (40, 60, 80, and 100 mm) were investigated. According to Rezaei *et al.* (2016), the duration of vibrations for trials was fixed at 5 s. The circular frequency was measured by a light tachometer on the slider-crank mechanism.

Before fruit harvesting, a sheet was spread under the tree. The mechanically removed fruits and fruits remaining on the branch (picked manually) were weighed separately to

determine harvesting efficiency. The fruit removal percentage is:

$$e = \frac{w_a}{w_b + w_a} 100 \quad (19)$$

Where e is the fruit harvesting percentage (%), w_a is the weight of fruits harvested from each branch, w_b is the weight of fruits remained on each branch.

The damages to the tree were not considered here. The method of determining damages that comprised of the leaves which were detached from the tree and fallen on the ground, the bark injured by the clamping device, and broken small stems with some leaves presented by (Chen *et al.*, 2012; Gambella *et al.*, 2013; Kargarpour *et al.*, 2018; Memari *et al.*, 2019).

Results and Discussions

The effects of shaking frequency and amplitude were both significant on fruit detachment, while no interacting effect was observed (Table 1). Figure 3 shows the comparison between mean values of detached fruits (%) from limb for different amplitudes and frequencies at 5% significance level. The oscillation mode with a shaking frequency of 10 Hz and amplitude of 80 mm, which caused 95% fruit detachment, passes the standard level of daily vibration dose of 11.4 Hz recommended by Aiello *et al.* (2019) where the damaging effect on the hand is reached. Oscillation of olive trees with a frequency of 24 Hz and amplitude of 60 mm (Sessiz and Özcan, 2006), 16 Hz and 100 mm (Rezai *et al.*, 2015), 23 Hz and 100 mm (Babanatsas *et al.*, 2018), 22-27 Hz (Leone *et al.*, 2015), 35 Hz and 25 mm, and 25 Hz and 25 mm (Alzoheiry *et al.*, 2020), 41 Hz and 25 mm, and 17 Hz and 100 mm (Ferguson *et al.*, 2010) have significant differences with the recommended frequency in this research. The low ratio of the weight of the fabricated machine (120 kg) to the limb weight (8 kg) couple them as an oscillating system. However, in tree shakers *i.e.*, (Pellenc, 2019; Solano, 2020) the large mass of the machine avoids coupling the machine with the tree.

Table 1- Analysis of variance of the percentage of detached fruits for different configurations of amplitude and frequency

Source of variation	Degrees of freedom	Sum of squares	Mean square	FS	P
Replication	2	0.172	0.08	0.0044	
Amplitude	3	9459.80	3153.26	162.71	0.01
Frequency	2	480.62	240.31	12.35	0.01
Amplitude × frequency	6	245.41	40.90	2.10	ns
Error	22	427.75	19.44		

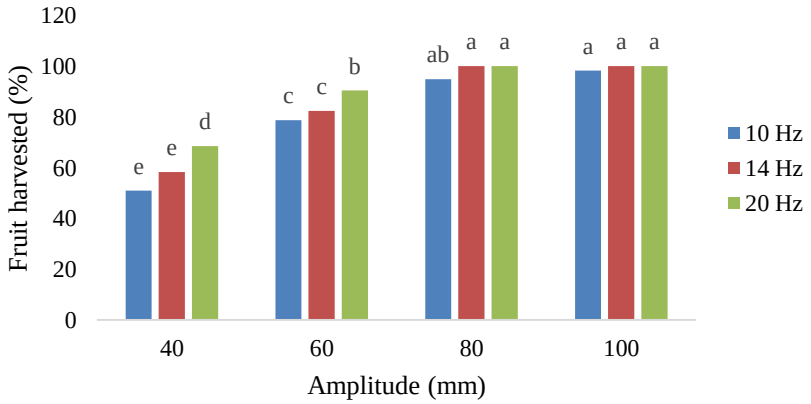

Fig.3. Percentage of detached fruits for different configurations of amplitude and frequency. The same letters do not have a significant difference with a probability of 5%.

By replacing the mean value of 13675N m^{-2} of elasticity and 8 kg for the mass of a limb (Golpira, 1998), the damping ratio of 0.1 for olive limbs (Adrian *et al.*, 1965; Hoshyarmanesh *et al.*, 2017) in (18) the limb's natural frequency (Hz).

$$\omega_n^2 = \frac{k}{m}(1+\delta^2) = \frac{13675}{8}(1+0.1^2) = 41.31 \quad (20)$$

According to (17), c (kg s^{-1}) is

$$c = 2 \times 8 \times 41.31 \times 0.1 = 66.15 \quad (21)$$

By replacing the frequency of 10 Hz in (15) the phase angle is:

$$\alpha = \tan^{-1} \frac{2\times 0.1\left(\frac{10}{41.31}\right)}{1-0.1\left(\frac{10}{41.31}\right)^2} = 0.05 \quad (22)$$

The same reasoning to introduce the concept of electromechanical modes can be extended to interpret (20). Any torque imbalance may cause several electro-mechanical modes with different frequencies (Golpîra *et al.*, 2021). The exciting vibration of 10 Hz to the limb may produce a natural frequency of 41.31 Hz in olive fruits. Natural frequencies of 20.2 and 37.7 Hz (García *et al.*, 2007), and 33.9, 31.9, and 28.0 Hz were calculated for olive limbs (Alzoheiry *et al.*, 2020).

By substituting the amplitude of 0.08 (m) in (12) the maximum power is

$$P_{max} = -\left(\frac{0.08^2}{8}\right) 10 \times 2 \times 3.14[(13675 - 8 \times (10 \times 2 \times 3.14)^2)^2 + 66.15 \times 2 \times 3.14 \times 10]^{\frac{1}{2}}(1 - sin0.05) = 1756 \quad (23)$$

By replacing the values of parameters in (14) the average power is

$$P_{av} = \left(\frac{0.08^2}{4}\right) 10[(13675 - 8 \times 10^2)^2 + 66.15 \times 2 \times 3.14 \times 10]^{\frac{1}{2}}(sin0.05) = 92 \quad (24)$$

The lower amount of energy regards to the lower shaking frequency and amplitude transmitted to the system could result in the higher fruit collection (He *et al.*, 2017b), lower tree damages (Gupta *et al.*, 2016), and lower human damages (Çakmak *et al.*, 2011; Deboli *et al.*, 2014b).

Conclusion

This paper merged field experimental data of the olive limb shaking mode with the dynamic model of the spring-mass system to redesign the fruit harvesters. Mathematical modeling of the olive limb identified the natural frequency of 41.31 Hz with a damping coefficient of 66 kg s^{-1}. The single-degree-of-freedom model showed the maximum and average power of 1756 and 92 W for limb oscillation of Shengy olives. The free exposure to harmful hand-arm vibration mode with a working frequency of 10 Hz and an amplitude of 80 mm detached 95% of olives in the field trial. Modeling the coupling system of the limb and the machine with two unequal masses and springs can further improve the results.

Acknowledgment

Partial financial support of the University of Kurdistan under grant agreement GRC96-00213-2 was appreciated. The authors would like to thanks Prof. Antonio Torregrosa Mira and Dr. Hemin Golpira for technical consultation.

References

1. Adrian, P. A., R. B. Fridley, and R. B. Fridley. 1965. Dynamics and design criteria of inertia-type tree shakers. Transactions of the ASAE 8: 12-0014.
2. Aiello, G., M. Vallone, and P. Catania. 2019. Optimizing the efficiency of olive harvesting considering operator safety. Biosystems Engineering 185: 15-24.
3. Alzoheiry, A., M. Ghonimy, E. Abd El Rahman, O. Abdelwahab, and A. Hassan. 2020. Improving olive mechanical harvesting using appropriate natural frequency. Journal of Agricultural Engineering 51: 148-154.
4. Amirante, P., P. Catalano, F. Giametta, A. Leone, and G. L. Montel. 2007. Vibration analysis of an olives mechanical harvesting system. Agricultural Engineering International: CIGR Journal.

5. Babanatsas, T., D. Glavan, R. B. Merce, M. Borzan, I. Radu, and S. Maris. 2018. Harvesting olive tree using accurate vibrations generated by a robotic system. Pages 012083. IOP Conference Series: Materials Science and Engineering: IOP Publishing.
6. Bentaher, H., M. Haddar, T. Fakhfakh, and A. Mâalej. 2013. Finite elements modeling of olive tree mechanical harvesting using different shakers. Trees 27: 1537-1545.
7. Blanco-Roldán, G. L., J. A. Gil-Ribes, K. Kouraba, and S. Castro-García. 2009. Effects of trunk shaker duration and repetitions on removal efficiency for the harvesting of oil olives. Applied Engineering in Agriculture 25: 329-334.
8. Blevins, R. D. 2015. Formulas for dynamics, acoustics and vibration. John Wiley & Sons.
9. Çakmak, B., T. Saraçoğlu, F. N. Alayunt, and C. Özarslan. 2011. Vibration and noise characteristics of flap type olive harvesters. Applied Ergonomics 42: 397-402.
10. Castro-García, S., G. L. Blanco-Roldán, J. A. Gil-Ribes, and J. Agüera-Vega. 2008. Dynamic analysis of olive trees in intensive orchards under forced vibration. Trees 22: 795-802.
11. Chen, D., X. Du, Q. Zhang, M. Whiting, P. Scharf, and S. Wang. 2012. Performance evaluation of mechanical cherry harvesters for fresh market grade fruits. Applied Engineering in Agriculture 28: 483-489.
12. Chen, J., Y. Wang, D. Liang, W. Xu, and Y. Chen. 2021. Design of Longitudinal Vibratory Compliant Picking Mechanism for Berry Shrub. Transactions of the ASABE: 64(4):1165-1171.
13. Costa, N., P. Arezes, C. Quintas, and R. Melo. 2013. Vibration exposure in mechanical olive harvesting: workers' perception. Occupational safety and hygiene. CRC Press, Boca Raton, FL, USA: 417-420.
14. Crooke, J., and R. Rand. 1969. Vibratory fruit harvesting: a linear theory of fruit-stem dynamics. Journal of Agricultural Engineering Research 14: 195-209.
15. Deboli, R., A. Calvo, C. Preti, and M. Inserillo. 2014a. Design and test of a device for acceleration reproducibility of hand held olive harvesters. International Journal of Industrial Ergonomics 44: 581-589.
16. Deboli, R., A. Calvo, F. Gambella, C. Preti, R. Dau, and E. C. Casu. 2014b. Hand arm vibration generated by a rotary pick-up for table olives harvesting. Agricultural engineering international: CIGR Journal 16: 228-235.
17. Dimarogonas, A. D. 1976. Vibration Engineering. West Group.
18. Du, X., D. Chen, Q. Zhang, P. A. Scharf, and M. D. Whiting. 2012. Dynamic responses of sweet cherry trees under vibratory excitations. Biosystems Engineering 111: 305-314.
19. Du, X., K. Chen, Z. Ma, C. Wu, and G. Zhang. 2020. Design, construction, and evaluation of a three-dimensional vibratory harvester for tree fruit. Applied Engineering in Agriculture 36: 221-231.
20. El Attar, M., M. El Awady, M. Rashwan, and M. Genaidy. 2004. Physical properties effects on shaker-model harvesting of olive-trees. Pages 4-5. 12th Conference of Miser Society of Agricultural Engineering, Giza, Egypt.
21. Ferguson, L., U. Rosa, S. Castro-Garcia, and S. Lee. 2010. Mechanical harvesting of California table and oil olives. Advances in Horticultural Science 24: 53-63.
22. Gambella, F., F. Paschino, and C. Dimauro. 2013. Evaluation of fruit damage caused by mechanical harvesting of table olives. Transactions of the ASABE 56: 1267-1272.
23. García, S. C., J. G. Ribes, G. B. Roldán, and J. A. Vega. 2007. Mode shapes evaluation of trunk shakers used in oil olive harvesting. Transactions of the ASABE 50: 727-732.
24. Giametta, G., and B. Bernardi. 2010. Olive grove equipment technology. Straddling trees: mechanized olive harvests. Advances in Horticultural Science 64-70.
25. Golpira, H. 1998. Design, development and evaluation of a tree shaker for investigation the effects of shaking amplitude and frequency on fruit detachment. M.Sc. Thesis. The University of Shiraz. (In Persian).

26. Golpîra, H., A. Román-Messina, and H. Bevrani. 2021. Renewable Integrated Power System Stability and Control. John Wiley & Sons.
27. Gupta, S. K., R. Ehsani, and N.-H. Kim. 2015. Optimization of a citrus canopy shaker harvesting system: Properties and modeling of tree limbs. Transactions of the ASABE 58: 971-985.
28. Gupta, S. K., R. Ehsani, and N.-H. Kim. 2016. Optimization of a citrus canopy shaker harvesting system: Mechanistic tree damage and fruit detachment models. Transactions of the ASABE 59: 761-776.
29. He, L., H. Fu, M. Karkee, and Q. Zhang. 2017a. Effect of fruit location on apple detachment with mechanical shaking. Biosystems Engineering 157: 63-71.
30. He, L., H. Fu, D. Sun, M. Karkee, and Q. Zhang. 2017b. Shake-and-catch harvesting for fresh market apples in trellis-trained trees. Transactions of the ASABE 60: 353-360.
31. Hoshyarmanesh, H., H. R. Dastgerdi, M. Ghodsi, R. Khandan, and K. Zareinia. 2017. Numerical and experimental vibration analysis of olive tree for optimal mechanized harvesting efficiency and productivity. Computers and Electronics in Agriculture 132: 34-48.
32. Kargarpour, H., T. Tavakoli Hashjin, A. Hemmat, and B. Ghobadian. 2018. Assessment of mechanical damage on olive fruit under impact loading. Journal of Agricultural Machinery 8: 365-376. (In Persian).
33. Lavee, S. 2010. Integrated mechanical, chemical and horticultural methodologies for harvesting of oil olives and the potential interaction with different growing systems: A general review. Advances in Horticultural Science 1000-1011.
34. Leone, A., R. Romaniello, A. Tamborrino, P. Catalano, and G. Peri. 2015. Identification of vibration frequency, acceleration, and duration for efficient olive harvesting using a trunk shaker. Transactions of the ASABE 58: 19-26.
35. Memari, A., H. Shamsabadi, M. Rahmati, and M. Razzaghi. 2019. Determination of damage index of olive fruit (Koroneiky variety) in different harvesting methods and times in Golestan province. Journal of Agricultural Machinery 9: 61-72. (In Persian).
36. Moreno, R., A. Torregrosa, E. Moltó, and P. Chueca. 2015. Effect of harvesting with a trunk shaker and an abscission chemical on fruit detachment and defoliation of citrus grown under Mediterranean conditions. Spanish Journal of Agricultural Research 13: 1-12.
37. Peça, J., A. B. Dias, A. Pinheiro, and J. Falcão. 2019. Continuous harvesting of olive orchards with wide canopies in hedge. 77th International Conference on Agricultural Engineering. Hanover, Germany, VDI-Berichte. 213-222.
38. PELLENC. 2019. MAVO olive harvester. https://pellenc.com/agri/produits/mavo-olive-harvester/?lang=en.
39. Ravetti, L., and S. Robb. 2010. Continuous mechanical harvesting in modern Australian olive growing systems. Advances in Horticultural Science 71-77.
40. Rezaei, A., M. Loghavi, S. Kamgar, and Y. Mehdipour. 2016. Determining the most suitable frequency and shaking time for olive harvesting by a pneumatic branch shaker. Journal of Agricultural Machinery 6: 417-428. (In Persian).
41. Rezai, A., M. Loghavi, S. Kamgar, and D. Rezaei. 2015. Design portable pneumatic branch shaker with programmable logic controller. Iranian Journal of Biosystems Engineering 46: 19-29. (In Persian).
42. Saraçoğlu, T., B. Cakmak, C. Özarslan, and F. N. Alayunt. 2011. Vibration and noise characteristics of hook type olive harvesters. African Journal of Biotechnology 10: 8074-8081.
43. Sarri, D., and M. Vieri. 2010. Criteria for introducing mechanical harvesting of oil olives: results of a five-year project in Central Italy. Advances in Horticultural Science 1000-1013.
44. Sessiz, A., and M. Özcan. 2006. Olive removal with pneumatic branch shaker and abscission chemical. Journal of Food Engineering 76: 148-153.

45. Sola-Guirado, R., F. Jimenez-Jimenez, G. Blanco-Roldan, S. Castro-Garcia, F. Castillo-Ruiz, and J. A. Gil-Ribes. 2016. Vibration parameters assessment to develop a continuous lateral canopy shaker for mechanical harvesting of traditional olive trees. Spanish Journal of Agricultural Research 14: 0204.
46. Sola-Guirado, R. R., G. L. Blanco-Roldan, S. Castro-Garcia, F. J. Castillo-Ruiz, and J. A. Gil-Ribes. 2018. Innovative circular path harvester for mechanical harvesting of irregular and large-canopy olive trees. International Journal of Agricultural and Biological Engineering 11: 86-93.
47. Sola-Guirado, R. R., S. Castro-García, G. L. Blanco-Roldán, F. Jiménez-Jiménez, F. J. Castillo-Ruiz, and J. A. Gil-Ribes. 2014. Traditional olive tree response to oil olive harvesting technologies. Biosystems Engineering 118: 186-193.
48. Solano, H. 2020. Front olive harvester. https://solano-horizonte.com/tree-harvesters/front-olive-harvester/.
49. Torregrosa, A., E. Ortí, B. Martín, J. Gil, and C. Ortiz. 2009. Mechanical harvesting of oranges and mandarins in Spain. Biosystems Engineering 104: 18-24.
50. Torregrosa, A., F. Albert, N. Aleixos, C. Ortiz, and J. Blasco. 2014. Analysis of the detachment of citrus fruits by vibration using artificial vision. Biosystems Engineering 119: 1-12.
51. Tous, J., A. Romero, and J. Hermoso. 2010. New trends in olive orchard design for continuous mechanical harvesting. Advances in Horticultural Science 43-52.
52. Tsatsarelis, C. 1987. Vibratory olive harvesting: the response of the fruit-stem system to fruit removing actions. Journal of Agricultural Engineering Research 38: 77-90.
53. Vieri, M., and D. Sarri. 2010. Criteria for introducing mechanical harvesting of oil olives: results of a five-year project in Central Italy. Advances in Horticultural Science 78-90.
54. Zhang, Z., P. H. Heinemann, J. Liu, T. A. Baugher, and J. R. Schupp. 2016. The development of mechanical apple harvesting technology: A review. Transactions of the ASABE 59: 1165-1180.
55. Zhou, J., L. He, Q. Zhang, X. Du, D. Chen, and M. Karkee. 2013. Evaluation of the influence of shaking frequency and duration in mechanical harvesting of sweet cherry. Applied Engineering in Agriculture 29: 607-612.

Nomenclature

c: Damping coefficient (kg s^{-1}), f: Force (N), F: Force vector, k: Spring constant (N m^{-1}), m: Mass (kg), $P(t)$: Power (W), S: Amplitude (m), $V(t)$: Velocity (m s^{-1}), t: Time of oscillation (s), x: Displacement of excitation (m), $\dot{x}$: First derivative of the x (m s^{-1}), $\ddot{x}$: Second derivative of the x (m s^{-2}), ω: Circular frequency (Rad s^{-1}), ω_n: Natural frequency (Hz), ζ: Damping ratio, α: Phase angle (Rad)

نشریه ماشین‌های کشاورزی
https://jame.um.ac.ir/

مقاله پژوهشی
جلد ۱۲، شماره ۱، بهار ۱۴۰۱، ص ۴۱-۳۳

مد ارتعاشی موثر برای برداشت مکانیکی زیتون رقم شنگی

هیوا گل‌پیرا[۱*]، محمد لغوی[۲]

تاریخ دریافت: ۱۳۹۹/۰۴/۰۸
تاریخ پذیرش: ۱۴۰۰/۰۳/۱۷

چکیده

هدف از انجام این تحقیق بهینه‌سازی عوامل طراحی ماشین‌های برداشت میوه برای برداشت موثر زیتون رقم شنگی بود. مدل جرم-فنر با یک درجه آزادی برای تعیین بسامد طبیعی و ضریب میرایی شاخه زیتون استفاده شد. یک شاخه‌تکان سوار که در آن ارتعاش از راه بازوی میل‌لنگی به شاخه و میوه انتقال می‌یافت برای ارزیابی مدهای ارتعاشی ساخته شد. به‌منظور تعیین تاثیر دامنه و بسامد ارتعاش بر میزان جداسازی میوه از شاخه یک آزمایش فاکتوریل (۴×۳) در قالب یک طرح کاملاً تصادفی اجرا شد. مد ارتعاشی با بسامد ۱۰ هرتز و دامنه ۸۰ میلی‌متر توان متوسط ۹۲ وات را برای برداشت ۹۵ درصد از میوه‌ها انتقال داد. برای برداشت موثر و منطبق بر استانداردهای سلامتی می‌توان از این مد ارتعاشی برای بازطراحی درخت تکان‌ها استفاده کرد.

واژه‌های کلیدی: ارتعاش، بسامد طبیعی، شاخه تکان، ماشین‌های برداشت میوه، مدل ریاضی

۱- استادیار گروه مهندسی بیوسیستم، دانشگاه کردستان، سنندج، ایران
۲- استاد گروه مهندسی بیوسیستم، دانشگاه شیراز، شیراز، ایران
(*- نویسنده مسئول: Email: h.golpira@uok.ac.ir)

DOI: 10.22067/jam.2021.58671.0

Journal of Agricultural Machinery

Homepage: https://jame.um.ac.ir/

Full Research Paper
Vol. 12, No. 1, Spring 2022, p. 43-54

Evaluating the Efficiency of Sugarcane Harvesting Units Using a Combined Approach to Data Envelopment Analysis and Data Mining

N. Monjezi[1*]

1- Assistant Professor, Biosystems Engineering Dept., Faculty of Agriculture, Shahid Chamran University of Ahvaz, Ahvaz, Iran

Received: 11-07-2020
Revised: 18-10-2020
Accepted: 22-12-2020
Available Online: 28-09-2021

How to cite this article:
Monjezi, N. 2022. Evaluating the Efficiency of Sugarcane Harvesting Units Using a Combined Approach to Data Envelopment Analysis and Data Mining. Journal of Agricultural Machinery 12 (1): 43-54.
DOI: 10.22067/jam.2020.58695.0

Abstract

Every organization needs an evaluation system in order to be aware of the level of performance and desirability of its units. It is more important for agricultural companies, including agro-industries. In this study, 20 sugarcane harvesting units were selected. After modeling based on input-oriented CCR and BCC models, efficiency values for sugarcane harvesting units were calculated and the CART decision tree was used to extract rules to predict the efficiency of these units. The results of a study of 20 sugarcane harvesting units in the CCR model showed that 6 units had an efficient score and 14 units had an inefficient score, and their technical efficiency score was in the range of 0.73-0.95. The results of the BCC model study also showed that out of a total of 20 sugarcane harvesting units, 8 units had efficient scores. As can be seen, in the BCC model, more units are introduced as efficient units and there is less dispersion between inefficient units. Also, the distribution of efficient units in the BCC model is less than the CCR model. The average technical efficiency, pure technical efficiency, and scale efficiency were 93%, 88%, and 93%, respectively. Also, the accuracy of the decision tree model for technical efficiency and pure technical efficiency was 86% and 93%, respectively.

Keywords: CART, DEA, Harvest, Sugarcane

Introduction

Harvesting crops and transporting them from two dimensions has a great impact on sugarcane production and the income of an agro-industry. In terms of cost, which accounts for the majority of sugarcane production costs, and in terms of income, due to the amount of sugarcane waste at harvest time and the quality of the product sent to the factory and the amount of damage to the farm and sugarcane stump, it has a great impact on the amount of yield in the same year, ratooning[2] years and eventually agro-industry income. In Iran, sugarcane is industrially produced by Khuzestan Sugarcane and By-Products Development Company, Haft Tappeh, Karun and Mian Ab agro-industries (about 135,000 hectares). In these agro-industries, there are four harvesting groups for sugarcane harvesting operations. Each harvesting team consisted of six harvesters. There are four active and stationary in the group and two as reserve units. There are also 20 transporters and 24 drivers (mechanic operators) of the harvester and the transporter in each group, along with an expert in the group (one person), mechanic technician (2 persons), electricians (3 persons), and service workers (3 persons) are used.

Data envelopment analysis (DEA) model is a useful tool in measuring the efficiency of several organizational units with the same structure. In other words, the DEA model

(*- Corresponding Author Email: n.monjezi@scu.ac.ir)

2- Sugarcane is a perennial plant and its operation does not end in a year. The sugarcane fields in the following years of operation are called ratoon.

minimizes the ratio of inputs to outputs. This study is an attempt to determine the efficiency of harvesting units located in sugarcane production companies to identify inefficient or less efficient units. On the other hand, due to the increase in data volume and the need to analyze information and predict variables, data mining, especially the decision tree, can be helpful. The decision tree is one of the data mining methods. A decision tree is a diagram that shows a classification system or a predictive model and is a way to display a series of rules that lead to a category or value (Jenhani *et al.*, 2008). In recent years, a wide range of researchers in various fields have used DEA model, data mining model, and a combination of the two methods (Rahman *et al.*, 2019; Liu *et al.*, 2019; Li *et al.*, 2018). Chiang *et al.* (2017) evaluated the performance of the information and communication technology (ICT) industry in Taiwan using a combination of DEA and decision tree and examined 16 relevant companies. Toloo *et al.* (2009), in a paper by using a combination of data mining and DEA evaluated different rules for evaluating performance. Wanke and Barros (2016) investigated the role of heterogeneity in the insurance sector. This study focused on predicting the performance of Brazilian insurance companies by proposing an integrative, two-stage approach, which involved the determination of a DEA meta-frontier in the first stage and the use of several data mining techniques in the second. Wu (2009) presented a hybrid model using DEA, decision trees, and neural networks (NNs) to assess supplier performance. The model consists of two modules: Module 1 applies DEA and classifies suppliers into efficient and inefficient clusters based on the resulting efficiency scores. Module 2 utilizes firm performance-related data to train decision trees, NNs model, and apply the trained decision tree model to new suppliers. Raorane and Kulkarini (2012) discussed the role of data mining as an effective tool for yield estimation in the agricultural sector. As crop production depends on geographical, biological, political, and economic factors, data mining can solve the challenge of extracting knowledge from this raw data and estimate the amount of crops production. Ferraro *et al.* (2009) analyzed a large production database describing crop yield patterns. They studied the influence of several factors controlling sugarcane productivity in one of the most important areas of sugarcane production in Argentina. They proposed using a data mining technique called classification and regression tree (CART) to identify the dependence of sugarcane yield on the variation of both environmental and management factors. Ramesh and Vardhan (2013) predicted agricultural products yield using different data mining techniques such as K-Means, K-Nearest Neighbor, Support Vector Machines, and Artificial Neural Networks. They wanted to find a model with high accuracy and ability for prediction of the yield of agricultural products. Jeysenthil *et al.* (2014) designed and predicted a support system for a database of sugarcane soil using the data mining clustering technique (k-means). Everinghama *et al.* (2009) in Australia and Fernandes *et al.* (2011) in Brazil have estimated the yield of sugarcane farms using data mining techniques. Medar and Rajpurohit (2014) presented various crop yield prediction methods using data mining techniques. Different Data Mining techniques such as K-Means, K-Nearest Neighbor (KNN), Artificial Neural Networks (ANN), and Support Vector Machines (SVM) for very recent applications of data mining techniques in the agriculture field.

This study examines how to evaluate the efficiency of sugarcane harvesting units using a combination of DEA and decision trees models and as a case study, sugarcane harvesting units in Amirkabir sugarcane agro-industry in Khuzestan province, Iran are considered. Because DEA evaluates the efficiency of harvesting units and a decision tree to predict their effectiveness, this research enables managers to use the results to improve performance in their future decisions.

Materials and Methods

Study area

The data for this study were collected from Amirkabir agro-industry Company of Khuzestan province in Iran. This agro-industry has 480 farms with 25.5 hectare area for each farm. It covers an area of about 14000 ha. Figure 1 shows the position of Khuzestan province in Iran and a map of Amirkabir agro-industry farms. The data is obtained for the years from 2015 to 2020. The study area is located in Khuzestan Province which is a major agricultural region in Iran. The geographical location of the study area is between latitudes 31° 15′ to 31° 40′ North, and longitudes 48° 12′ to 48° 30′ East. The average elevation of the study area is 8 m above sea level. Mean annual rainfall within the study area is 147.1 mm, mean annual temperature is approximately 25 °C, and mean soil temperature at 50 cm depth is 21.2 °C.

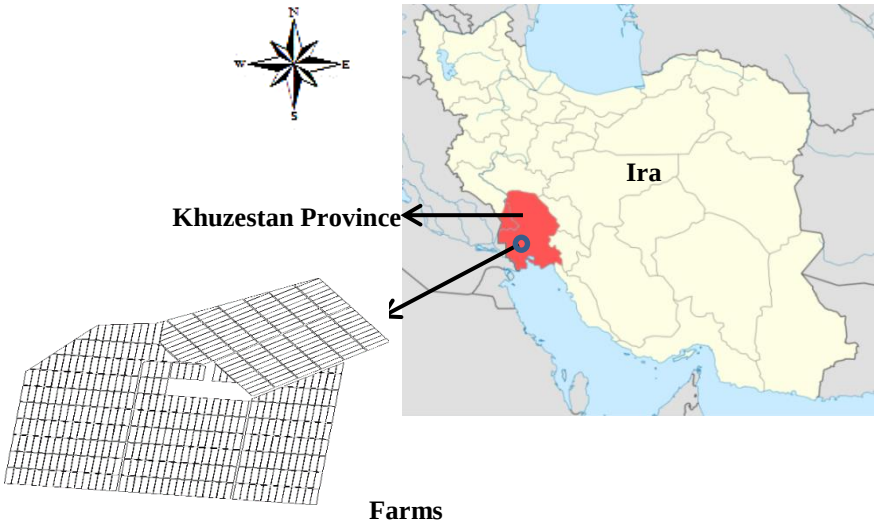

Fig.1. Amirkabir Agro-Industry position

Criteria for measuring the efficiency of sugarcane harvesting units

In this study, to measure the efficiency of sugarcane harvesting units and the best way to identify which unit has the best harvesting performance, nine indicators including the actual amount of hydraulic oil consumed during harvest after the overhaul of the harvester (litre), fuel consumption (litre), repair costs and the costs of consumable parts of harvesters (Rials), the amount of crop harvested (ton), harvest time (day), the amount of area harvested (hectare), factory no-cane hours, the amount of trash sent to the factory (percentage), and the amount of sugarcane waste on the farm (kilogram). To analyze the data, the DEA model has been used to measure the efficiency of sugarcane harvesting units, and the classification and regression trees (CART) model has been used in modeling and predicting the efficiency of these units. Software used also includes IBM SPSS MODELER 14.2 and DEA SOLVER. The research steps are shown in Figure 2.

Data envelopment analysis (DEA)

The DEA has four main models: Constant Return to Scale-CRS, Variable Return to Scale-VRS, Increase Return to Scale–IRS, and Decrease Return to Scale-DRS. Each of the above models has two directions of output-oriented and input-oriented (Liu *et al.*, 2019). In DEA, an inefficient DMU can be made efficient either by reducing the input levels while holding the outputs constant (input-oriented); or symmetrically, by increasing the output levels while holding the inputs constant (output-oriented). Data analysis will be performed with two models CCR[1] and BCC[2]. The CCR DEA model assumes constant

1- Charns, Cooper and Rhodes
2- Banker, Charns and Cooper

returns to scale. It measures the technical efficiency by which the DMUs are evaluated for their performance relative to other DMUs in a sample. On the other hand, the BCC DEA model assumes variable returns to scale conditions. Choosing the right DEA model depends on the level of control over the inputs and outputs; by making each one more controllable, the appropriate model is selected based on that. In this study, because the increase and decrease of inputs are more practical, CCR and BCC input-oriented models are used (Equations 1 and 2). In both models, efficient and inefficient units are identified and the types of technical efficiency, pure technical efficiency, and scale efficiency were calculated .

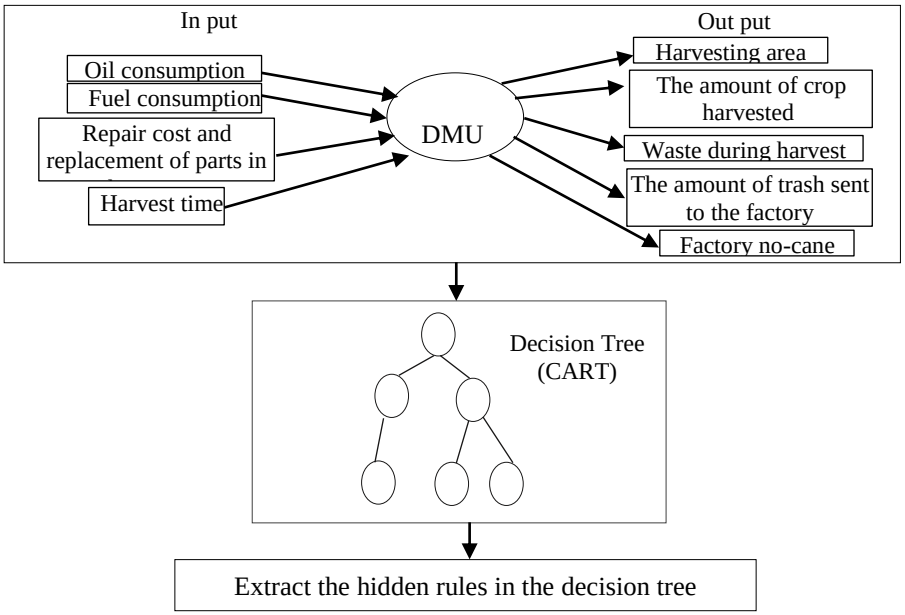

Fig.2. Research model

$$\begin{aligned} &\max E_p = \sum_{r=1}^{r=s} U_r Y_{rp} \\ &\sum_{i=1}^{i=m} V_i X_{ip} = 1 \\ &\sum_{r=1}^{r=s} U_r Y_{rj} - \sum_{i=1}^{i=m} V_i X_{ij} \le o,\ j = 1,2,...,n \\ &V_i \ge \varepsilon, U_r \ge \varepsilon \end{aligned} \quad (1)$$

$$\begin{aligned} &\max E_p = \sum_{r=1}^{r=s} U_r Y_{rp} + w \\ &\sum_{i=1}^{i=m} V_i X_{ip} = 1 \\ &\sum_{r=1}^{r=s} U_r Y_{rj} - \sum_{i=1}^{i=m} V_i X_{ij} + w \le o,\ j = 1,2,...,n \\ &U_r \ge \varepsilon, V_i \ge \varepsilon, w \ \textit{free} \end{aligned} \quad (2)$$

In the above Equations: j= 1,2,…, n, n: the number of DMUs, s: the number of outputs, m: the number of inputs, X_{iP}: the amount of input ith for DMUp, Y_{rP}: the amount of output rth for DMUp, U_k and V_j, respectively, the weight of the outputs, The weight of the inputs and E_p the efficiency of the unit ith. (Banker *et al.*, 1984.)

The relationship between technical efficiency (TE), pure technical efficiency (PTE) (managerial efficiency), and scale efficiency (SE) is defined as Equation 3:

$$\frac{\text{TE}}{\text{PTE}} = \text{SE} \quad (3)$$

The scale efficiency will not be more than one. The efficiency of the CCR model is called total technical efficiency because it is not affected by scale and size. On the other hand, the BCC model shows pure technical efficiency under variable returns to scale. The above relationship shows the efficiency analysis, which shows the efficiency sources.

Which determines whether the inefficiency is due to managerial inefficiency or is due to conditions that indicate the scale efficiency or to both factors.

Data mining

A CART tree is a binary decision tree that is constructed by splitting a node into two child nodes repeatedly, beginning with the root node that contains the whole learning sample. Each node of a tree has two branches, which are related to the outcome of a test on one of the contextual variables. Data used in this study include 11 variables obtained from 20 sugarcane harvesting units during the years 2015-2020. The variables used were divided into two categories: predictive variables and target variables. The variables of pure technical efficiency and technical efficiency were considered as target variables (dependent variable) and other variables were considered as predictive variables (independent variable). In the CART model, the input data includes: harvesting area, the amount of crop harvested (ton), waste during harvest, fuel consumption, oil consumption, repair cost and replacement of parts in harvesters, harvest time, amount of trash sent to the factory (percentage), factory no-cane hours, technical efficiency and pure technical efficiency units of sugarcane harvesters. In this algorithm, 70% of the data were used for training and 30% of the data were used for testing. The Gini index was used to build the tree. Decision tree algorithm try to minimize diversity in the nodes. This non-uniformity in nodes can be measured using the impurity measure, the most important and most widely used method is the Gini index (Yoneyama *et al.*, 2002). Figure 3 depicts the data modeling process using IBM SPSS Modeler 14.2.

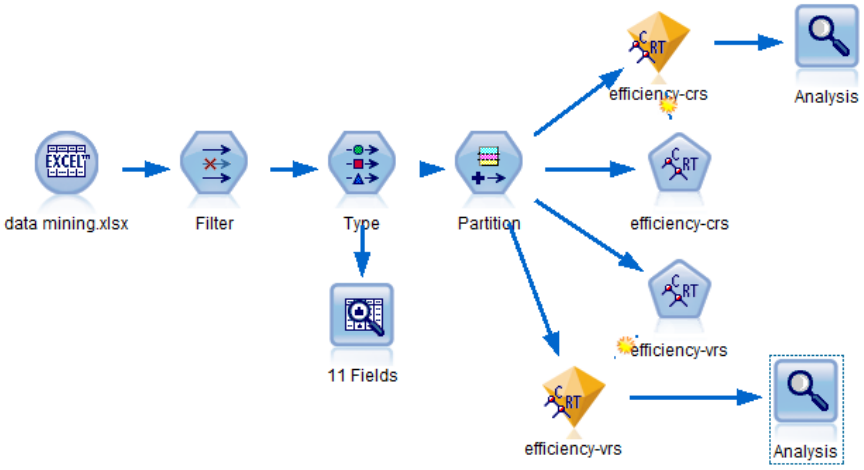

Fig.3. Data modeling process using IBM SPSS Modeler 14.2

Results and Discussion

Determining efficient and inefficient sugarcane harvesting units

The results of a study of 20 sugarcane harvesting units in the CCR model showed that 6 units had an efficient score (30%) and 14 units (70%) had an inefficient score, and their technical efficiency score was in the range of 0.73-0.95 (Table 1). The results of the BCC model study also showed that out of a total of 20 sugarcane harvesting units, 8 units (40%) had efficient scores (Table 1). On the other hand, the remaining harvest units, which were 12 units (60%), scored less than 100 points and were inefficient. In the BCC model, more units are introduced as efficient units and there is less dispersion between inefficient units. Also, the distribution of efficient units in

the BCC model is less than the CCR model. The average values of pure technical efficiency, technical efficiency, and scale efficiency for all 20 units are 0.93, 0.88, and 0.93, respectively (Table 2). Ullah *et al.* (2019) analyzed the efficiency of different sugarcane production systems of Thailand. The result showed that the average efficiency score of sugarcane production systems is approximately 52%. The efficiency analysis indicates a huge potential for the improvement in efficiency through a reduction in the current pattern of farm inputs. The efficiency can also be improved by providing good management practices for sugarcane farms. Kaab *et al.* (2019) reported mean scores of technical efficiency, scale efficiency, and pure technical efficiency in sugarcane production in Iran as 0.91, 0.98, and 0.93, respectively. Khai and Yabe (2011) reported TE for paddy production in Vietnam as 0.816. Elhami *et al.* (2016) computed that TE, PTE, and SE for chickpea production in Isfahan province of Iran were 0.94, 0.99, and 0.94, respectively.

The average technical efficiency of inefficient units is 0.83, which shows that by using 83% of inputs and remaining the same output of them, these units can reach the efficiency limit and save 17% of inputs by increasing their efficiency (Table 1). The BCC analysis results in this table show that units 1, 5, 8, 11, 12, 13, 15, and 16 are efficient. The efficiency of the units means that each unit must be able to reduce its consumption of inputs by (1-θ)% without reducing the amount of production. The efficiency of unit 2 is 0.81%. This means that unit 2 should be able to reduce its consumption from all inputs by 19% to reach the efficiency limit. In Table 1, the ranking results of the harvest units are based on the BBC and CCR input-oriented models, which rank the inefficient units, and all efficient units are prioritized in the rankings on the inefficient units and assigned the first rank. Ranking of efficient units will be based on the number of inefficient units to which reference is made. The ranking of inefficient units is based on the value of efficiency points they have earned. According to the CCR model, after six efficient units, unit No. 14 is ranked first among inefficient sugarcane harvesting units and 7th among all harvest units, followed by harvesting units number 18, 6, 12, 20, 17, etc., respectively. In the BBC model, after eight efficient units, the inefficient unit No. 14 ranks first among the inefficient harvesting units and 9th among the total units, and then the harvesting units number 18, 6, 17, 20, 19, etc., respectively, have the next ranks. If a unit is quite efficient in terms of the BBC model but has a low efficiency of the CCR model, then it is relatively efficient but not overall efficiency. So basically it is reasonable to determine the efficiency of the scale of a unit by these two functions. The technical efficiency of a unit with a constant return to scale (CRS) is obtained from the CCR model. However, in the case of variable efficiency compared to the variable scale (VRS) of the BCC model, technical efficiency can be calculated. The relationship between technical efficiency, pure technical efficiency (management), and scale efficiency is defined in Equation 3. The scale efficiency will not be more than one. The efficiency of the CCR model is called total technical efficiency, because it is not affected by scale and size. On the other hand, BCC shows pure technical efficiency under variable returns to scale. Relationship 3 shows the efficiency analysis that shows the relationship between the sources of inefficiency, i.e. it determines whether the inefficiency is due to managerial inefficiency or is due to the conditions that indicate the scale efficiency or from both factors. According to the results obtained in Table 1, units 12 and 13 operate locally efficiently (pure technical efficiency = 1) and total inefficiency (1 <total efficiency) is due to scale inefficiency. The inefficiencies of units 2, 3, 4, 6, 7, 9, 10, 14, 17, 17, 18, 19, and 20 are due to management inefficiency and also due to the condition of the units (scale inefficiency).

The structure of the CART tree was created to predict the technical efficiency and pure technical efficiency of sugarcane harvesting units is shown in Figures 3 and 4. In the

technical efficiency model, this tree consists of 4 nodes. Three of these nodes are the final nodes.

CART algorithm

The information and description of the input data in the CART model are given in Table 3.

Table 1- Evaluation results of sugarcane harvesting units

DMU NO.	DMU Name	Technical efficiency score (CRS)	Ranking CCR	Pure technical efficiency score (VRS)	Ranking BCC	Scale efficiency score	RTS
1	2015-2016...1	1	1	1	1	1	Constant
2	2015-2016…2	0.81	15	0.86	17	0.94	Constant
3	2015-2016…3	0.73	18	0.88	16	0.82	Constant
4	2015-2016…4	0.89	13	0.91	15	0.97	Constant
5	2016-2017...1	1	1	1	1	1	Constant
6	2016-2017…2	0.93	9	0.96	11	0.96	Increasing
7	2016-2017…3	0.75	16	0.78	20	0.96	Constant
8	2016-2017…4	1	1	1	1	1	Constant
9	2017-2018...1	0.70	19	0.86	18	0.81	Constant
10	2017-2018…2	0.68	20	0.79	19	0.86	Constant
11	2017-2018…3	1	1	1	1	1	Constant
12	2017-2018…4	0.91	10	1	1	0.91	Constant
13	2018-2019...1	0.74	17	1	1	0.74	Constant
14	2018-2019…2	0.95	7	0.97	9	0.97	Decreasing
15	2018-2019…3	1	1	1	1	1	Constant
16	2018-2019…4	1	1	1	1	1	Constant
17	2019-2020...1	0.90	12	0.95	12	0.94	Decreasing
18	2019-2020…2	0.94	8	0.96	10	0.97	Decreasing
19	2019-2020…3	0.88	14	0.92	14	0.95	Decreasing
20	2019-2020…4	0.91	11	0.92	13	0.98	Decreasing

Source: Own calculation

Table 2- Efficiency average of harvesting units

Efficiency	Average	Standard deviation
Pure technical efficiency (efficiency in BCC model)	0.93	0.07
Technical efficiency (efficiency in CCR model)	0.88	0.11
Scale efficiency	0.93	0.07

Table 3- Description of variables used for this study

Variable name	Unit	Average	Minimum amount	Maximum amount	Standard deviation
Harvesting area	ha	2311	2017	2679	166.71
The amount of crop harvested	ton	179321	140942	215033	28501.01
Waste during harvest	kg	11856.5	8341	15032	1755.52
Fuel consumption	lit	364150	301000	448000	39205.63
Oil consumption	lit	10965.90	8600	13984	2003.51
Repair cost and replacement of parts in harvesters	Rials	766850000	5800000000	12530000000	1763173798.02
Harvest time	day	113.60	98	140	14.37
The amount of trash sent to the factory (percentage)	ton	6.24	5.51	6.80	0.42
Factory no-cane hours	hr	23.95	0	59	17.17

Source: Own calculation

The first variable selected to create a branch in the tree is the amount of fuel consumed with the Gini index, 0.002. The next division is using the cost of repairs and replacement of parts in harvesters, which is divided into two branches, costs more than 1,200,000,000 Rials and less than 1,200,000,000 Rials. Also, in the pure technical efficiency model, the tree consists of 2 nodes. The variable selected to create a branch in the tree is the amount of fuel consumed with the Gini index, 0.001. The tree is divided into two branches, the amount of fuel consumed is more than 348,000 liters and less than 348,000 liters.

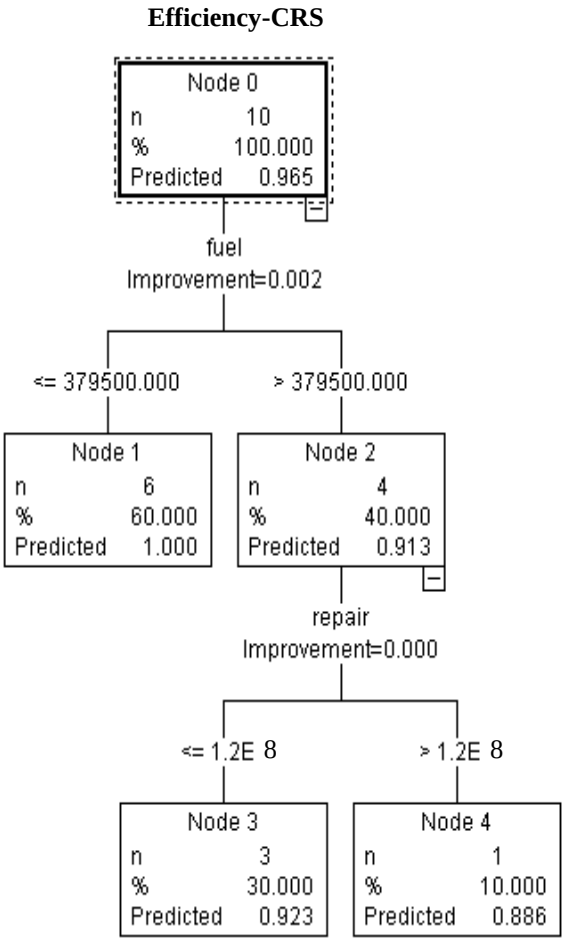

Fig.3. CART model predicting technical efficiency of sugarcane harvesting units

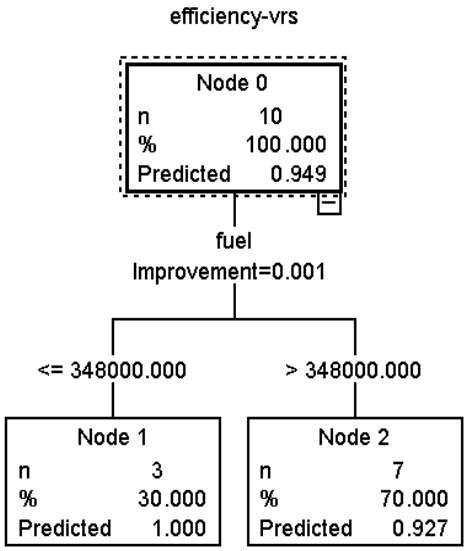

Fig.4. CART model predicting pure technical efficiency of sugarcane harvesting units

Modeling accuracy

Using the linear correlation relationship between the results predicted by the model and the actual results, it can be seen to what extent the resulting model has been successful in predicting the technical efficiency and pure technical efficiency of sugarcane harvesting units. According to Table 4, the accuracy of the CART model for predicting technical efficiency and pure technical efficiency was 86% and 93%, respectively.

Table 4- Results for CART algorithm

Variable	Technical efficiency	Pure technical efficiency
Minimum Error	-0.036	-0.031
Maximum Error	0.077	0.017
Mean Error	0.008	-0.003
Mean Absolute Error	0.013	0.005
Standard Deviation	0.027	0.01
Linear correlation	0.86	0.93

Conclusion

In this study, using the DEA method, technical efficiency, pure technical efficiency, and scale efficiency in sugarcane harvesting units in Khuzestan province, in Iran were investigated. The results of CCR and BCC input-oriented models showed that the average technical efficiency, pure technical efficiency, and scale efficiency in the sugarcane harvesting units were 93%, 88%, and 93%, respectively. Since both CCR and BCC models used for calculating the technical and pure technical efficiencies are unit invariant, the extended models are recommended for future study. In the next step, using the CART decision tree method, the efficiency of sugarcane harvesting units was predicted. In the CART model, the input data includes 11 variables. The results showed that the fuel consumption variable in the CART model for predicting technical efficiency and pure technical efficiency has emerged as the most important independent variable in modeling. This study results showed that the accuracy of the CART model for the variables of technical efficiency and pure technical efficiency were 86% and 93%, respectively. Therefore, it can be clearly seen that the decision tree model has

a very good accuracy in estimating the values of technical efficiency and pure technical efficiency of sugarcane harvesting units. Finally, the results of this study show that the use of predictive methods, by providing an accurate picture of the situation of sugarcane harvesting in Amirkabir agro-industry, allows increasing the productivity of inputs.

References

1. Banker, R. D., A., Charnes, and W. W. Cooper. 1984. Some Models for Estimating Technical and Scale Inefficiencies in Data Envelopment Analysis. Management Science 30 (9): 1078-1092.
2. Charnes, A., W. W., Cooper, and E. Rhodes. 1978. Measuring the efficiency of decision making units. European Journal of Operational Research 2: 429-44.
3. Chiang, T. C., P. Y., Cheng, and F. Y. Leu. 2017. Prediction of technical efficiency and financial crisis of Taiwan's information and communication technology industry with decision tree and DEA. Soft Computing 21 (18): 5341-5353.
4. Elhami, B., A. Akram, and M. Khanali. 2016. Optimization of energy consumption and environmental impacts of chickpea production using data envelopment analysis (DEA) and multi objective genetic algorithm (MOGA) approaches. Information Processing in Agriculture 3: 190-205.
5. Everinghama, Y. L., C. W., Smyth and N, G. Inman-Bamber. 2009. Ensemble data mining approaches to forecast regional sugarcane crop production. Agricultural and Forest Meteorology 149: 689-696.
6. Ferraro, D. O., D. E. Rivero and C. M. Ghersa. 2009. An analysis of the factors that influence sugarcane yield in Northern Argentina using classification and regression trees. Field Crops Research 112: 149-157.
7. Jenhani, I., N. B. Amor, and Z. Elouedi. 2008. Decision Trees as Possibilistic Classifiers. International Journal of Approximate Reasoning 48 (3): 784-807.
8. Jeysenthil, K. M. S., T. Manikandan and E. Murali. 2014. Third Generation Agricultural Support System Development Using Data Mining. International Journal of Innovative Research in Science, Engineering and Technology 3 (3): 9923-9930.
9. Kaab, A., M. Sharifi, H. Mobli, A. Nabavi-Pelesaraei, and K. Chau. 2019. Use of optimization techniques for energy use efficiency and environmental life cycle assessment modification in sugarcane production. Energy 181: 1298-1320.
10. Khai, H., and M. Yabe. 2011. Technical efficiency analysis of rice production in Vietnam. Journal of the International Society for Southeast Asian Agricultural Sciences 17: 135-146.
11. Li, N., Y. Jiang, H. Mu, and Z. Yu. 2018. Efficiency evaluation and improvement potential for the Chinese agricultural sector at the provincial level based on data envelopment analysis (DEA), Energy 164: 1145-1160.
12. Liu, X., P. Guo, and S. Guo. 2019. Assessing the eco-efficiency of a circular economy system in China's coal mining areas: emergy and data envelopment analysis, Journal of Cleaner Production 206: 1101-1109.
13. Medar, R. A., and V. S., Rajpurohit. 2014. A survey on Data Mining Techniques for Crop Yield Prediction. International Journal of Advance Research in Computer Science and Management Studies 2 (9): 59-64.
14. Rahman, M. T., R., Nielsen, M. A., Khan, and M., Asmild. 2019. Efficiency and production environmental heterogeneity in aquaculture: A meta-frontier DEA approach. Aquaculture 509: 140-148.
15. Ramesh, D., and B. Vishnu Vardhan. 2013. Data Mining Techniques and Applications to Agricultural Yield Data. International Journal of Advanced Research in Computer and Communication Engineering 2 (9): 3477-3480.

16. Raorane, A. A., and R. V. Kulkarni. 2012. Data Mining: An effective tool for yield estimation in the agricultural sector. International Journal of Emerging Trends and Technology in Computer Science 1 (2): 75-79.
17. Toloo, M., B. Sohrabi, and S. Nalchigar. 2009. A New Method for Ranking Discovered Rules from Data Mining by DEA. Journal of Expert Systems with Applications 36 (4): 8503-8508.
18. Torgo, L. 2011. Data Mining with R: Learning with Case Studies. CRC Press, Boca Raton.
19. Ullah, A., T. Silalertruksa, P. Pongpat, and S. H. Gheewala. 2019. Efficiency analysis of sugarcane production systems in Thailand using data envelopment analysis. Journal of Cleaner Production 238: 1-11.
20. Wanke, P., and C. P., Barros. 2016. Efficiency drivers in Brazilian insurance: A two-stage DEA meta-frontier-data mining approach. Economic Modelling 53: 8-22.
21. Yoneyama, Y., S., Suzuki, R., Sawa, K., Yoneyama, G. G. Power, and Araki, T. 2002. Increased plasma adenosine concentrations and the severity of preeclampsia. Obstetrics & Gynecology 100 (6): 1266-1270.
22. Wu, D. 2009. Supplier selection: A hybrid model using DEA, decision tree and neural network. Expert Systems with Applications 36: 9105-9112.

نشریه ماشین‌های کشاورزی
https://jame.um.ac.ir/

مقاله پژوهشی

جلد ۱۲، شماره ۱، بهار ۱۴۰۱، ص ۵۴-۴۳

ارزیابی کارآیی واحدهای برداشت نیشکر با استفاده از یک رویکرد ترکیبی از تحلیل پوششی داده‌ها و داده‌کاوی

نسیم منجزی[۱*]

تاریخ دریافت: ۱۳۹۹/۰۴/۲۱
تاریخ پذیرش: ۱۳۹۹/۱۰/۰۲

چکیده

هر سازمانی به‌منظور آگاهی از میزان عملکرد و مطلوبیت فعالیت واحدهای خود به یک نظام ارزشیابی جهت سنجش این مطلوبیت نیاز دارد و این موضوع برای موسسات کشاورزی از جمله کشت و صنعت‌ها اهمیت بیشتری دارد. در تحقیق حاضر، ۲۰ واحد برداشت نیشکر انتخاب گردید. پس از مدل‌سازی بر مبنای مدل‌های CCR و BCC ورودی محور، مقادیر کارایی برای واحدهای برداشت نیشکر محاسبه گردید و با استفاده از درخت تصمیم CART به استخراج قوانین برای پیش‌بینی کارایی این واحدها پرداخته شد. نتایج مطالعه ۲۰ واحد برداشت نیشکر در مدل CCR نشان داد که ۶ واحد دارای امتیاز کارآمد و ۱۴ واحد دارای امتیاز ناکارآمد بودند و امتیاز کارایی فنی آن‌ها در محدوده ۰/۷۳ تا ۰/۹۵ بود. نتایج مطالعه مدل BCC همچنین نشان داد که از مجموع ۲۰ واحد برداشت نیشکر، ۸ واحد دارای امتیاز کارآمد بودند. همان‌طور که مشاهده می‌شود، در مدل BCC، واحدهای بیشتری به‌عنوان واحدهای کارآمد معرفی می‌شوند و پراکندگی کمتری بین واحدهای ناکارآمد وجود دارد. همچنین، توزیع واحدهای کارآمد در مدل BCC کمتر از مدل CCR است. میانگین کارایی فنی، کارایی فنی خالص و کارایی مقیاس به‌ترتیب برابر ۹۳، ۸۸ و ۹۳ درصد به‌دست آمد. همچنین دقت مدل درخت تصمیم تولید شده برای کارایی فنی و کارایی فنی خالص نیز به‌ترتیب برابر ۸۶ و ۹۳ درصد به‌دست آمد.

واژه‌های کلیدی: CART، برداشت، تحلیل پوششی داده‌ها، نیشکر

۱- استادیار گروه مهندسی بیوسیستم، دانشکده کشاورزی، دانشگاه شهید چمران اهواز، اهواز، ایران
(*- نویسنده مسئول: Email: n.monjezi@scu.ac.ir)

DOI: 10.22067/jam.2020.58695.0

Journal of Agricultural Machinery

Homepage: https://jame.um.ac.ir/

Full Research Paper
Vol. 12, No. 1, Spring 2022, p. 55-66

Evaluation of the Plateau Honing on the Friction and Wear Cylinder Liners in Agricultural Tractors

R. Khodabakhshian[1*], S. Sajadi[2]

1- Assistant Professor, Department of Biosystems Engineering, Ferdowsi University of Mashhad, Mashhad, Iran
2- MSc Student, Department of Biosystems Engineering, Ferdowsi University of Mashhad, Mashhad, Iran

Received: 27-09-2020
Revised: 26-10-2020
Accepted: 24-11-2020
Available Online: 28-09-2021

How to cite this article:
Khodabakhshian, R., and S. Sajadi. 2022. Evaluation of the Plateau Honing on the Friction and Wear Cylinder Liners in Agricultural Tractors. Journal of Agricultural Machinery 12 (1): 55-66.
DOI: 10.22067/jam.v12i1.88869

Abstract

To enhance the fuel efficiency of the engines of agricultural tractors, the optimal control of interacting surfaces for improving engine performance becomes extremely significant, especially in developing the surface of cylinder liners. Therefore, plateau honing technology was designed on the cylinder liner of automotive and tractor engines. A substantially flat or plateau is left on the sliding surfaces along with more bearing areas, although a cross hatch model of valleys is kept for retaining oil. On the contrary, the created valley by honing functions as an oil repository can negatively affect creating fluid dynamic pressure on the surfaces. Accordingly, a better understanding of generated surfaces during plateau honing is essential for optimizing process. To this end, some experiments were performed on a cylinder liner of the Perkins 4-248 engine (related to the Massey Ferguson 285 tractor) which was manufactured by Keyhan Sanat Ghaem Company. Then, friction and wear tests with reciprocating motions were conducted to compare the lubricity of sliding cylinder liner surfaces with each different mark of plateau honing. Then, a comparison was made between the friction and wear of the surfaces including various depth of profiles, which were used as the honing mark of the agricultural tractors diesel engine, and those which had randomly ground surfaces. Based on this study results, higher amounts of wear volumes were produced by creating more interactions from asperity contacts and relatively thin films, compared to the test with the shallow-grooved honing marks.

Keywords: Cylinder liner, Friction, Plateau honing, Tractor engine, Wear

Introduction

Nowadays, the process of mechanization development highlights that an increase in the application of tractors in agriculture and the share of mechanical power in operations improves production (Khodabakhshian, 2013; Keshvari and Marzban, 2019). However, improved engine performance and reduced fuel and oil consumptions are among the requirements which challenge the agricultural tractor industry. In agricultural tractors, nearly 11.5% of the energy is utilized for the actual power while the remaining energy is lost. In addition, 18% of the energy loss occurs in mechanical parts, and the energy waste is related to friction losses. Fuel and oil consumption may be reduced by 2% when a 10% reduction occurs in friction losses. According to Khodabakhshian and Shakeri (2011), piston assembly and interface between piston rings and cylinder liners are considered as the most losses in the tractor engine.

Recently, controlling interacting surfaces optimally for increasing the engine performance has been highlighted, especially in designing the surface of cylinder liners to enhance the fuel efficiency related to the agricultural tractor engine. Recent approaches in improving high-speed engines necessitate having an engine with lighter weight, higher

(*- Corresponding Author Email: khodabakhshian@um.ac.ir)

performance, lower exhaust gasifiers, as well as less fuel consumption compared to previous ones (Grabon *et al*., 2018). Further such engines should have the ability for severe loading, which necessitates a reduction in the amount of wear. The process of making some grooves on the surface for lubricating purposes and controlling contact surfaces are considered as one of such methods in this regard. Thus, plateau honing technology was designed on the cylinder liner related to the tractor and automotive engines (Tomanik *et al*., 2018). A plateau honing results in producing flat or plateau finishes on sliding surfaces with a more bearing area while maintaining a cross hatch model of valleys for retaining oil (Kim *et al*., 2018a; Sadizade *et al*., 2020).

Texturing surface is considered as one of the most useful technologies for handling the friction between cylinder liners and piston rings. Some studies focused on a multi-stage honing operation and texturing laser surface on cylinder liners for reducing the friction (e.g., Kligerman *et al*., 2005; Anderberg *et al*. 2018). Ramadan *et al*. (2009) indicated that the honing process enhances the geometric shape of the cylinder liner in terms of its geometric properties, including ovality and roundness. The ovality of the cylinder increases frictions in the engine and the wear between the ring and the cylinder liner wall since it establishes an asymmetric contact surface between rings and pistons with the cylinder liner wall. This phenomenon leads to an increase in fuel consumption while it decreases the output power of the engine and thus the service life of engine parts through time, with additional wear between the ring and piston with the cylinder wall (Kim *et al*., 2018b). Accordingly, tractor manufacturing companies now employ more rigid standards with tight tolerances in the permitted level of cylinder liner roughness although these standards differ relying on the type of the engine and the diameter of the cylinder and piston.

To the best of our knowledge, no study has evaluated the influence of honing or plateau honing on friction and wear of tribological cylinder liner surfaces in agricultural tractors, as well as the effect of honing parameters on the functional parameters of the engine. Most studies in this area predicted the maintenance and repair costs of agricultural tractors and estimated the economic life of tractors (e.g., Almasi and Yeganeh, 2000; Khodabakhshian and Shakeri, 2011; Rohani *et al*., 2011). Furthermore, some studies investigated the application of the preventive net in maintenance and repair programs of agricultural machines (e.g., Khodabakhshian and Shakeri, 2011; Khodabakhshian, 2013). Contrarily, various studies evaluated honing and plateau honing technology on the cylinder liner of automotive and ship engines. For example, Buj-Corral *et al*. (2015) designed several models for optimizing the honing equipment of the driving liner by comparing the obtained data from the surface roughness test device in the laboratory and the existing Honing machine. Additionally, Cabanettes *et al*. (2015) obtained data regarding the surface roughness of the cylinder liner and its related wear. In addition, Yousfi *et al*. (2015) studied the effect of plateau honing parameters on the surface roughness of the driving cylinder liner. In another study, Kim *et al*. (2018b) examined the effect of the parameters related to plateau honing on creating friction and wear for the driving cylinder liner.

Considering the above-mentioned explanations, the present study attempted to assess the impact of plateau honing on creating the tribological cylinder liner surfaces for friction and wear in agricultural tractors. A change occurred in profile depth from 0.05 μm to 0.8 μm in R_a, which often uses the honing mark related to the agricultural tractor engine. Further, a comparison was made between these surfaces and the randomly ground surface with a surface roughness of 0.15 and 0.25 μm in R_a. To this end, a cylinder liner of the Perkins 4-248 engine (related to the Massey Ferguson 285 tractor and manufactured by Keyhan Sanat Ghaem Company) was applied to perform the test.

Materials and Methods

The spatial and temporal domain of the study

Keyhan Sanat Ghaem Company, as one of the largest manufacturers of cylinder liners in Iran and the Middle East, was selected as the case study. The current study was conducted in 2017 in this company. Given the aim of the present study regarding evaluating the cylinder liner of the agricultural tractor, the cylinder liner of the Perkins 4-248 engine was selected, which was associated with the Massey Ferguson 285 tractor. Fig. 1 depicts a sample of this cylinder liner.

Tribological tests

A reciprocating ring-liner tribometer driven by a slider-crank mechanism with a stroke length of 80 mm (Fig. 4) was implemented for evaluating the friction and wear characteristics of cylinder liner surfaces with different honing marks against piston ring surfaces with 27±2 °C temperature. Then, the contact surface was lubricated by using a 10W40 semi-synthetic oil (μ_D equal to 0.08 Pas at 40 °C). It should be noted that the total wear test took 120 min in which extra amounts of lubricant were summed (2-3 mL) every 20 min. In addition, the normal force and engine velocity used for these tests were 100 N and 120 rpm, respectively (Yousfi *et al*., 2015; Kim *et al*., 2018b).

Fig.1. A sample of the cylinder liner

The measured cylinder liner material involves high-quality cast iron (GG 25) which has a 101 mm bore diameter and 233 length. The chemical compositions of the grey cast iron are shown in Table 1. The inner surface of cylinder liners has a hardness of 225-272 HB. The metallography (ASTM A247) results indicated that the liner consists of cast iron along with the pearlite matrix and an insignificant amount of the steadite (iron phosphide eutectic network). Further, the form of graphite is type I, graphite distribution is pattern A, E, and graphite size is 4.5.

Table 1– Cylinder liner material specifications

Element*	Cr%	S%	P%	%Mn	%Si	%C
% By weight	0.5	0.1	0.4	0.9	2.4	3.35

**Note*. Cr: Chrome; S: Sulfur; P: Phosphorus; Mn: Manganese; C: Carbon.

Sample preparation

First, the honing process from cylinder liners in the Perkins 4-248 engine block honing station was used for producing specimens by utilizing a mono spindle vertical honing machine by a developed instrument (NAGEL no. 28-8470) (Fig. 2). Cylinder blocks are delivered to the honing station after pressing and boring liners in the machining

line. Then, liner specimens were prepared with varied honing depths, representing a surface roughness of 0.05, 0.15, 0.25, 0.5, and 0.8 µm in Ra (Fig. 3). In addition, five honing marks were produced to assess the impact of the honing mark on the wear and friction related to the contacting surfaces. The final surface of engine liners in plateau honing should become 0.8 µm in R_a (in other words R_k 3.712, R_{pk} 0.895, and R_{vk} 2.321 values should be seen on the final surface) on the surface processed by long-stroke honing. Additionally, two surfaces were created by random grinding without any honing marks, and the surface roughness of which were 0.15 and 0.25 µm in Ra. Next, all liner specimens were mounted on a reciprocating tester along with cleaning with acetone. Finally, scanning electron and optical microscopes were utilized to examine worn tracks on surfaces.

Friction tests undertake a load level of 100 N and reciprocating velocity of 120 rpm (Yousfi *et al*, 2015; Kim *et al*., 2018b). The contact pressure is high and can reach up to 50 MPa thanks to a small contact surface between the liner and ring surface (nearly 2-3 mm^2). Then, the friction was measured after 0, 15, 30, 60, and 120 min. Finally, the friction coefficient was calculated by applying the ratio between the average normal force (F_N) over the mean tangential force (F_T) assessed by strain gauges. The Rtec Multi-Function Tribometer software was used. A balanced Wheatstone bridge has been constructed by mounting four strain gauges over F_T. Two strain gauges have been mounted over the outer surface (for F_N), while rests are placed at the inner surface.

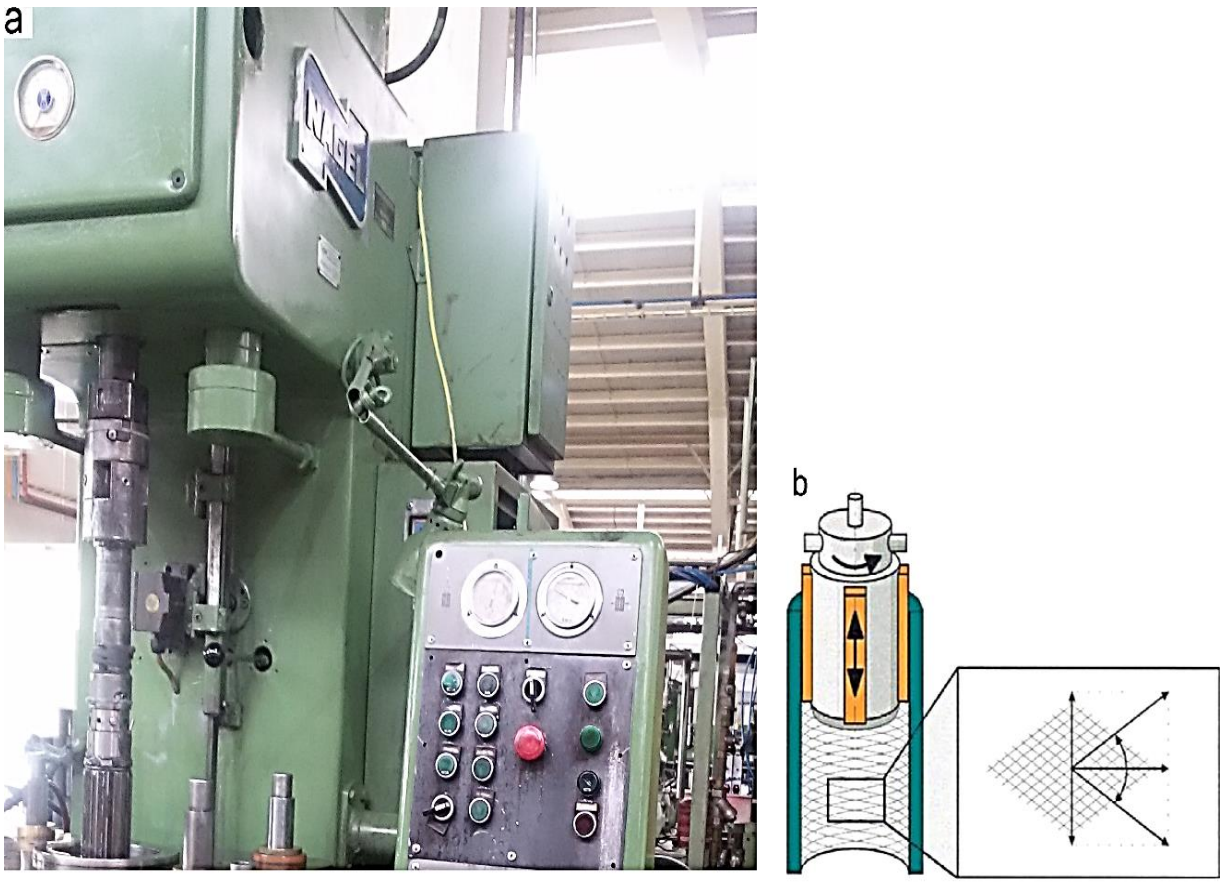

Fig.2. (a) Vertical honing machine with an expansible tool and (b) Schematic representation of a honing head and its motion

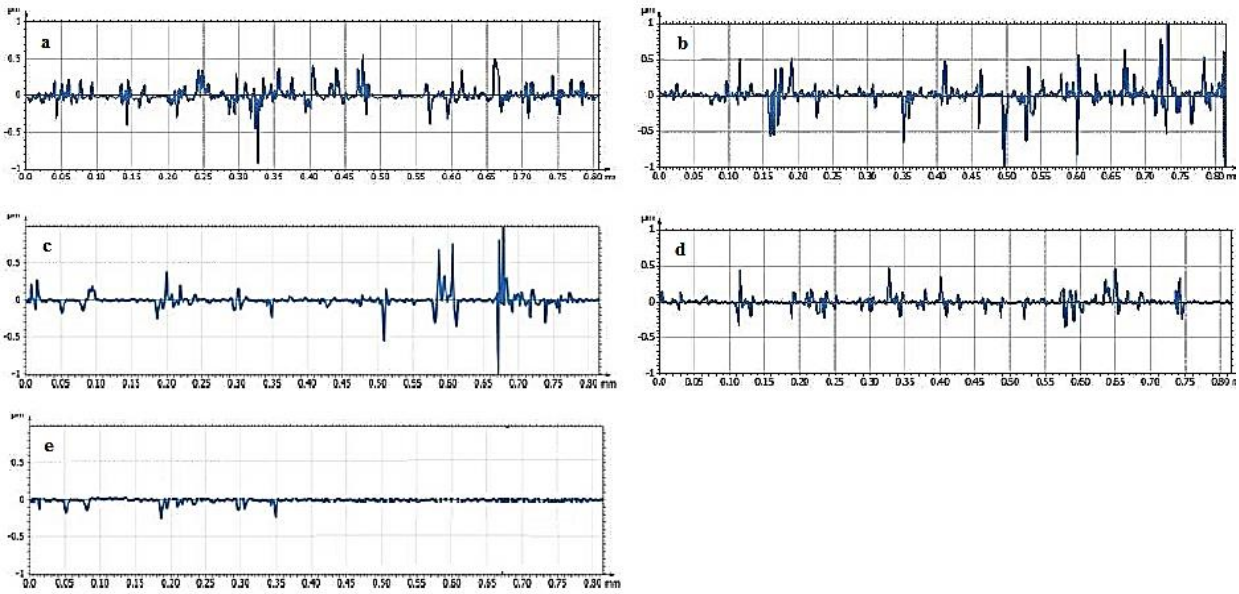

Fig.3. Honing processed surface roughness: (a) R_a 0.8 μm, (b) R_a 0.5 μm 5, (c) R_a 0.25 μm, (d) R_a 0.15 μm, and (e) R_a 0.05 μm– polishing processed surface

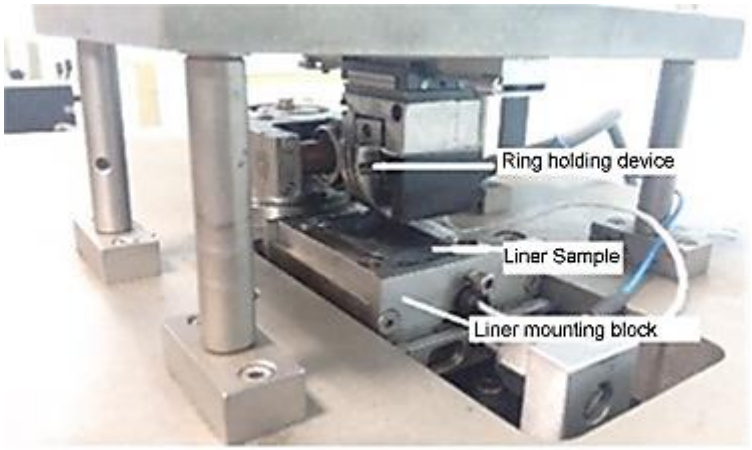

Fig.4. Reciprocating ring-liner tribometer

Results and Discussion

Running-in friction dependence on surface

Fig. 5 illustrates the specimen friction coefficient made by utilizing different surface processes. As displayed, compared to the surfaces with a grinding process with similar surface roughness, honing processed surfaces involve the coefficients with lower friction. Based on the results, no difference was observed in the friction performance related to the surface roughness of 0.8 μm in R_a in comparison to those of smoother surfaces. However, the highest friction coefficient was reported for polishing processed surfaces which confirmed some numerical results in the mixed lubrication regime (Mezghani *et al*., 2013; Yousfi *et al*., 2014). However, these findings should be approved by firing engine experiments that consider real engine conditions. These findings corroborate with those of Yousfi *et al*. (2015), Kim *et al*. (2018b), Anderberg *et al*. (2018), and Grabon *et al*. (2018).

Wear evolution during running-in

The evaluation method related to the wear volume of the cylinder liner during the plateau honing process compares the surface bearing as a curve of the original and plateau honed surface (Kumar *et al*., 2000; Srivastava *et al*., 2007). Further, this method represents that original surface depth is not eliminated when there is a negligible amount of wear. Fig. 6 illustrates the wear volumes related to cylinder liners with different roughness of the surface. The least volume of wear is created by the surfaces with the honing marks of 0.1-0.2 µm in R_a.

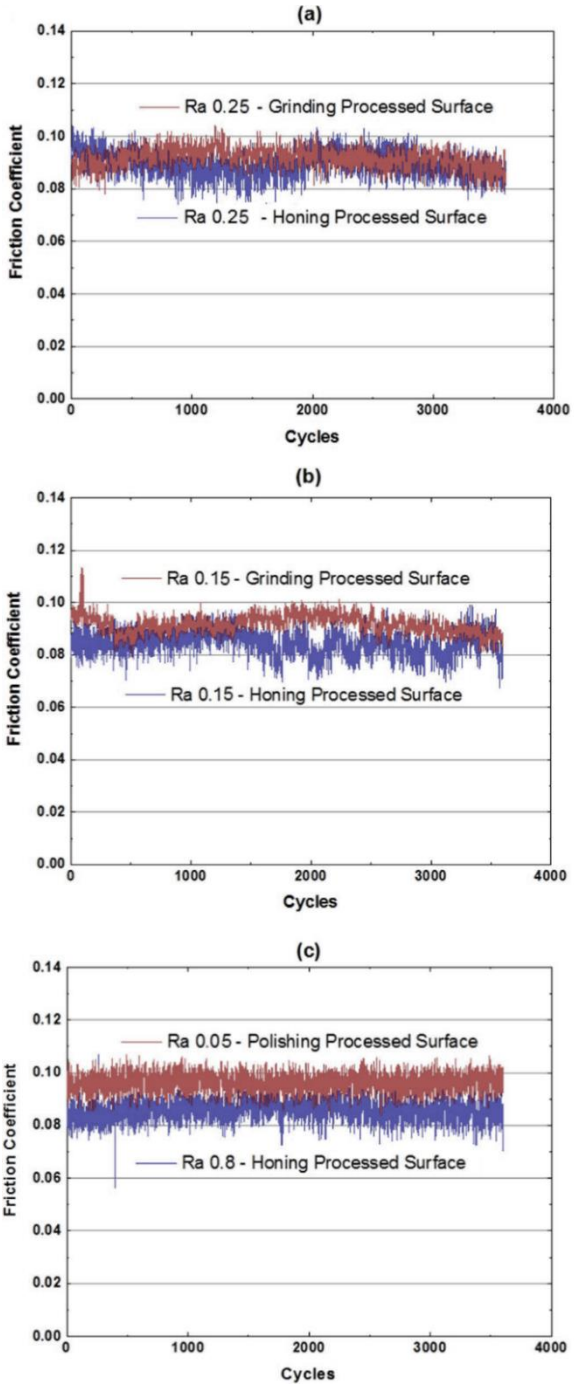

Fig.5. The friction coefficient related to surface roughness: (a) R_a 0.25 µm, (b) R_a 0.15 µm, and (c) R_a 0.8 and 0.05 µm

However, the highest wear volume was observed in the surface roughness of 0.8 µm in R_a. Based on the results, the volumes of wear increased by enhancing the surface roughness from 0.2 µm since colliding jagged asperities resulted in increasing in polishing effects. Contrarily, a decrease in the surface roughness from 0.1 µm led to an increase in the volumes of the wear by considering the fact that an increase in the real contact area between steel ball and cylinder liner results in creating more severe wear by adhesion. Other studies such as Yousfi *et al*. (2015) and Kim *et al*. (2018b) reported a similar trend for the wear volumes related to cylinder liners with different surface roughness.

In addition, the randomly ground surface indicated identical or better wear resistance after comparing the wear volumes related to the two machined surfaces, in comparison to the honing processed surface. It is worth noting that the surface valleys interrupt the maintaining hydrodynamic pressure of the lubricant film which results in creating partially metal-to-metal contact and plastic deformations by interacting asperities.

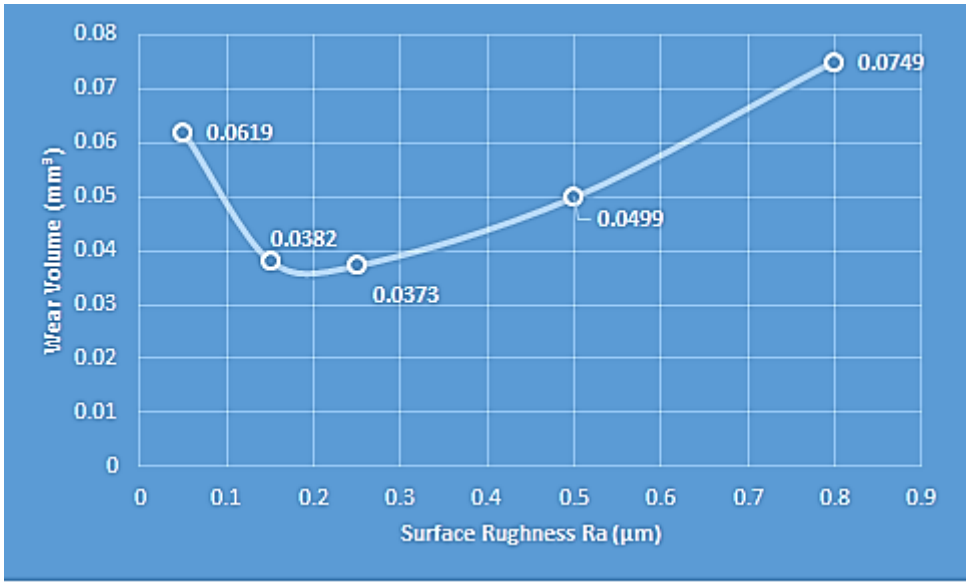

Fig.6. Wear volume of the cylinder liner

Scanning electron microscope (SEM) observations

To evaluate the effect of the honing mark on the wear, the honed surfaces with different surface roughness were considered for comparison. As shown in Fig. 7, the rough surface with 0.8 µm in R_a is rather damaged due to its plowing action and deep valley. In addition, the polished surface indicated a deep wear depth and higher plowing, while the wear mark related to the surface roughness of 0.5 µm in R_a is less than those of other surfaces.

As shown in Fig. 8, the surface with R_a 0.8 µm, which involves deeper grooves and a less contact area, demonstrates severe plastic deformations due to the interaction existing in colliding asperities. Based on the results, the grooves smeared by sliding surface and plastic deformations became smooth. Kim *et al*. (2012) evaluated the effect of reserving oils on grooves as well. The results of the current study further represented that surfaces with R_a 0.25 and 0.15 µm still indicate several groove patterns after the sliding test. Furthermore, adhesive wear was observed by the smoothest surface with polishing, which produced higher

volumes of wear (Fig. 6). Thus, there is an optimum range of surface roughness to reduce the wear amount of the plateau honing process ranged between 0.15 and 0.25 μm in R_a.

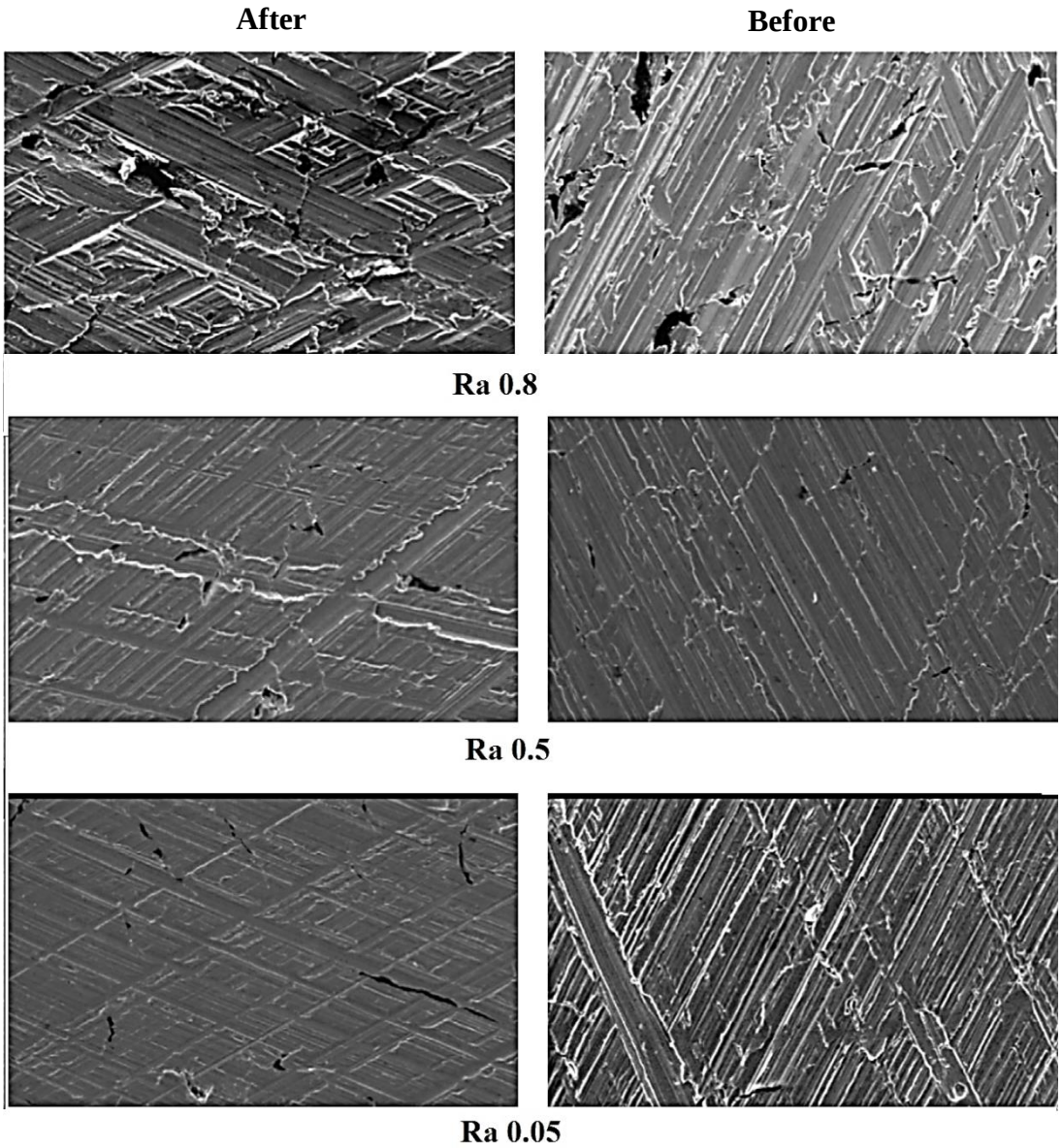

Fig.7. Microscopic images before and after the experiment

Fig. 9 depicts SEM images measured by ground surfaces without any honing process. The amounts of the wear were almost similar in comparison to similar surfaces with honing. Although the optimum groove depth of plateau honing is available for reducing the amounts of wear, the effect of the groove by using the plateau honing process which is considered as an oil reservoir is insufficient for reducing the wear compared to using only the grinding process.

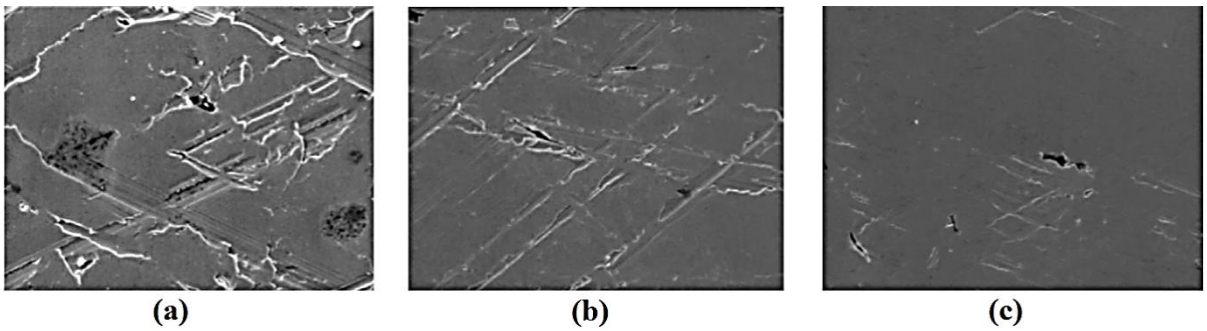

Fig.8. SEM images analysis of honing processed surface: (a) R_a 0.8 μm, (b) R_a 0.25 μm, and (c) R_a 0.15 μm

Note. SEM: Scanning electron microscope.

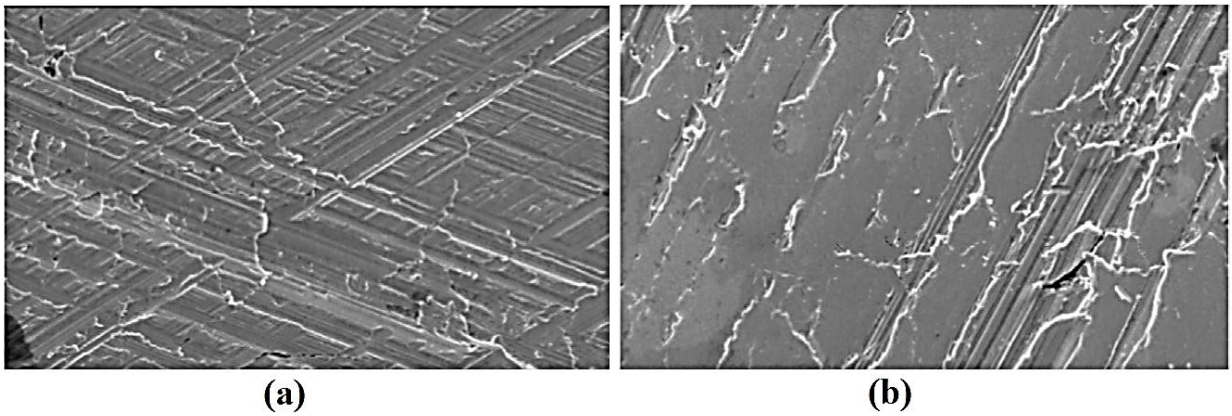

Fig.9. SEM images analysis of grinding processed surface: (a) Ra 0.25 μm and (b) Ra 0.15 μm

Note. SEM: Scanning electron microscope.

Conclusion

In general, increasing the fuel efficiency of the agricultural tractor engine requires a better understanding of the generated surfaces during the honing of cylinder liners. Therefore, the present study evaluated the impact of plateau honing marks on the cylinder liner of the Perkins 4-248 engine (related to the Massey Ferguson 285 tractor). To this end, five types of honing marks (with the surface roughness of 0.05, 0.15, 0.25, 0.5, and 0.8 μm in R_a) and two randomly ground surfaces including 0.15 and 0.25 μm in R_a for the surface roughness were used for testing friction and wear. The tests were performed under the load level of 100 N and reciprocating velocity of 120 rpm with a 10W40 semi-synthetic oil. The main findings of the present study are as follows.

1. Based on the results of deep-grooved honing marks, higher amounts of wear volumes were created after severe interactions due to asperity contacts and the formation of relatively thin films in comparison to the test related to shallow-grooved honing marks.

2. The least volume of wear occurred for the surface with the honing mark ranged 0.15 and 0.25 μm in R_a.

3. Similar amounts of wear were observed for the tests without honing with a similar R_a of 0.25 μm in comparison to the wear test with the honed surface.

4. Lubricant films were not enough for decreasing the surface interaction resulting from deep grooves regarding surfaces with the honing mark, which resulted in disrupting fluid film formation.

Acknowledgment

The present study was conducted as a research project (No. 47948) with the support

and cooperation of the Faculty of Agriculture of Ferdowsi University of Mashhad.

References

1. Almasi, M., and H. M. Yeganeh. 2000. Determining the appropriate mathematical model for forecasting the costs of maintenance and repair of agricultural tractors used in the Karun Sugar Crop Industry. Iranian Journal of Agricultural Science 4 (33): 707-716.
2. Anderberg, C., Z. Dimkovski, B. G. Rosén, and T. R. Thomas. 2018. Low friction and emission cylinder liner surfaces and the influence of surface topography and scale. Tribology International 133: 224-229.
3. Buj-Corral, I., J. Vivancos-Calvet, L. Rodero-de-Lamo, and L. Marco-Almagro. 2015. Comparison between Mathematical Models for Roughness Obtained in Test Machine and in Industrial Machine in Semifinish Honing Processes. Procedia Engineering 132: 545-552.
4. Cabanettes, F., Z. Dimkovski, and B. G. Rosén. 2015. Roughness variations in cylinder liners induced by honing tools' wear. Precision Engineering 41: 40-46.
5. Grabon, W., P. Pawlus, S. Wos, W. Koszela, and M. Wieczorowski. 2018. Effects of cylinder liner surface topography on friction and wear of liner-ring system at low temperature. Tribology International 12: 148-160.
6. Keshvari, A., and A. Marzban. 2019. Prioritizing the Power Arrival in Khuzestan Province Agriculture using FAHP and FTOPSIS. Journal of Agricultural Machinery 9 (1): 235-251. (In Persian).
7. Khodabakhshian, R. 2013. A review of maintenance management of tractors and agricultural machinery: preventive maintenance systems. Commission of Agricultural and Biosystems Engineering (CIGR) 15 (4): 147-159.
8. Khodabakhshian, R., and M. Shakeri. 2011. Prediction of repair and maintenance costs of farm tractors by using of Preventive Maintenance. International Journal of Agriculture Sciences 3 (1): 39-44.
9. Kim, J. S., D. H. Cho, K. M. Lee, and Y. Z. Lee. 2012. The signal parameter for monitoring fretting characteristics in real-time. Tribology Transactions 55: 730-737.
10. Kim, E. S., S. M. Kim, and Y. Z. Lee. 2018a. Effect of waviness and roughness on cylinder liner friction. Wear 400-401: 207-212.
11. Kim, E. S., S. M. Kim, and Y. Z. Lee. 2018b. The effect of plateau honing on the friction and wear of cylinder liners. Wear 400-401: 207-212.
12. Kligerman, Y., I. Etsion, and A. Shinkarenko. 2005. Improving tribological performance of piston rings by parial surface texturing. Journal of Tribology 127: 632-638.
13. Kumar, R., S. Kumar, B. Prakash, and A. Sethuramiah. 2000. Assessment of engine liner wear from bearing area curves. Wear 239: 282-286.
14. Mezghani, S., I. Demirci, M. Yousfi, and M. EL Mansori. 2013. Mutual influence of cross hatch angle and superficial roughness of honed surfaces on friction in ring pack tribo-system. Tribology International 66: 54-59.
15. Ramadan Ali, S. H., H. H. Mohamed, and M. K. Bedewy. 2009. Identifying Cylinder Liner Wear using Precise Coordinate Measurements. International Journal of Precision Engineering and Manufacturing 10: 19-25.
16. Rohani, A., M. H. Abbaspour-Fard, and S. Abdolahpour. 2011. Prediction of tractor repair and maintenance costs using Artificial Neural Network. Expert Systems with Applications 38: 8999-9007.
17. Sadizade, B., A. Araee, S. N. Bavil Oliaei, and V. Rezaeizad Farshi. 2020. Plateau honing of a diesel engine cylinder with special topography and reasonable machining time. Tribology International 146: 106204.

18. Srivastava, D. K., A. K. Agarwal, and J. Kumar. 2007. Effect of liner surface properties on wear and friction in a non-firing engine simulator. Materials & Design 28: 1632-1640.
19. Tomanik, E., M. EL Mansori, R. Souza, and F. Profito. 2018. Effect of waviness and roughness on cylinder liner friction. Tribology International 120: 547-555.
20. Yousfi, M., S. Mezghani, I. Demirci, and M. EL Mansori. 2014. Mutual effect of groove size and anisotropy of cylinder liner honed texture son engine performances. Advanced Materials Research 966-967: 175-183.
21. Yousfi, M., S. Mezghani, I. Demirci, and M. EL Mansoria. 2015. Smoothness and plateauness contributions to the running-in friction and wear of stratified helical slide and plateau honed cylinder liners. Wear 332-333: 1238-1247.

نشریه ماشین‌های کشاورزی
https://jame.um.ac.ir/

مقاله پژوهشی

جلد ۱۲، شماره ۱، بهار ۱۴۰۱، ص ۶۶-۵۵

بررسی تاثیر هونینگ پلاتو بر روی اصطکاک و سایش بوش سیلندر در تراکتورهای کشاورزی

رسول خدابخشیان کارگر[۱*]، ستایش سجادی[۲]

تاریخ دریافت: ۱۳۹۹/۰۷/۰۶
تاریخ پذیرش: ۱۳۹۹/۰۹/۰۴

چکیده

به‌منظور افزایش بازده سوخت موتورهای تراکتورهای کشاورزی، کنترل بهینه سطوح برهم‌کنش برای بهبود عملکرد موتور به‌ویژه در توسعه سطح بوش سیلندر بسیار چشمگیر می‌شود. از این رو، فن‌آوری هونینگ پلاتو بر روی بوش سیلندر موتورهای خودرو و تراکتور طراحی شد. یک سطح صاف یا پلاتو در واقع به‌جا گذاشتن سطوح لغزشی همراه با مناطق تنش پسماند بالا می‌باشد، اگرچه یک مدل هاشور متقاطع از شیارهای سطح برای نگهداری روغن نگهداری وجود دارد. در مقابل، شیارهای سطح ایجاد شده از طریق عملیات هونینگ به‌عنوان مخزن روغن می‌تواند بر ایجاد فشار دینامیکی سیال بر روی سطوح، تأثیر منفی بگذارد. بر این اساس، درک بهتری از سطوح تولید شده در طی فرآیند هونینگ پلاتو برای بهینه‌سازی فرآیند ضروری است. بدین منظور، برخی آزمایش‌های روی یک بوش سیلندر موتور پرکنیز ۴/۲۴۸ (مربوط به تراکتور مسی فرگوسن ۲۸۵) تولیدی شرکت کیهان صنعت قائم انجام شد. سپس، آزمون‌های اصطکاک و سایش با حرکات رفت و برگشتی برای مقایسه روانکاری سطوح بوش سیلندر با تیمارهای مختلف هونینگ پلاتو انجام شد. درنهایت، مقایسه‌ای بین اصطکاک و ساییدگی سطوح از جمله عمق‌های مختلف پروفیل‌ها، که به‌عنوان تیمارهای مختلف هونینگ موتور دیزل دریایی استفاده شده و آن‌هایی که دارای سطوح تصادفی بوده انجام گردید. بر اساس نتایج، مقادیر بالای سایش با ایجاد فعل و انفعالات بیشتر از تماس‌های زبری و فیلم‌های نسبتاً نازک، در مقایسه با آزمون با تیمارهای هونینگ شیار کم عمق تولید شد.

واژه‌های کلیدی: اصطکاک، بوش سیلندر، سایش، موتور تراکتور، هونینگ پلاتو

۱- استادیار گروه مهندسی بیوسیستم، دانشگاه فردوسی مشهد، مشهد، ایران
۲- دانشجوی کارشناسی ارشد مهندسی بیوسیستم، دانشگاه فردوسی مشهد، مشهد، ایران
(*- نویسنده مسئول: Email: khodabakhshian@um.ac.ir)

DOI: 10.22067/jam.v12i1.88869

Journal of Agricultural Machinery

Homepage: https://jame.um.ac.ir/

Full Research Paper
Vol. 12, No. 1, Spring 2022, p. 67-79

Effect of Infrared Drying on Drying Kinetics and Color Changes of Wild Sage Seed Mucilage

Gh. Amini[1], F. Salehi[2], M. Rasouli[3*]

1- MSc Student, Faculty of Agriculture, Bu-Ali Sina University, Hamedan, Iran
2- Associate Professor, Faculty of Agriculture, Bu-Ali Sina University, Hamedan, Iran
3- Assistant Professor, Faculty of Agriculture, Bu-Ali Sina University, Hamedan, Iran

Received: 07-12-2020
Revised: 13-01-2021
Accepted: 02-03-2021
Available Online: 28-09-2021

How to cite this article:
Amini, Gh., F. Salehi, and M. Rasouli. 2022. Effect of Infrared Drying on Drying Kinetics and Color Changes of Wild Sage Seed Mucilage. Journal of Agricultural Machinery 12 (1): 67-79.
DOI: 10.22067/jam.2021.67448.1002

Abstract

In this study, the effects of infrared (IR) dryer system parameters such as IR power, the distance of mucilage from lamp surface, mucilage thickness on drying kinetics and, color indexes (L*, a*, b* and ΔE) of wild sage seed mucilage (WSSM) were investigated in an IR dryer system. Experimental moisture ratio (MR) data were fitted to 7 various empirical thin-layer models. It was found that the Page model has the best fit to show the kinetic behavior and acceptably described the IR drying behavior of WSSM with the lowest mean square error (MSE), root mean square error (RMSE), mean absolute error (MAE), and standard error (SE) values and the highest correlation coefficient (r) value. The values of MSE, RMSE, and MAE for all experiments were in the range of 0.1×10^{-3}-1.1×10^{-3}, 1.04×10^{-2}-3.25×10^{-2} and 8.7×10^{-3}-27.1×10^{-3}, respectively. The average effective moisture diffusivity (D_{eff}) increased from 4.61×10^{-9} m^2s^{-1} to 15.8×10^{-9} m^2s^{-1} with increasing lamp power from 150 W to 375 W, while it was decreased from 14.4×10^{-9} m^2s^{-1} to 5.16×10^{-9} m^2s^{-1} and 13.2×10^{-9} m^2s^{-1} to 4.31×10^{-9} m^2s^{-1} with increasing the distance of mucilage from 4 to 12 cm and the reduction of mucilage thickness from 1.5 to 0.5 cm, respectively. Increasing in IR radiation power has a positive influence on the yellowness (increasing 19.78% in b^* index) of dried WSSM. Also, it increased the color changes index (ΔE) from 16.05 to 17.59.

Keywords: Color indexes, Effective moisture diffusivity, Gum, Moisture ratio, Page model

Introduction

Fruits and vegetables drying is a commonly used process for improving product safety as it greatly decreases the microbial activity and enzymatic changes during the storage period, hence, increasing the shelf life of the product. One of the best ways to reduce the drying time is to provide heat by infrared (IR) radiation. IR methods could be used as a substitution to the current drying methods for producing high-quality dried hydrocolloids. IR heating has many advantages including high heat transfer rate, uniform heating, short processing time, high efficiency (80-90%), lower energy consumption, lower energy costs, and improving final product quality (Salehi, 2020a). In addition, the use of IR dryers in combination with other dryers helped to decrease the drying time by rising the drying rate that leads to reduced energy utilization. Also, symmetrical temperature sharing by IR improved final product quality (Baeghbali *et al.*, 2019).

The dispersion of water-soluble hydrocolloids (gums) in the aqueous system provides great technical importance, since they can improve the gelling or thickening properties of food products (Zameni *et al.*, 2015). The genus *Salvia* (*Labiatae*) contains more than 700 species of mucilaginous

(*- Corresponding Author Email: m.rasouli@basu.ac.ir)

endemic plant. Wild sage (*Salvia macrosiphon* L.) is the mucilaginous native plant that is grown in different regions of Asia, Europe, and Middle East, especially in various regions of Iran and its seeds have a high content of mucilage (gums or hydrocolloids) with outstanding useful characteristics that is comparable with marketable food gums. Wild sage seeds are round small seeds, with a mucilage layer on their surface, which could swell in water, giving a viscous suspension. Wild sage seed mucilage (WSSM) is a gum extracted from the wild sage seed. Salehi and Kashaninejad (2015) reported that the apparent viscosity of WSSM solution (0.6% w/w), was varied from 0.162 to 0.344 Pa.s (60 s^{-1}), and freeze-dried WSSM exhibited the highest viscosity value among all dried gums. Also, the amounts of hardness, stickiness, consistency and adhesiveness of WSSM gel (3% w/w) were changed from 45.7 to 78.2 g, 9.8 to 17.0 g, 340.4 to 794.8 g.s, and 91.4 to 159.2 g.s at different drying conditions. In the bakery products gums have been used to improve dough performance, breads and cakes characteristics, textural and sensorial quality and extend the shelf life of the products (Salehi, 2019a). For example, the effect of the WSSM (at four levels of 0, 0.5, 1 and 1.5%, w/w) on physicochemical characteristics and sensorial properties of apple cake was studied by Salehi (2017). The authors reported that adding WSSM to apple cake batter reduced the density and improved its volume, lightness (L*), and sensorial parameters (appearance, crumb color lightness, porosity, flavor, texture, and overall acceptance).

The physicochemical properties and rheological behavior of dried seed gums depend on the method and condition of drying. Also, the color of the dried products is an important quality factor, which is affected by the drying conditions. For example, the effect of different drying methods (oven drying with temperature changes 40-80°C, freeze-drying and, vacuum oven-drying) on rheological behavior, color and physicochemical characteristics of basil seed mucilage was investigated by Salehi and Kashaninejad (2017). The color of oven-dried gum was darker (lower L* index values) in comparison to the freeze-dried or vacuum oven dried gums. In addition, the drying procedure can provide a broad range of molecular weight depending on the type and condition of drying. Nep and Conway (2011) reported that the grewia gum demonstrated the various degrees of viscosity varying from 0.2 to 0.32Pa.s depending on the drying method. However, there is no study available in the literature regarding the effect of IR drying techniques on the drying kinetics, D_{eff} and color changes of WSSM. Therefore, this study aimed to investigate the effect of IR drying on the drying kinetics, D_{eff} and color changes of WSSM.

Materials and Methods

Gum extraction

Wild sage seeds were purchased from a local market in Hamedan, Iran. They were physically cleaned and all foreign materials were removed. Then, the pure wild sage seeds were immersed in water for 20 min at a seed/water portion of 1:20 at 25°C. In the next step, the gum was separated from the inflated seeds by passing the seeds through an extractor (M-J-376-N, Nikko Electric Industry Company, Iran) with a rotating disc that scratched the mucilage layer on the seed surface. The initial moisture content (MC) of the WSSM was 99.4% (wet basis). The moisture content of WSSM was determined in an atmospheric oven at 105°C for 4 h (AOAC, method no. 934.06). Finally, the obtained WSSM was immediately placed into the IR dryer (Figure 1).

IR drying

The extracted WSSM was transferred in the cylindrical aluminum containers and then dried in an IR dryer (length 44 cm, width 20 cm, and height 40 cm). The effect of IR lamp (IR radiation lamp (NIR), Noor Lamp Company, Iran) power (at three levels 150, 250 and 375 W), the distance of sample from lamp (at three levels 4, 8, and 12 cm), mucilage thickness (at three levels 0.5, 1 and 1.5 cm) and time on the drying kinetics of WSSM was investigated (Amini *et al.*, 2021).

The weight changes of WSSM were measured using a LutronGM-300p digital balance (Taiwan, sensitivity of ±0.01 gr).

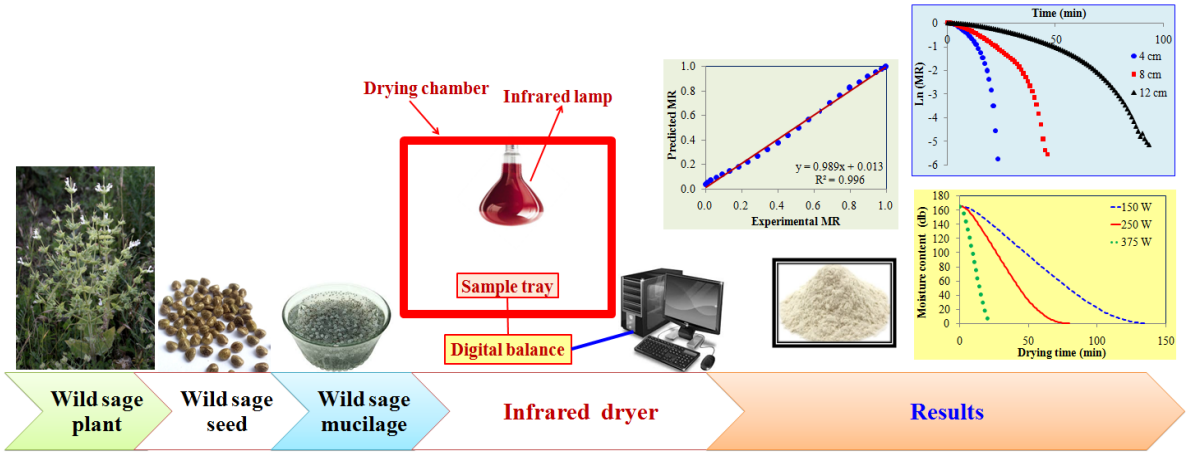

Fig.1. Schematic of Wild sage seed mucilage drying in an infrared dryer

Drying kinetics

Numerical modeling is one of the appropriate methods for describing the drying kinetics of food products (Salehi, 2020b). For numerical modeling the drying kinetic behavior of WSSM, 7 commonly used thin-layer models including Quadratic, Page, Newton, Midilli, Logarithmic, Verma, and Two terms were examined (Akpinar and Bicer, 2005; Doymaz, 2011). In these models, dimensionless MR were defined as equation (1):

$$MR = \frac{M_t - M_e}{M_0 - M_e} \quad (1)$$

Where M_t is MC of the sample (gr water/gr dry matter) at time t; M_e and M_0 are equilibrium and initial MC (gr water/gr dry matter), respectively. In equation (1), since $M_e << M_t$ and $M_e << M_0$, the value of M_e is negligible and the equation was simplified to M_t/M_0 (Arunsandeep and Chandramohan, 2018; Ceylan *et al.*, 2007; Doymaz, 2011).

Regression analysis was done using Curve Expert software (Version 1.34, Hyams, D. G., Microsoft Corporation) to evaluate equations parameters. Mean square error (MSE), root mean square error (RMSE), mean absolute error (MAE), standard error (SE), and correlation coefficient (r) values were calculated using equations 2 to 6 to evaluate the accuracy of models. It is noted that the highest r-value (closer to one) and the lowest MSE, RMSE, MAE, and SE values (closer to zero) represent the best model (good fitting).

$$MSE = \frac{\sum_{i=1}^{N}(O_i - T_i)^2}{N} \quad (2)$$

$$RMSE = \sqrt{\frac{\sum_{i=1}^{N}(O_i - T_i)^2}{N}} \quad (3)$$

$$MAE = \frac{1}{N}\sum_{i=1}^{N}|O_i - T_i| \quad (4)$$

$$SE = \frac{\sigma}{\sqrt{N}} \quad (5)$$

$$r = \sqrt{1 - \frac{\sum_{i=1}^{N}[O_i - T_i]^2}{\sum_{i=1}^{N}[O_i - T_m]^2}} \quad (6)$$

Where O_i is the i^{th} actual value, T_i is the i^{th} predicted value, N is the number of data, σ is the standard deviation, and T_m is given by:

$$T_m = \frac{\sum_{i=1}^{N} O_i}{N} \quad (7)$$

Calculation of Moisture Diffusivity (D_{eff})

Drying of food products occurs in two periods of constant and falling rates and drying of them is controlled by internal diffusion phenomenon. Fick's second law of diffusion

can be used to describe the thin layer drying of these products at the falling rate (Sacilik, 2007). According to this law, MR for different geometries including cylinder, slab and sphere is defined as equation 8:

$$\frac{\partial MR}{\partial t} = D_{eff} \nabla^2 MR \quad (8)$$

Analytical solution of this equation for infinite slab geometry and with assuming a constant moisture distribution, one-dimensional moisture, negligible shrinkage, and negligible external resistance used to predict moisture diffusion in samples. The dimensionless MC values were calculated with the equilibrium moisture content determined by dynamic equilibrium data of samples. It is given as equation (9):

$$MR = \frac{8}{\pi^2} \sum_{n=1}^{\infty} \frac{1}{(2n+1)^2} \exp(-(2n+1)^2 \frac{\pi^2 D_{eff} t}{4L^2}) \quad (9)$$

Where t is the drying time (s), D_{eff} is the effective moisture diffusivity (m^2s^{-1}); L is half-thickness of WSSM samples which are equal to 0.25×10^{-2}, 0.5×10^{-2}, and 0.75×10^{-2} m in this study.

For long drying process period, Eq. (10) can be further simplified to:

$$MR = \frac{8}{\pi^2} \exp\left[\frac{-\pi^2 D_{eff} t}{4L^2}\right] \quad (10)$$

Hence, a logarithmic form was introduced as follows:

$$LnMR = Ln(\frac{8}{\pi^2}) - \frac{\pi^2 D_{eff} t}{4L^2} \quad (11)$$

The D_{eff} was calculated through Eq. (11) by using the method of slopes. From Eq. 12, a plot of experimental drying data in terms of lnMR versus time gives a straight line with a slope (K) of:

$$Slope(K) = -\frac{\pi^2 D_{eff}}{4L^2} \quad (12)$$

Color measurement

WSSM chromaticity was measured before and after drying in CIE lab system using the digital imaging method cited in the literature. CIE lab color parameters of L*, a* and b* represent darkness-lightness (0-100), color of greenness (-a*) to redness (+a*), and color of blueness (-b*) to yellowness (+b*), respectively (Salehi, 2019b). Therefore, the fresh and dried WSSM of each experiment were placed on the scanner surface and samples photos (RGB signals) were obtained (Hp Scanjet 300). Then, the taken photos from dried WSSM were loaded to a computer, and L*, a* and, b* indexes values were measured via ImageJ (1.42e, USA) software.

Another color parameter that was calculated is color changes index (ΔE) which was calculated by total color difference as follow:

$$\Delta E = \sqrt{(\Delta L^*)^2 + (\Delta a^*)^2 + (\Delta b^*)^2} \quad (13)$$

Where ΔL is L_2-L_1, Δa is a_2-a_1 and Δb is b_2-b_1.

Statistical analysis

The experimental data were subjected to an analysis of variance (ANOVA) for a completely random design using a statistical analysis system (SAS 9.1, 2003, Institute, Inc.). Significant difference between data means was determined using Duncan's multiple range test at P-value<0.05 and it was performed to establish the impact of IR radiation power (150, 250, and 375 W), the distance of the sample from lamp (4, 8 and, 12 cm), mucilage thickness (0.5, 1 and 1.5 cm) on drying time of WSSM (P-value<0.05). All measurements were conducted in triplicate.

Results and Discussion

Drying time

Statistical analysis of experimental results (data) demonstrated that the IR power, samples distance and mucilage thickness have a significant effect on the evolution of drying time of WSSM (p<0.01) (Table 1). In conclusion, experimental results showed that the infrared power, mucilage distance, mucilage thickness, infrared power × mucilage distance, infrared power × thickness, and mucilage distance × mucilage thickness, have significant effects on the drying time of WSSM. The interaction effects of IR lamp power, and mucilage distance, IR lamp power, and mucilage thickness, and mucilage distance and mucilage thickness on the drying time of WSSM are shown in Figure 2.

Table 1- Results of analysis of variance for drying time parameters of wild sage seed mucilage drying

Sources of changes	Degrees of freedom	Sum of squares	Mean square	P
Power	2	174988	87494	0.000
Distance	2	109956	54978	0.000
Thickness	2	189562	94781	0.000
Power × Distance	4	6611	1653	0.006
Power × Thickness	4	24752	6188	0.000
Distance × Thickness	4	24980	6245	0.000
Power × Distance × Thickness	8	3031	379	0.490
Error	54	21698	402	
Total	80			

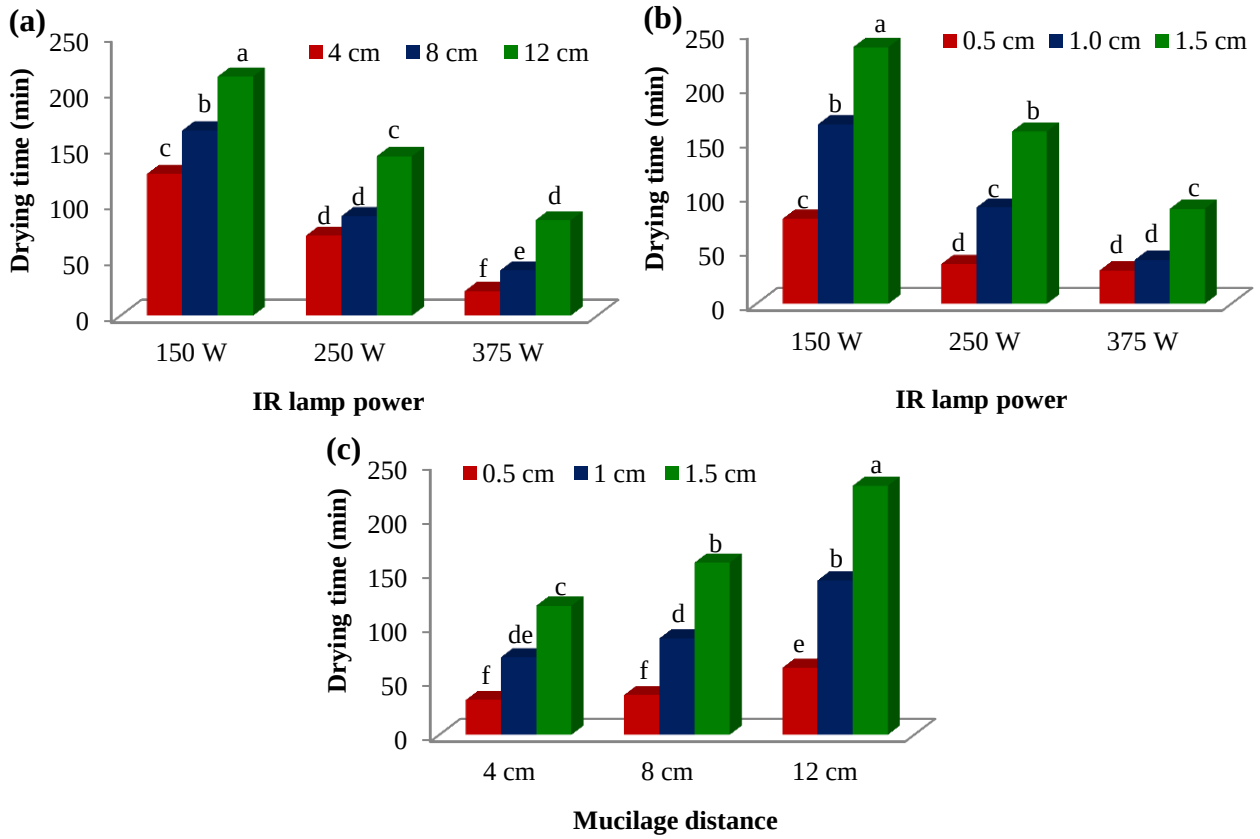

Fig.2. The interaction effects of IR lamp power and mucilage distance (a), IR lamp power and mucilage thickness (b), and mucilage distance and mucilage thickness (c) on the drying time of wild sage seed mucilage. Means with different superscripts differ significantly ($P<0.05$).

As expected, drying time was decreased by increasing the power because of increased temperature and heat transfer gradient between air and samples. The average drying times of WSSM were 172.04, 104.26, and 58.93 min at 150, 250 and 375 W, respectively. In addition, the drying time of WSSM was increased by increasing the distance of mucilage from the lamp surface and mucilage thickness. The average drying time reduced from 160.81 min to 72.03 min and from 173.67 min to 55.59 min when the mucilage distance and mucilage thickness were decreased from 12 to 4 cm, and from 1.5 to 0.5 cm, respectively.

The effects of IR power, samples distance and mucilage thickness on the MC of WSSM are shown in Figure 3. MC of WSSM was decreased with increasing the power because of the increasing temperature and heat transfer gradient between the air and samples. With

increasing IR intensity, due to the increase in mucilage temperature and increasing evaporation rate and the decrease in drying time, the specific energy for drying of WSSM decreases.

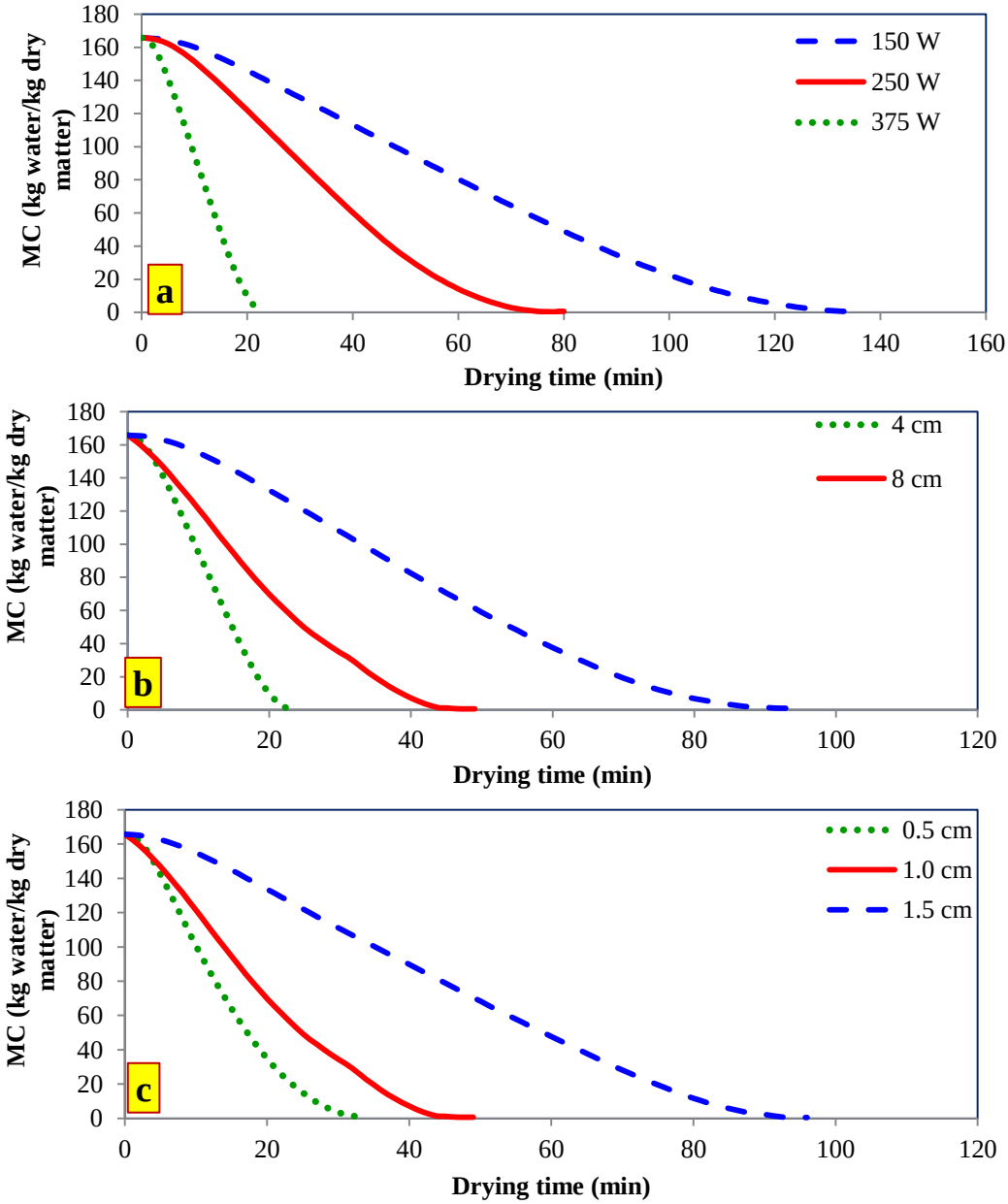

Fig.3. Variations of moisture content (MC) with drying time of wild sage seed mucilage at different: a) IR power (4 cm distance and 1.0 cm thickness); b) Sample distance (375W and 1.0 cm thickness); c) Sample thickness (375W and 8 cm distance).

Fitting of the Drying Curves

To estimate the drying kinetics of food products, numerous empirical models have been used by researchers. In this study, 7 thin-layer equations were selected and fitted to experimental data to choose the best and most suitable equation. The model with the highest r value and the lowest MSE, RMSE, MAE, and SE values was selected as the best suitable model describing the IR drying processes of WSSM. The model that satisfied these features was the Page model (Eq. 14):

$$MR = exp\ (-kt^n) \quad (14)$$

Where MR and t are moisture ratio and drying time, respectively. The estimated parameters (fitting data) of the Page model including drying constants, k, and n, are tabulated in Table 2 along with corresponding statistical data (MSE, RMSE, MAE, SE and r) for all experiments conditions. The values of MSE, RMSE and MAE for all experiments were in the ranges of 0.1×10^{-3}-1.1×10^{-3}, 1.04×10^{-2}-3.25×10^{-2} and 8.7×10^{-3}-27.1×10^{-3}, respectively. Also, the values of r and SE for all experiments were in the ranges of 0.995-0.999 and 0.010-0.031, respectively.

Figure 4 shows the comparison of fitted MR data by Page model with experimental results (375 W, 4 cm distance, and 1.0 cm thickness). These results indicate that Page model is appropriate in describing the drying characteristics of WSSM under the various IR drying conditions.

Table 2- Model constants of Page model for all experiments

Power (W)	Distance (cm)	Thickness (cm)	k	n	MSE	RMSE	MAE	SE	r
150	4	0.5	0.00097	1.918	0.00074	0.0272	0.0234	0.027	0.996
150	4	1.0	0.00047	1.805	0.00044	0.0210	0.0177	0.021	0.997
150	4	1.5	0.00031	1.784	0.00039	0.0197	0.0159	0.019	0.998
150	8	0.5	0.00099	1.829	0.00055	0.0235	0.0206	0.023	0.997
150	8	1.0	0.00031	1.765	0.00094	0.0307	0.0250	0.029	0.995
150	8	1.5	0.00025	1.702	0.00059	0.0243	0.0207	0.024	0.997
150	12	0.5	0.00048	1.788	0.00051	0.0226	0.0198	0.022	0.997
150	12	1.0	0.00028	1.701	0.00106	0.0325	0.0271	0.031	0.995
150	12	1.5	0.00024	1.592	0.00057	0.0239	0.0214	0.023	0.997
250	4	0.5	0.00446	1.898	0.00026	0.0162	0.0143	0.016	0.998
250	4	1.0	0.00099	1.890	0.00027	0.0165	0.0140	0.015	0.998
250	4	1.5	0.00068	1.727	0.00057	0.0239	0.0189	0.021	0.998
250	8	0.5	0.00286	1.937	0.00047	0.0217	0.0191	0.023	0.998
250	8	1.0	0.00052	1.922	0.00054	0.0233	0.0199	0.023	0.997
250	8	1.5	0.00068	1.641	0.00040	0.0201	0.0148	0.017	0.998
250	12	0.5	0.00185	1.782	0.00050	0.0224	0.0199	0.022	0.997
250	12	1.0	0.00042	1.798	0.00045	0.0211	0.0187	0.020	0.998
250	12	1.5	0.00038	1.644	0.00025	0.0158	0.0109	0.013	0.999
375	4	0.5	0.01189	2.109	0.00018	0.0134	0.0105	0.015	0.999
375	4	1.0	0.00479	2.073	0.00043	0.0208	0.0172	0.022	0.998
375	4	1.5	0.00185	2.051	0.00061	0.0247	0.0205	0.025	0.997
375	8	0.5	0.00932	1.718	0.00011	0.0104	0.0087	0.010	0.999
375	8	1.0	0.00836	1.555	0.00038	0.0195	0.0158	0.018	0.998
375	8	1.5	0.00081	1.809	0.00070	0.0264	0.0226	0.025	0.996
375	12	0.5	0.00247	1.799	0.00024	0.0156	0.0140	0.015	0.999
375	12	1.0	0.00073	1.872	0.00034	0.0186	0.0163	0.018	0.998
375	12	1.5	0.00059	1.662	0.00035	0.0187	0.0138	0.015	0.999

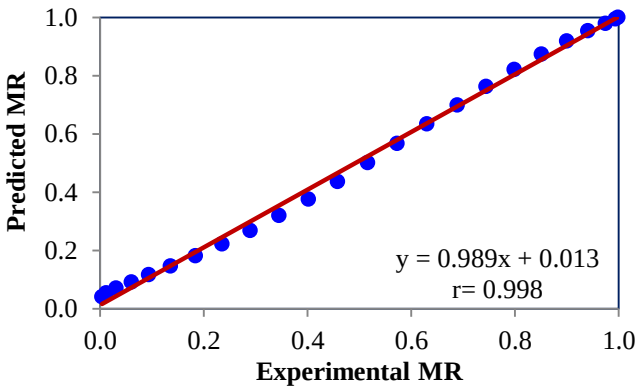

Fig.4. Comparison of fitted data by Page model with experimental results (375 W, 4 cm distance and 1.0 cm thickness).

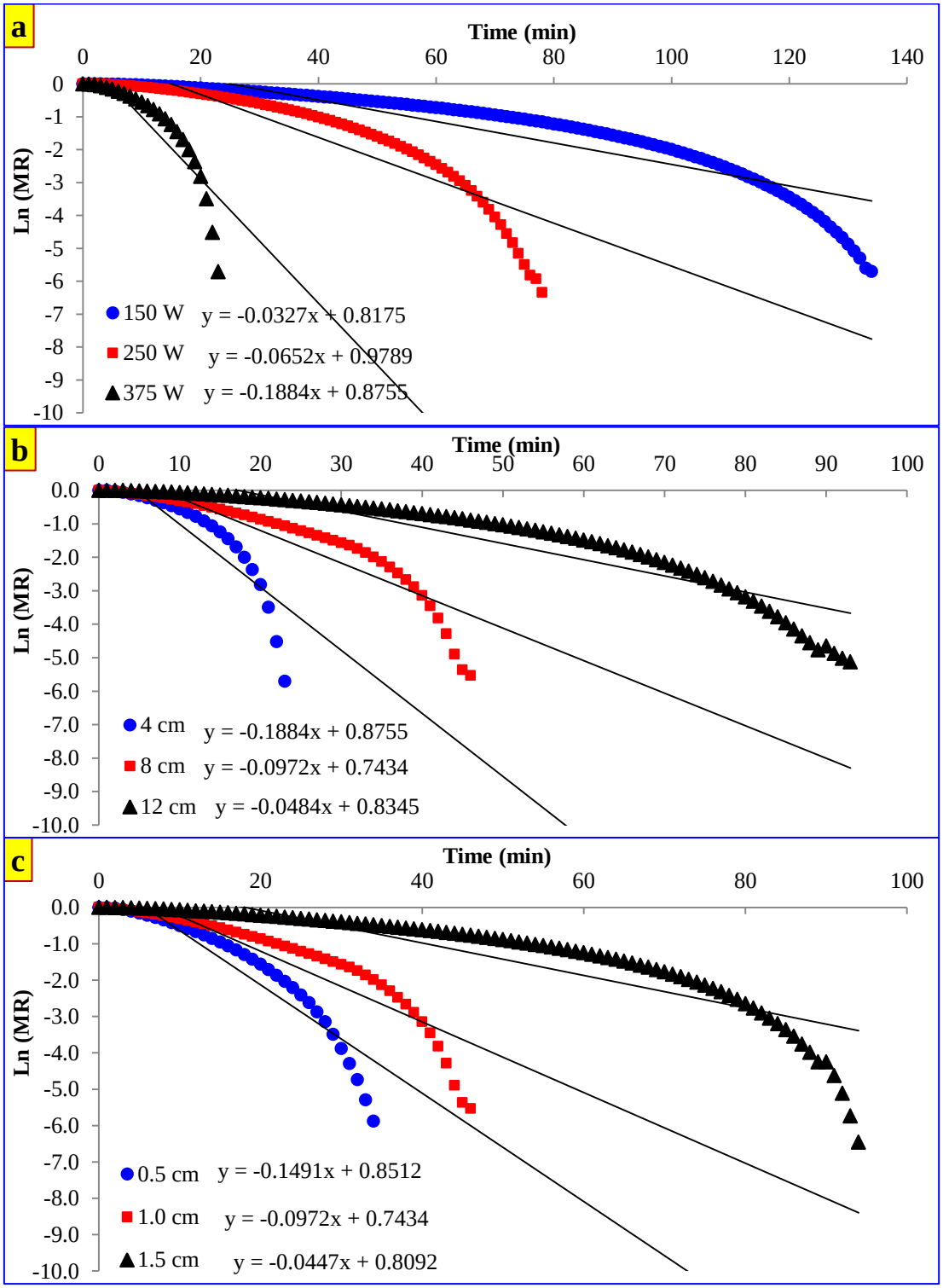

Fig.5. Variations of the Ln (MR) with drying time of wild sage seed mucilage at different: a) IR power (4 cm distance and 1.0 cm thickness); b) Sample distance (375W and 1.0 cm thickness); c) Sample thickness (375W and 8 cm distance).

Moisture Diffusivity

The effect of IR drying systems on the D_{eff} of some fruits and vegetables was studied by Salehi (2020a). The D_{eff} values lie within in range of 10^{-8} to 10^{-10} m^2s^{-1} for fruits and vegetables. The D_{eff} values are determined by plotting experimental drying data in terms of lnMR versus time. The effects of IR radiation power, samples distance, and mucilage thickness on the lnMR are shown in Figure 5. The values of D_{eff} at different conditions drying of WSSM obtained by using Eq. (19) and estimated values are shown in Table 3. The D_{eff} values of WSSM were ranged from 1.31×10^{-9} and 41.5×10^{-9} m^2s^{-1}. D_{eff} values increased with increasing IR radiation power because of the rapid movement of water at high temperatures (Doymaz, 2011).

Table 3- Effective moisture diffusivity values (D_{eff}) of wild sage seed mucilage at different IR drying conditions

Power (W)	Distance (cm)	Thickness (cm)	Effective diffusivity (m^2s^{-1})	r
150	4	0.5	2.57×10^{-9}	0.902
150	4	1.0	5.56×10^{-9}	0.909
150	4	1.5	9.5×10^{-9}	0.911
150	8	0.5	2.32×10^{-9}	0.923
150	8	1.0	4.52×10^{-9}	0.899
150	8	1.5	6.86×10^{-9}	0.900
150	12	0.5	1.31×10^{-9}	0.937
150	12	1.0	4.06×10^{-9}	0.882
150	12	1.5	4.82×10^{-9}	0.944
250	4	0.5	5.49×10^{-9}	0.951
250	4	1.0	1.09×10^{-8}	0.909
250	4	1.5	1.35×10^{-8}	0.866
250	8	0.5	5.52×10^{-9}	0.917
250	8	1.0	8.59×10^{-9}	0.882
250	8	1.5	9.83×10^{-9}	0.878
250	12	0.5	2.62×10^{-9}	0.925
250	12	1.0	5.81×10^{-9}	0.913
250	12	1.5	6.58×10^{-9}	0.917
375	4	0.5	9.32×10^{-9}	0.931
375	4	1.0	3.14×10^{-8}	0.877
375	4	1.5	4.15×10^{-8}	0.880
375	8	0.5	6.21×10^{-9}	0.937
375	8	1.0	1.59×10^{-8}	0.920
375	8	1.5	1.66×10^{-8}	0.889
375	12	0.5	3.4×10^{-9}	0.942
375	12	1.0	8.07×10^{-9}	0.924
375	12	1.5	9.74×10^{-9}	0.913

The average D_{eff} values increased with increasing mucilage thickness and they were equal to 4.31×10^{-9}, 10.5×10^{-9} and 13.2×10^{-9} m^2s^{-1} for 0.5, 1.0 and 1.5 cm thickness of mucilage, respectively. In addition, the average D_{eff} values decreased from 14.4×10^{-9} to 5.16×10^{-9} m^2s^{-1} with increasing distance of mucilage from 4 to 12 cm.

The values of D_{eff} are comparable with the reported values of 1.00×10^{-8} to 3.72×10^{-8} m^2s^{-1} for dried quince in the IR system (Mehrnia *et al.*, 2017) and 0.87×10^{-9} to 2.64×10^{-9} m^2s^{-1} for dried pomegranate arils in the IR system (Briki *et al.*, 2019). These values are consistent with the present estimated D_{eff} values for WSSM. The results of such fitting gave an average regression coefficient of 0.91 indicating that the quality of such fitting was satisfactory.

Color measurement

The quality attributes of WSSM during IR drying at various conditions as measured by the changes in color parameters of L*, a*, b* and, ΔE are shown in Table 4. The fresh WSSM exhibited a light color, with L_1*, a_1*

and, b_1* equal to 87.69, -0.11 and, -0.90, respectively. The IR radiation power was found to have a significant effect on the color of WSSM. The rise in power has a negative effect on the ΔE and with increasing in IR radiation power from 150 to 375 W, it was increased from 16.05 to 17.59. As shown in Table 4, the L^* values varied from 85.82 to 87.01 at various drying conditions. The rise in power has a positive effect on the b^* index and with increasing in IR power from 150 to 375 W, it was increased from 13.65 to 16.35. Onwude *et al.* (2018) reported similar changes in the color values of sweet potatoes undergoing IR drying.

Table 4- Color parameters results of IR dried wild sage seed mucilage.

Power (W)	Distance (cm)	Thickness (cm)	L^*	a^*	b^*	ΔE
150	4	0.5	96.67±0.69	-1.28±0.14	7.33±0.66	12.24
150	4	1.0	83.13±0.86	1.38±0.16	19.63±0.91	21.08
150	4	1.5	80.25±0.75	1.68±0.08	18.70±0.27	21.04
150	8	0.5	94.98±0.31	-0.47±0.06	4.71±0.52	9.20
150	8	1.0	85.67±0.33	1.24±0.10	12.98±0.33	14.09
150	8	1.5	80.63±0.26	1.78±0.10	16.90±0.19	19.24
150	12	0.5	92.98±0.79	-0.34±0.13	9.75±0.13	11.89
150	12	1.0	87.88±0.22	0.14±0.06	9.81±0.64	10.72
150	12	1.5	80.93±0.14	1.58±0.16	23.03±0.59	24.92
250	4	0.5	89.82±1.34	-0.60±0.16	15.69±2.11	16.73
250	4	1.0	85.92±0.89	0.61±0.13	18.63±1.38	19.62
250	4	1.5	81.25±0.37	1.29±0.11	23.68±0.25	25.45
250	8	0.5	95.88±0.28	-0.70±0.06	6.00±0.69	10.72
250	8	1.0	86.02±0.70	0.41±0.08	15.70±0.44	16.69
250	8	1.5	82.20±0.30	1.69±0.04	18.84±0.35	20.57
250	12	0.5	94.47±0.19	-0.49±0.06	9.16±0.72	12.14
250	12	1.0	85.57±0.17	1.24±0.07	14.86±0.03	15.96
250	12	1.5	82.53±0.35	1.88±0.03	17.55±0.49	19.26
375	4	0.5	80.45±1.36	3.37±0.39	21.04±0.89	23.36
375	4	1.0	83.87±0.54	1.37±0.14	23.30±0.52	24.54
375	4	1.5	87.26±0.89	0.76±0.25	24.95±0.97	25.86
375	8	0.5	86.26±1.52	-0.12±0.12	10.47±0.21	11.46
375	8	1.0	86.77±1.97	-0.19±0.25	13.12±0.32	14.05
375	8	1.5	88.81±1.44	0.34±0.15	11.69±0.55	12.65
375	12	0.5	90.21±0.44	-0.21±0.09	7.21±0.39	8.50
375	12	1.0	84.89±0.85	0.41±0.05	18.34±0.22	19.45
375	12	1.5	83.85±1.00	2.07±0.18	16.99±0.41	18.42

L^* (darkness/lightness, 0 to 100), a^* (greenness/redness, -120 to 120) and b^* (blueness/yellowness, -120 to 120).

Conclusion

The IR lamp power, the distance of mucilage from lamp and, mucilage thickness influenced the drying time of WSSM. The average drying time of WSSM samples was 172.04, 104.26 and 58.93 min at 150, 250 and, 375 W, respectively. The drying characteristics were satisfactorily described by the Page model with the highest r value (greater than 0.99) and the lowest MSE, RMSE, MAE and SE values (a good fit). Values for the D_{eff} of WSSM samples were obtained in the range of 1.31×10^{-9} and, 41.5×10^{-9} m^2s^{-1} and, they were increased with increasing lamp power while decreased with increasing distance of mucilage from lamp and mucilage thickness. Color parameters were estimated in terms of L*, a* and, b* indexes and total color difference (ΔE) measurements. The increases in IR radiation power have a negative influence on ΔE and with rising in IR power from 150 to 375 W, it was increased from 16.05 to 17.59.

Conflict of Interests: Authors declare that there no conflict of interest exists.

List of symbols

ΔE	Color changes index
D_0	Pre-exponential factor (m^2s^{-1})
D_{eff}	Effective moisture diffusivity (m^2s^{-1})
k	Drying rate constants in models (s^{-1})
K	Slope

L	Half slab thickness of the samples (m)	MR	Moisture ratio
M_0	Initial MC (kg water/kg dry matter)	n	Number of constants
Me	Equilibrium MC (kg water/kg dry matter)	N	Number of observations
		r	Correlation coefficient
M_t	MC at time t (kg water/kg dry matter)	t	Drying time (min)

References

1. Akpinar, E. K., and Y. Bicer. 2005. Modeling of the drying of eggplants in thin layers. International Journal of Food Science & Technology 40: 273-281.
2. Amini, G., F. Salehi, and M. Rasouli. 2021. Drying kinetics of basil seed mucilage in an infrared dryer: Application of GA-ANN and ANFIS for the prediction of drying time and moisture ratio. Journal of Food Processing and Preservation: 45(3): e15258.
3. Arunsandeep, G., and V. P. Chandramohan. 2018. Numerical Solution for Determining the Temperature and Moisture Distributions of Rectangular, Cylindrical, and Spherical Objects During Drying. Journal of Engineering Physics and Thermophysics 91: 895-906.
4. Baeghbali, V., M. Niakousari, M. O. Ngadi, and M. Hadi Eskandari. 2019. Combined ultrasound and infrared assisted conductive hydro-drying of apple slices. Drying Technology 37: 1793-1805.
5. Briki, S., B. Zitouni, B. Bechaa, and M. Amiali. 2019. Comparison of convective and infrared heating as means of drying pomegranate arils (*Punica granatum* L.). Heat and Mass Transfer 55: 3189-3199.
6. Ceylan, I., M. Aktaş, and H. Doğan. 2007. Mathematical modeling of drying characteristics of tropical fruits. Applied Thermal Engineering 27: 1931-1936.
7. Doymaz, I. 2011. Drying of eggplant slices in thin layers at different air temperatures. Journal of Food Processing and Preservation 35: 280-289.
8. Mehrnia, M. A., A. Bashti, and F. Salehi. 2017. Experimental and modeling investigation of mass transfer during infrared drying of Quince. Iranian Food Science and Technology Research Journal 12: 758-766.
9. Nep, E. I., and B. R. Conway. 2011. Physicochemical characterization of grewia polysaccharide gum: Effect of drying method. Carbohydrate Polymers 84: 446-453.
10. Onwude, D. I., N. Hashim, K. Abdan, R. Janius, and G. Chen. 2018. Modelling the mid-infrared drying of sweet potato: kinetics, mass and heat transfer parameters, and energy consumption. Heat and Mass Transfer 54: 2917-2933.
11. Sacilik, K. 2007. Effect of drying methods on thin-layer drying characteristics of hull-less seed pumpkin (*Cucurbita pepo* L.). Journal of Food Engineering 79: 23-30.
12. Salehi, F. 2017. Rheological and physical properties and quality of the new formulation of apple cake with wild sage seed gum (*Salvia macrosiphon*). Journal of Food Measurement and Characterization 11: 2006-2012.
13. Salehi, F. 2019a. Improvement of gluten-free bread and cake properties using natural hydrocolloids: A review. Food Science & Nutrition 7: 3391-3402.
14. Salehi, F. 2019b. Color changes kinetics during deep fat frying of kohlrabi (*Brassica oleracea var. gongylodes*) slice. International Journal of Food Properties 22: 511-519.
15. Salehi, F. 2020a. Recent applications and potential of infrared dryer systems for drying various agricultural products: A review. International Journal of Fruit Science 20: 586-602.
16. Salehi, F. 2020b. Recent advances in the modeling and predicting quality parameters of fruits and vegetables during postharvest storage: A review. International Journal of Fruit Science 20: 506-520.

17. Salehi, F., and M. Kashaninejad. 2015. Effect of drying methods on rheological and textural properties, and color changes of wild sage seed gum. Journal of Food Science and Technology 52: 7361-7368.
18. Salehi, F., and M. Kashaninejad. 2017. Effect of drying methods on textural and rheological properties of basil seed gum. International Food Research Journal 24: 2090-2096.
19. Zameni, A., M. Kashaninejad, M. Aalami, and F. Salehi. 2015. Effect of thermal and freezing treatments on rheological, textural and color properties of basil seed gum. Journal of Food Science and Technology 52: 5914-5921.

نشریه ماشین‌های کشاورزی
https://jame.um.ac.ir/

مقاله پژوهشی

جلد ۱۲، شماره ۱، بهار ۱۴۰۱، ص ۷۹-۶۷

تأثیر خشک‌کردن فروسرخ بر سینتیک خشک شدن و تغییرات رنگ موسیلاژ دانه مرو

غزاله امینی[۱]، فخرالدین صالحی[۲]، مجید رسولی[۳*]

تاریخ دریافت: ۱۳۹۹/۰۹/۱۷
تاریخ پذیرش: ۱۳۹۹/۱۲/۱۲

چکیده

در این مطالعه، تأثیر پارامترهای سیستم خشک‌کن فروسرخ شامل توان فروسرخ، فاصله موسیلاژ از سطح لامپ، ضخامت موسیلاژ بر روی سینتیک خشک شدن و شاخص‌های رنگ (L*، a*، b* و ΔE) موسیلاژ دانه مرو در سیستم خشک‌کن فروسرخ بررسی شد. داده‌های آزمایشگاهی نسبت رطوبت با ۷ مدل تجربی لایه‌نازک مختلف برازش داده شد. مشخص شد که مدل پیج بهترین تناسب را برای نشان دادن رفتار سینتیکی دارد و به‌طور قابل قبولی رفتار خشک‌کردن فروسرخ موسیلاژ دانه مرو را با کمترین مقادیر میانگین خطای مربع (MSE)، جذر میانگین مربعات خطا (RMSE)، میانگین خطای مطلق (MAE) و خطای استاندارد (SE) و بیشترین مقدار ضریب همبستگی (r). مقادیر MSE، RMSE و MAE برای همه آزمایش‌ها به‌ترتیب در محدوده ۰/۰۰۱۱-۰/۰۰۰۱، ۰/۰۳۲۵-۰/۰۱۰۴ و ۰/۰۲۷۱-۰/۰۰۸۷ بود. متوسط نفوذ مؤثر رطوبت (D_{eff}) با افزایش توان لامپ از ۱۵۰ به ۳۷۵ وات از $۴/۶۱\times۱۰^{-۹}$ به $۱۵/۸\times۱۰^{-۹}$ مترمربع بر ثانیه افزایش یافت، اما با افزایش فاصله موسیلاژ از ۴ به ۱۲ سانتی‌متر و کاهش ضخامت موسیلاژ از ۱/۵ به ۰/۵ سانتی‌متر، این ضریب به‌ترتیب از $۱۴/۴\times۱۰^{-۹}$ به $۵/۱۶\times۱۰^{-۹}$ مترمربع بر ثانیه و از $۱۳/۲\times۱۰^{-۹}$ به $۴/۳۱\times۱۰^{-۹}$ مترمربع بر ثانیه کاهش یافت. افزایش توان تابش فروسرخ تأثیر مثبتی بر شاخص زردی (افزایش ۱۹/۷۸ درصدی در شاخص b*) موسیلاژ دانه مرو خشک‌شده داشت. همچنین، شاخص تغییرات رنگ (ΔE) را از ۱۶/۰۵ به ۱۷/۵۹ افزایش داد.

واژه‌های کلیدی: شاخص‌های رنگی، صمغ، مدل پیج، نسبت رطوبت، نفوذ مؤثر رطوبت

۱- دانشجوی کارشناسی ارشد، دانشکده کشاورزی، دانشگاه بوعلی سینا، همدان، ایران
۲- دانشیار، دانشکده کشاورزی، دانشگاه بوعلی سینا، همدان، ایران
۳- استادیار، دانشکده کشاورزی، دانشگاه بوعلی سینا، همدان، ایران
(*- نویسنده مسئول: Email: m.rasouli@basu.ac.ir)

DOI: 10.22067/jam.2021.67448.1002

Journal of Agricultural Machinery

Homepage: https://jame.um.ac.ir/

Full Research Paper
Vol. 12, No. 1, Spring 2022, p. 81-94

Diagnosis of Early Blight Disease in Tomato Plant based on Visible/Near-Infrared Spectroscopy and Principal Components Analysis- Artificial Neural Network Prior to Visual Disease Symptoms

F. Azadshahraki[1*], K. Sharifi[2], B. Jamshidi[3], R. Karimzadeh[4], H. Naderi[5]

1- Agricultural Engineering Research Institute, Agricultural Research, Education and Extension Organization (AREEO), Karaj, Iran
2- Assistant Professor, Research Department of Plant Pathology, Iranian Research Institute of Plant Protection, Agricultural Research, Education and Extension Organization (AREEO), Tehran, Iran
2- Agricultural Engineering Research Institute, Agricultural Research, Education and Extension Organization (AREEO), Karaj, Iran
4 Department of Physics, Shahid Beheshti University, Tehran, Iran
5- MSc. in Remote Sensing and Geographic Information System, Vanda Atlas Technologists Company, Karaj, Iran

Received: 13-12-2020
Revised: 08-01-2021
Accepted: 15-02-2021
Available Online: 28-09-2021

How to cite this article:
Azadshahraki, F., K. Sharifi, B. Jamshidi, R. Karimzadeh, and H. Naderi. 2022. Diagnosis of Early Blight Disease in Tomato Plant based on Visible/Near-Infrared Spectroscopy and Principal Components Analysis- Artificial Neural Network Prior to Visual Disease Symptoms. Journal of Agricultural Machinery 12 (1): 81-94.
DOI: 10.22067/jam.2021.67436.1001

Abstract

Early diagnosis of plant diseases before the occurrence of symptoms can reduce the loss of the yield and increase the quality of agricultural crops. It also reduces the consumption of pesticides, environmental risks, and the cost of production. For this reason, the objectives of the present study were non-destructive diagnosis of early blight of tomato plant and discrimination of the most important agents of early blight (*A. solani* and *A. alternate*) in the primary stages of incidence of the disease before appearing visual symptoms using Vis-NIR spectroscopy (400-900 nm). The spectral data were acquired from the leaves of the plants infected with *A. solani* and *A. alternate*, 48 hours, 72 hours, 96 hours, and 120 hours after inoculation. To develop the recognition model based on the spectral data, principal components analysis (PCA) coupled with artificial neural network (ANN) was used. The results showed that the PCA-ANN model could diagnose the infected plants and pathogen species with accuracy of 93-100% for test set samples. In 96 hours after inoculation, in addition to the simpler model (8 PCs and 3 neurons in hidden layer), accuracy of 100% was obtained. At all times after inoculation, there was no error in diagnosis of the plants infected with *A. solani* that is more pathogenic and aggressive than other species, from healthy plants. Early blight in tomato plant and the type of pathogen before visual symptoms, without any plant sample preparation, could be diagnosed non-destructively (with accuracy of 93-100%) using Vis-NIR (400-900 nm) spectroscopy coupled with PCA-ANN. It was concluded that this technology could be used for rapid, low-cost, and early diagnosis of this disease in tomato plant instead of time-consuming, expensive, and destructive laboratory methods.

Keywords: Early blight, NIR spectroscopy, Principal components analysis, Tomato plants

Introduction

Tomato (*Solanum lycopersicum* L.) is one of the most popular plants in the world and is grown in a wide range of climates (Song *et al.*, 2015). Tomatos are widely consumed because of its high nutritional value and are a well-known source of vitamins and minerals. They can be eaten as raw vegetables or processed products (Sigmund and Gustav, 1991; Minich *et al.*, 2019). However, diseases can affect the yield and quality of tomato fruits

(*- Corresponding Author Email: farzad_shahrekian@yahoo.com)

during the growing season (Chaerani and Voorrips, 2006).

Early blight is a serious disease in tomato growing regions and has been reported under a wide range of climatic conditions. This disease weakens tomato plants and increases susceptibility of the plants to infection (Adhikari *et al.,* 2017; Zhang *et al.,* 2018). Leaf spots and leaf drop caused by early blight, reduce the photosynthetic area and increase the imbalance between nutrient demand and nutrient supply (Ding *et al.,* 2019). Failure to control early blight at the right time leads to foliar damage, the serious losses of the yield and quality, and excessive consumption of fungicides in tomato production. Therefore, early diagnosis and control of this disease has great economic importance (Ershad, 2009; Adhikari *et al.,* 2017).

Species of the genus *Alternaria* causes early blight in tomato plants. *Alternaria solani* and *A. alternata* are the most important pathogenic species of the genus *Alternaria* in many countries such as Iran (Ershad, 2009; Zhang *et al.,* 2018). These two species are different in terms of the secreted enzymes involved in pathogenesis. Morphologically, *A. alternata* produces small spores and *A. solani* produces larger spores than those because of *A. alternata*. In tomato plants, pathogenicity of *A. alternata* is lower than that of *A. solani* (Simmons, 2000).

Because of climatic conditions of tomato cultivation, high humidity and moderate temperatures may spread early blight, especially in the southern and northern regions of Iran (Ershad, 2009; Babagoli and Behdad, 2012). As mentioned above, different chemical fungicides are used to control early blight. Early diagnosis of this disease can reduce the consumption of fungicides. On the other hand, identifying the disease before its incidence allows the application of biological fungicides to prevent the spreading of the disease agents (Zitter *et al.,* 2004).

Plant diseases, are usually diagnosed by visual assessments or common laboratory methods. Common diagnostic techniques such as polymerase chain reaction (PCR), enzyme linked immune sorbent assay (ELISA), and fluorescence in situ hybridization (FISH) are destructive, time-consuming, and expensive. In addition, such diagnostic techniques require highly skilled technicians and advanced equipment (Xie *et al.,* 2015; Ghanei Ghooshkhaneh, 2018).

Some non-destructive methods have been used to classify, forecast, diagnose or warn the occurrence of crop diseases, and various models have been developed for these non-destructive techniques. Near-infrared (NIR) spectroscopy as an advanced and innovative technology utilizes the spectral range from 780 to 2,500 nm (12,800 cm^{-1}– 4,000 cm^{-1}) and provides internal structural information of organic materials in food, pharmaceutical, chemical, and petrochemical industries (Cen and He, 2007; Jamshidi *et al.,* 2015). This technology coupled with the advanced mathematical and statistical methods has become a reliable, fast, and powerful non-destructive tool for analyzing the internal properties of organic materials (Tey *et al.,* 2013; Nicolai *et al.,* 2014).

NIR spectroscopy equipment (with a full spectral range) is expensive and its use in rapid detection systems depends on economic feasibility. The equipment with a narrower spectral range such as visible/near-infrared (Vis-NIR) spectroscopy equipment are low cost and more economically feasible for use in rapid and on-line detection systems (Mouazen *et al.,* 2005). Some studies have confirmed the fitness of Vis-NIR or NIR spectroscopy for the classification of the leaves infected with citrus canker (Sankaran and Ehsani, 2013), diagnosis of the avocado leaves infected with laurel wilt (Sankaran and Ehsani, 2012), diagnosis of virus-infected soybean (Jinendra *et al.,* 2010), diagnosis of huanglongbing in citrus orchards (Sankaran *et al.,* 2011), and prediction of disease ratings for leaf gall in sugarcane clones (Purcell *et al.,* 2009). However, relatively few reports have been found about the non-destructive diagnosis of crop diseases before the onset of symptoms. No reports have been found about the non-destructive diagnosis of

early blight on tomato plants before appearing visual symptoms using Vis-NIR or NIR spectroscopy.

This research aimed to evaluate the feasibility of non-destructive method of Vis-NIR spectroscopy for diagnosis of early blight diseases (*A. solani* and *A. alternate*, as the main agents in tomato plants in Iran) in the primary stages of the disease incidence before occurrence of visual symptoms. Moreover, different PCA-ANN models were also developed for different times of establishment and progression of pathogens to select optimum diagnosis models for diagnosing the disease and discrimination of pathogen type.

Material and Methods

Pathogenicity on tomato plants

Susceptible tomato seedlings (cv. Peto Early CH), planted in trays containing peat moss, were transferred to 1.5-liter pots in four-leaf stage. Ten milliliters of spore suspension of each of isolates of *A. solani* and *A. alternata* were prepared with sterile distilled water. Using a hemocytometer, the concentration of the suspensions was adjusted to 10^5 and 10^6 conidia per milliliter for *A. solani* and *A. alternate*, respectively,. Spores were suspended in sterile distilled water. Plants were inoculated with conidia suspensions one month after transplanting. Each plant was inoculated again after 24 hours. The control treatment leaflets were sprayed with sterile distilled water. The inoculated plants were incubated at 20-22°C and 95% relative humidity (Rotem, 1994; Fulton *et al.*, 1995). Figures 1(a) and 1(b) show the symptoms of the disease in the leaves inoculated with *A. alternata* and *A. solani* 10 to 12 days after inoculation.

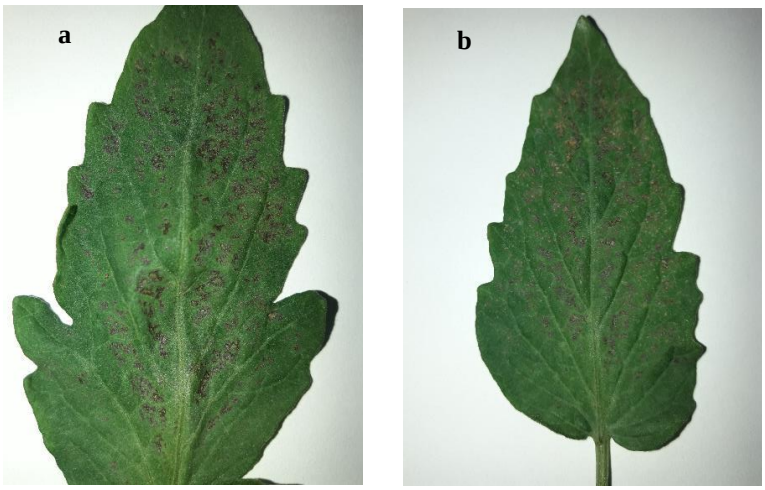

Fig.1. Symptoms of the disease in *A. solani*–inoculated leaf (a) and *A. alternata*–inoculated leaf (b) 10 to 12 days after inoculation.

Spectral data collection

Spectroscopy System

The Vis-NIR spectral data of tomato leaves were acquired using a V700 UV-Vis-NIR spectrophotometer (OPTC, Co., Iran) equipped with a CCD sensor (Toshiba, Ltd., Japan) that can operate in the spectral range of 350-1,100 nm at the resolution of 1.8 nm. The light source was a 120W tungsten halogen lamp and the spectroscopy mode was reflectance one. Two optical fibers, which had a 45-degree angle with the leaf sample, were used to guide the light from the source to the leaf and from the leaf to the spectrophotometer.

Samples and Spectroscopy times

Collecting the spectral data was performed at four times after inoculation, including two days (48 hours), three days (72 hours), four days (96 hours), and five days (120 hours) after inoculation. Occurrence of symptoms of

early blight on tomato plants depends on many factors and under the best condition; the symptom is visualized for five to seven days after conidia establishment on the leaves (Sherf and MacNab 1986; Chaerani *et al.,* 2007).

The lower and upper leaves of each plant were excluded from the experiment. For each pathogenic species, the spectral data were acquired from 50 leaves of the infected plants (from 4-6 plants), in each day after inoculation. On the fifth day (120 hours after inoculation), five spectral samples of the leaves infected with *A. solani* were lost because of incorrect spectra collection, and the total number of the samples infected with *A. solani* in this day was 45. In each day of spectroscopy, along with acquiring the spectra from the inoculated samples, the spectral data from the leaves of two healthy plants (control treatment) were also acquired (approximately 23 leaves per day). In total, the number of spectral samples of healthy leaves was 91. Therefore, the total number of samples on each of the second, third, and fourth days after inoculation was 191, and in the fifth day was 186. For each leaf sample, five measurements from five different points were obtained. The average of these five spectra was used as a representative spectrum for one leaf sample.

PCA-ANN models

In this experiment, the ANN method was used for the classification of *A. alternate*-inoculated, *A. solani*-inoculated, and healthy leaves. An ANN is a non-linear computing model inspired by biological neural networks (Salchenberger *et al.,* 1992; Kia, 2010; Castro *et al.,* 2017). ANNs modeling technique have been widely used for prediction and classification based on the spectral data (Mireei *et al.,* 2010; Pan *et al.,* 2016; Dai *et al.,* 2015; Yoplac *et al.,* 2019).

Multilayer feed forward network with back-propagation (BP) learning algorithm, which is the most popular neural network, was used for the recognition of the leaf samples. One BP network is a feed forward multilayer perceptron network that consists of one input layer with the neurons as independent variables, one or more hidden layers, and one output layer with the neurons as a dependent variable (leaf classes in this study) (Kia, 2010; Omid *et al.,* 2010). In this study, a single-hidden layer ANN was established for classification. The transfer function was tansig, the training function was trainscg, and epoch was 1,000. Wavelengths shorter than 400 and longer than 900 nm were eliminated to reduce the noise and thus, the spectral range of 400 to 900 nm was used for developing the model.

The spectral data in the range of 400-900 nm was used as the input layer in ANN, but they were not directly used because of the large number of the data for each spectrum sample. In order to reduce the data in each spectrum, PCA was used. PCA is a well-known technique for the data mining and is commonly used in spectroscopy (Wold *et al.,* 2101). PCA is an orthogonal linear transformation that transforms the spectral data to a new coordinate system whose axes are the PCs. In this transformation, the greatest variance of the data comes to lie on the first coordinate (called the first principal component), the second greatest variation on the second PC, and so on. This process continues until the cumulative variance of the principal components is equal to 100% of the variance of the original data. In PCA, the data components that have the greatest effect on the variance, are selected and can be used instead of the original data and reduce the data volume (Nicolai *et al.,* 2007). It is clear that the first component, then the second component, and the subsequent components have the greatest impact on recognition, respectively. The optimum number of PCs in the PCA-ANN models was chosen based on the cumulative explained data variance (Brown *et al.,* 2005).

For the classification of the leaves in each day based on PCs, the samples were divided into a training (70%), validation (15%), and test (15%) subsets, randomly. The training datasets were used to fit the model, and the validation datasets were used to stop the training ones and avoid overfitting when the error in the validation datasets increases. The

test datasets were used to evaluate the model fitted at the training stage. In this paper, the developed models were also evaluated by training and validation subsets, in addition to evaluation by test subset.

The optimum number of neurons in the hidden layer was determined by trial and error and examining several networks with the different number of neurons in the hidden layer, and finding the optimum model. A 3-byte binary code was assumed for the output vectors of three output neurons (Kia, 2010; Omid *et al.*, 2010). Therefore, the output vectors (100), (010), and (001) were denoted as the healthy leaf, *A. alternate*-inoculated leaf, and *A. solani*-inoculated leaf, respectively.

In the PCA-ANN models, of the variance explained by PCs should be at least 85% of variance of the original data (Mireei *et al.*, 2010). The models with the lower number of PCs have lower classification accuracy, while using the higher number of PCs makes more complex models without a significant difference in the discrimination power (Nicolai *et al.*, 2007). In this study, the maximum number of PCs as the input for ANN was considered 10. Finally, the optimum number of PCs as the input for ANN was selected by trial and error. These PCs were selected instead of the original spectral data.

For each time after inoculation (48 hours, 72 hours, 96 hours, and 120 hours), one PCA-ANN model was developed to discriminate healthy, *A.* -infected and *A. solani* -infected leaves. In this paper, principal components analysis and BP-ANN were carried out using Matlab12.

The procedure of this study is shown in Figure 2.

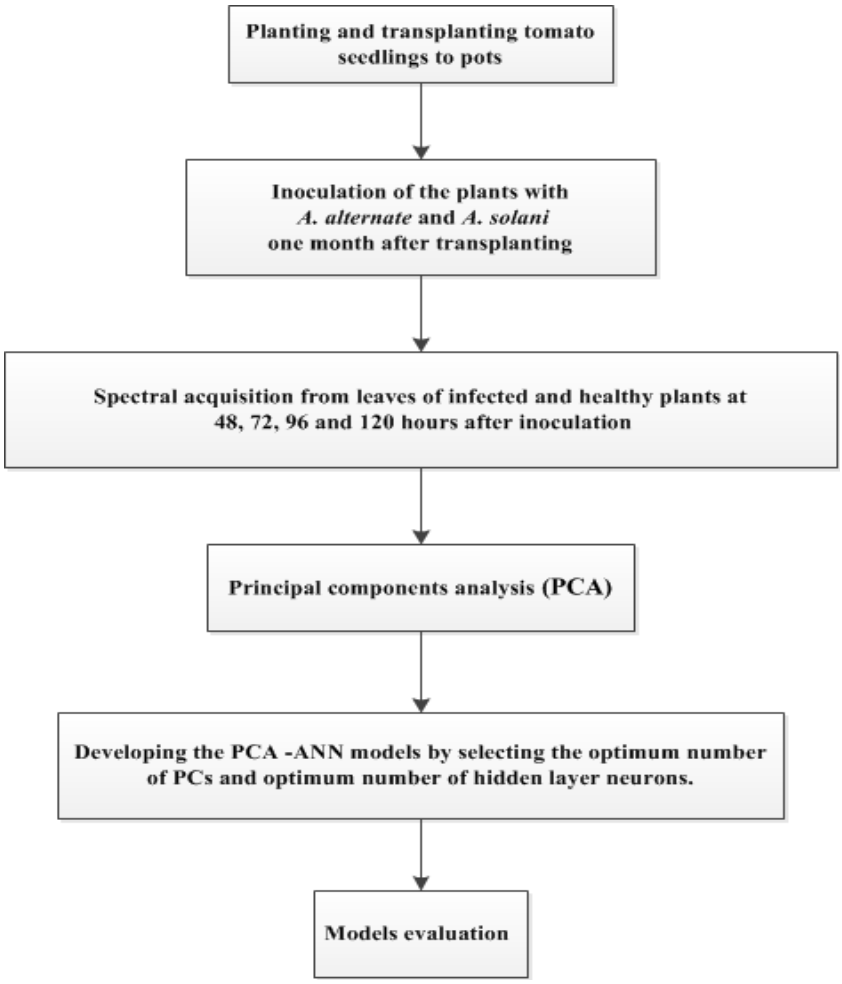

Fig.2. Research procedure

Results and Discussion

Effect of early blight pathogens and time on the absorbance spectra

Figures 3(a), (b), (c), and (d) show the mean absorbance spectrum of healthy, *A. alternata*–inoculated, and *A. solani*-inoculated leaves in 48 hours, 72 hours, 96 hours, and 120 hours after inoculation at the wavelength range of 400-900 nm, respectively. For the better interpretation of spectra, absorbance values (Log (1/R)) of spectra are shown instead of raw spectra in Figure 2 (Azadshahraki *et al.*, 2018).

All spectra had two broad peaks around 470 nm and 680 nm, which were due to the chlorophyll of the photosystem I and II reaction centers (Taiz and Zeiger, 2002). In 48 hours and 72 hours after inoculation, the mean absorbance spectra were clearly very similar. As mentioned above, spores of *A. solani* are larger than those of *A. alternate.* In 48 hours after inoculation, the absorption (height of spectrum) of *A. solani* samples was lower than that of other samples and this might have been due to the greater light reflection because of large spores. Over time, as the spores multiply and grow, the reaction between spores and leaves increases, and the light absorption (height of the spectrum) increases in both species of diseases. At other times after inoculation (96 hours and 120 hours after inoculation), absorbance spectra of the inoculated leaves changed and the shape of the second peaks was quite different from that of the second peaks of spectra in the second and third day after inoculation. The height of the mean absorbance spectra of the inoculated leaves was increased in the fourth and fifth days after inoculation, and these means were higher than the mean absorbance spectrum of healthy leaves. These changes in the spectra of the infected leaves and the differences between the spectra of the infected and healthy leaves in fourth and fifth days could be due to the impact of diseases on the leaves and might have been effective in discriminating the infected leaves. The absorption increment in spectra of both *A. alternata*–infected and *A. Solani*–infected leaves in 96 hours and 120 hours after inoculation indicated that early blight disease increased the absorption of chlorophyll over time, and this increment around 470 nm was more than around 680 nm. In general, the height changes in *A. solani*-infected spectrum was more than that in *A. alternate*-infected spectrum. Because the pathogen (*Alternaria* spp.) is a necrotrophic fungus, within 48 to 72 hours after inoculation, it is possible that the fungal spores could be plasmolyzed and the contents of them could be transferred to the host cells. The reduction in the spore volume caused in order that the spectrum of the inoculated leaves could be closer to the control treatment leaves. However, 72 hours after inoculation, the intracellular host changes were begun, and the spectrum absorption increased in the infected leaves. Research has shown that members of the genus *Alternaria* cause quiescent infections, in which the fungus enters the tissue where it remains dormant until changed conditions favor infection (Thomma, 2003).

Diagnosis of healthy and infected plants at each time after inoculation

Tables 1, 2, 3, and 4 show the results of the classification of training, validation and test sample sets of healthy, *A. alternate*-infected, and *A. solani*-infected leaves of tomato plants for 48 hours, 72 hours, 96 hours, and 120 hours after inoculation using Vis-NIR spectroscopy (400-900 nm) and the PCA-ANN model. According to these Tables, the optimum developed PCA-ANN model for each time after inoculation had the specific number of PCs as well as neurons in the hidden layer. All selected PCs could explain more than 99% of the variance of the original data and had high power of discriminating the infected leaves. In the second and third day after inoculation, the models were more complex (had more PCs and more hidden layer neurons).

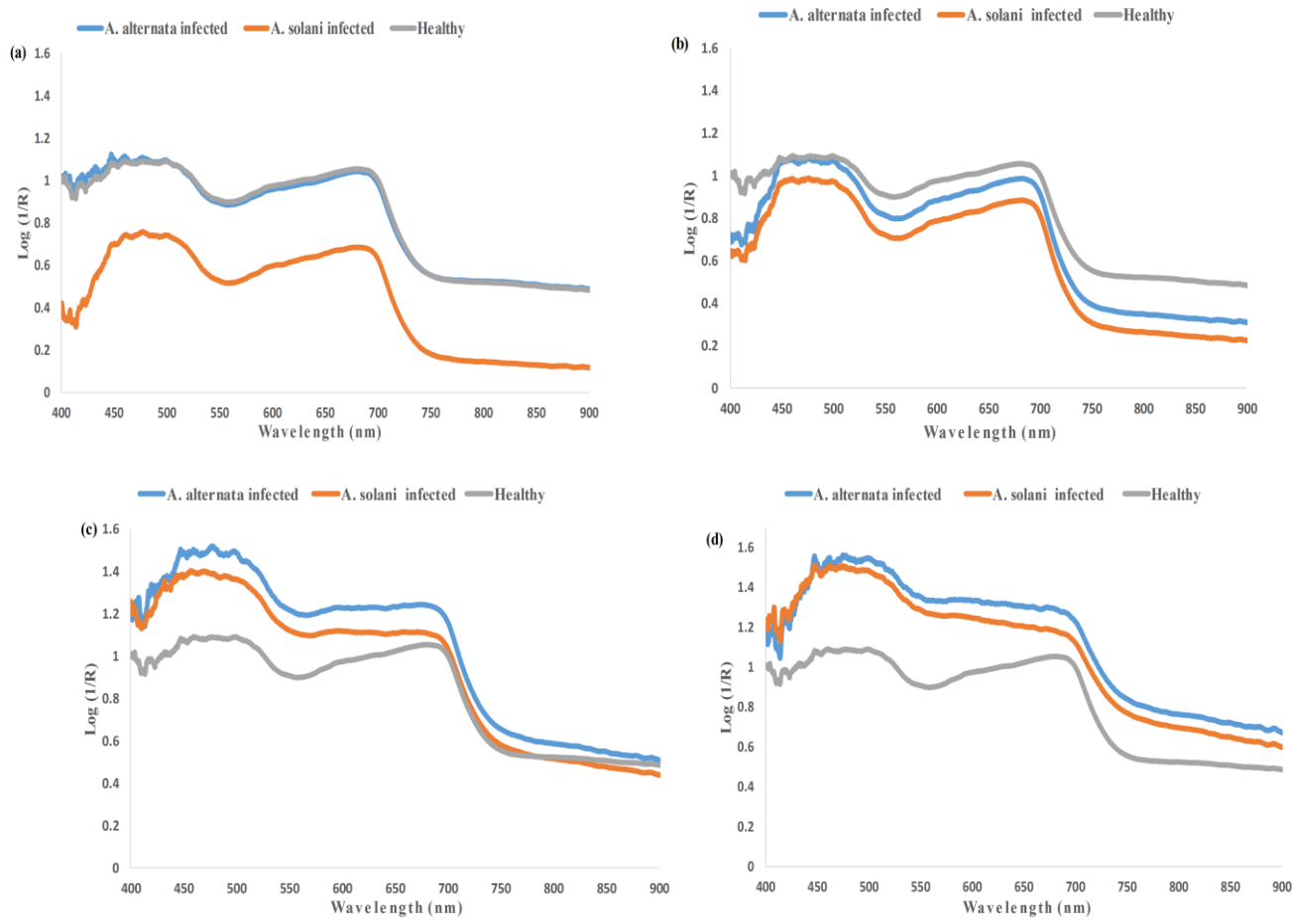

Fig.3. The mean absorbance spectrum (Log (1/R)) of healthy, *A. alternata*–inoculated, and *A. solani*-inoculated leaves of tomato plants in 48 hours (a), 72 hours (b), 96 hours (c), and 120 hours (d) after inoculation

As mentioned above, with the impact of pathogens on the inoculated leaves and deformation of their absorbance spectra over time, fewer PCs were needed to develop the best model. At all times after inoculation, the developed models were able to accurately discriminate healthy, *A. alternate*-infected, and *A. solani*-infected leaves from each other. In 48 hours, 72 hours, and 120 hours after inoculation, the discrimination accuracy were 98.5%, 99.2%, and 98.5% for training sample sets and 96.6%, 100%, and 100% for validation sample sets. These models were used for diagnosis of test sample sets, and accuracy of 100%, 93.1%, and 96.4% were obtained. In 96 hours after inoculation, the discrimination accuracy for all subsets was 100%. In other words, Vis-NIR spectroscopy with the developed PCA-ANN models could diagnose early blight-infected leaves and the type of pathogen at the accuracy of 93. 1%-100% of test samples in the early stages of disease before visual symptoms. The lowest accuracy in the test samples was related to 72 hours after inoculation, which the absorbance spectra of healthy samples and both infected samples were more similar. For all samples, discrimination accuracies were 98.4%, 98.4%, 100%, and 98.4% in the second, third, fourth, and fifth days after inoculation, respectively. The results showed that at all times after inoculation and in all subset samples, there was no error in the discrimination of the leaves infected with *A. solani* pathogen (which is

more pathogenic and more damaging in tomato plants) and healthy leaves.

Occurrence of symptom of early blight disease in tomato plants depends on many factors, including temperature, relative humidity, and host sensitivity. Two days after infection, *Alternaria conidia* penetrates the cells by producing germ tube. After penetration and colonization, the pathogen degrades the host cell wall by enzymes, and the lesions become visible three days after infection. Under the best condition, the symptom visualized in five to seven days after the establishment of conidia in the leaves (Sherf and MacNab 1986; Chaerani *et al.*, 2007). After this relatively short period, the disease cycle allows a polycyclic infection and rapidly spreads in all leaves. Early diagnosis can be prevented disease incidence before colonization and spore production, allowing a polycyclic infection (Sherf and MacNab 1986).

Table 1- Diagnosis results in training, validation and test sets of optimum PCA-ANN model at 48 hours after inoculation

The optimum number of PCs	The optimum number of neurons in hidden layer	Subsets	Leaf class	Diagnosis results				Accuracy (%)	Overall accuracy (%)
				No.	Healthy	*A. alternata*	*A. solani*		
10	14	Training	Healthy	67	67	0	0	100	98.5
			A. alternata	33	2	31	0	93.9	
			A. solani	33	0	0	33	100	
		Validation	Healthy	10	10	0	0	100	96.6
			A. alternata	10	1	9	0	90	
			A. solani	9	0	0	9	100	
		Test	Healthy	14	14	0	0	100	100
			A. alternata	7	0	7	0	100	
			A. solani	8	0	0	8	100	
		All	-	-	-	-	-	-	98.4

Table 2- Diagnosis results in training, validation and test sets of optimum PCA-ANN model at 72 hours after inoculation

The optimum number of PCs	The optimum number of neurons in hidden layer	Subsets	Leaf class	Diagnosis results				Accuracy (%)	Overall accuracy (%)
				No.	Healthy	*A. alternata*	*A. solani*		
10	9	Training	Healthy	59	59	0	0	100	99.2
			A. alternata	40	0	40	0	100	
			A. solani	34	0	1	33	97.1	
		Validation	Healthy	21	21	0	0	100	100
			A. alternata	4	0	4	0	100	
			A. solani	4	0	0	4	100	
		Test	Healthy	11	10	1	0	90.9	93.1
			A. alternata	6	0	6	0	100	
			A. solani	12	0	1	11	91.7	
		All	-	-	-	-	-	-	98.4

Table 3- Diagnosis results in training, validation and test sets of optimum PCA-ANN model at 96 hours after inoculation

The optimum number of PCs	The optimum number of neurons in hidden layer	Subsets	Leaf class	Diagnosis results				Accuracy (%)	Overall accuracy (%)
				No.	Healthy	*A. alternata*	*A. solani*		
8	3	Training	Healthy	63	63	0	0	100	100
			A. alternata	37	0	37	0	100	100
			A. solani	33	0	0	33	100	100
		Validation	Healthy	16	16	0	0	100	100
			A. alternata	7	0	7	0	100	100
			A. solani	6	0	0	6	100	100
		Test	Healthy	12	12	0	0	100	100
			A. alternata	6	0	6	0	100	100
			A. solani	11	0	0	11	100	100
		All	-	-	-	-	-	-	100

Table 4- Diagnosis results in training, validation and test sets of optimum PCA-ANN model at 120 hours after inoculation

The optimum number of PCs	The optimum number of neurons in hidden layer	Subsets	Leaf class	Diagnosis results				Accuracy (%)	Overall accuracy (%)
				No.	Healthy	*A. alternata*	*A. solani*		
9	9	Training	Healthy	61	61	0	0	100	98.5
			A. alternata	38	0	37	1	97.4	
			A. solani	31	0	1	30	96.8	
		Validation	Healthy	14	14	0	0	100	100
			A. alternata	8	0	8	0	100	
			A. solani	6	0	0	6	100	
		Test	Healthy	16	16	0	0	100	96.4
			A. alternata	4	0	4	0	100	
			A. solani	8	0	1	7	87.5	
		All	-	-	-	-	-	-	98.4

In present study, the accuracy of using Vis-NIR spectroscopy and the PCA-ANN model for early diagnosis of the tomato leaves infected with early blight was close to that of diagnosis of *A. alternata* in the eggplant leaves (over 88.46% in the testing sets) using the hyperspectral image technique reported by Xie and He (2016). Yin and Zhao (2013) reported the accuracy of 80.68% for recognition of early blight in tomato plants using the hyperspectral data and the support vector machine. Atherton *et al.* (2015) reported that hyperspectral spectroscopy could discriminate more heavily the potato plants diseased with early blight (*A. solani*) from healthy potato plants in different growth stages. Atherton *et al.* (2017) used hyperspectral remote sensing spectroscopy for advanced diagnosis of early blight (*A. solani*) in potato plants prior to visual disease symptoms, and reported that the technique could distinguish moderately the diseased plants from healthy and minimally diseased plants. An investigation of the potential of using hyperspectral imaging for diagnosing early blight and late blight diseases in tomato leaves by Xie *et al.* (2015) showed that using a hyperspectral imaging technique and extreme learning machine (ELM)

classifier model or successive projection algorithm (SPA) could excellently diagnose the diseases at the accuracy of 97.1-100% in the testing sets. Diagnosis accuracy of present study for test set samples (93.1-100%) was close to the results reported by Xie *et al.* (2015). However, different studies for non-destructive diagnosis of diseases have different results because of different instruments, stage of diseases, plant types and varieties. Because of the high cost of hyperspectral imaging equipment and good results of present study, Vis–NIR spectroscopy can be recommended for diagnosis of early blight disease prior to visual symptoms. The results of this research compared to other studies are summarized in Table 5.

Table 5- Comparison of the performance of early and nondestructive diagnosis of early blight disease in this study with other studies

Research	Vegetable	Accuracy (%)
Tis research	Tomato	93.1-100
Xie *et al.*, 2015	Tomato	97.1-100
Gold *et al.*, 2020	Potato	89-95
Xie and He, 2016	Eggplant	88.46
Yin and Zhao, 2013	Tomato	80.68

Conclusion

This study evaluated the feasibility of utilizing Vis–NIR spectroscopy (range of 400-900nm) using a CCD spectrometer coupled with the PCA-ANN modeling method for early and non-destructive diagnosis of early blight disease in tomato plants and diagnosis of type of pathogen (*A. alternate* and *A. solani*) before the appearance of the symptoms. The results of this study indicated that, when optimum PCs and optimum number of neurons in the hidden layer of ANN were selected, the PCA-ANN model could accurately diagnose the infected plants and type of pathogen (accuracy of 93.1-100%). Over time, the shape of the infected spectra changed and this change was effective in diagnosing the infected leaves. At all times after inoculation, the developed models could discriminate *A. solani*-infected plants from healthy leaves at the accuracy of 100%. This was a noticeable result because of more pathogenicity and more damage of *A. solani* species. On fourth day after inoculation, Vis-NIR spectroscopy combined with the PCA-ANN computing method could diagnose the infected leaves and type of pathogen without any error by the simpler model. Therefore, it was concluded that Vis-NIR spectroscopy could be utilized for rapid and non-destructive early diagnosis of early blight on tomato plants before visual symptoms without any plant sample preparation. It is recommended that diagnosis of other causes of tomato leaf spots, including manganese deficiency, and fungi of *Septoria* sp. and *Cercospora* sp., in which some cases have similar symptoms to early blight, be evaluated by NIR spectroscopy in the future research.

Acknowledgement

This research was supported by Iranian Research Institute of Plant Protection and Agricultural Engineering Research Institute of Iran (Project number: 3-16-1614-039-970295).

References

1. Adhikari, P., Y. Oh, and D. R. Panthee. 2017. Current status of early blight resistance in tomato: an update. International Journal of Molecular 18 (10): 2019.
2. Atherton, D., D. G. Watson, M. Zhang, Z. Qin, and X. Liu. 2015. Hyperspectral spectroscopy for detection of early blight (*Alternaria solani*) disease in potato (*Solanum tuberosum*) plants at two different growth stages. In 2015 ASABE Annual International Meeting (p. 1). American Society of Agricultural and Biological Engineers.

3. Atherton, D., R. Choudhary, and D. Watson. 2017. Hyperspectral remote sensing for advanced detection of early blight (*Alternaria solani*) disease in potato (*Solanum tuberosum*) plants prior to visual disease symptoms. In 2017 ASABE Annual International Meeting (p. 1). American Society of Agricultural and Biological Engineers.
4. Azadshahraki, F., B. Jamshidi, and V. R. Sharabiani. 2018. Non-destructive determination of vitamin C and lycopene contents of intact cv. Newton tomatoes using NIR spectroscopy. Yuzuncu Yil University Journal of Agricultural Sciences 28 (4): 389-397.
5. Babagoli, M. A., and E. Behdad. 2012. Effects of three essential oils on the growth of the fungus *Alternaria solani.* Journal of Research in Agricultural Science 8 (14): 45-57.
6. Brown, D. J., R. S. Bricklemyer, and P. R. Miller. 2005. Validation requirements for diffuse reflectance soil characterization models with a case study of VNIR soil C prediction in Montana. Geoderma 129 (3-4): 251-267.
7. Castro, W., J. Oblitas, R. Santa-Cruz, and H. Avila-George. 2017. Multilayer perceptron architecture optimization using parallel computing techniques. PloS One 12 (12): 1-17.
8. Cen, H., and Y. He. 2007. Theory and application of near infrared reflectance spectroscopy in determination of food quality. Trends in Food Science & Technology 18 (2): 72-83.
9. Chaerani, R., and R. E. Voorrips. 2006. Tomato early blight (*Alternaria solani*): the pathogen, genetics, and breeding for resistance. Journal of General Plant Pathology 72 (6): 335-347.
10. Chaerani, R., R. Groenwold, P. Stam, and R. E. Voorrips. 2007. Assessment of early blight (*Alternaria solani*) resistance in tomato using a droplet inoculation method. Journal of General Plant Pathology 73 (2): 96-103.
11. Dai, Q., J. H. Cheng, D. W. Sun, H. Pu, X. A. Zeng, and Z. Xiong. 2015. Potential of visible/near-infrared hyperspectral imaging for rapid detection of freshness in unfrozen and frozen prawns. Journal of Food Engineering 149: 97-104.
12. Ding, S., K. Meinholz, K. Cleveland, S. A. Jordan, and A. J. Gevens. 2019. Diversity and virulence of Alternaria spp. causing potato early blight and Brown spot in Wisconsin. Phytopathology 109 (3): 436-445.
13. Ershad, D. 2009. Fungi of Iran. 3rd edition, Iranian Research Institution of Plant Protection. 531 pp.
14. Fulton, T. M., J. Chunwongse, and S. D. Tanksley. 1995. Microprep protocol for extraction of DNA from tomato and other herbaceous plants. Plant Molecular Biology Reporter 13 (3): 207-209.
15. Gold, K. M., P. A. Townsend, A. Chlus, I. Herrmann, J. J. Couture, E. R. Larson, and A. J. Gevens. 2020. Hyperspectral measurements enable pre-symptomatic detection and differentiation of contrasting physiological effects of late blight and early blight in potato. Remote Sensing 12 (2): 286.
16. Ghanei Ghooshkhaneh, N., M. R. Golzarian, and M. Mamarabadi. 2018. Detection and classification of citrus green mold caused by Penicillium digitatum using multispectral imaging. Journal of the Science of Food and Agriculture 98 (9): 3542-3550.
17. Jamshidi, B., S. Minaei, E. Mohajerani, and H. Ghassemian. 2015. Pattern recognition of near-infrared spectroscopy for non-destructive discrimination of oranges based on taste index. Journal of Agricultural Machinery 5 (1): 101-110. (In Persian).
18. Jinendra, B., K. Tamaki, S. Kuroki, M. Vassileva, S. Yoshida, and R Tsenkova. 2010. Near infrared spectroscopy and aquaphotomics: Novel approach for rapid in vivo diagnosis of virus infected soybean. Biochemical and Biophysical Research Communications 397 (4): 685-690.Kia, M. 2010. Neural network using MATLAb. Tehran: Kiyan Rayane.408pp.
19. Mireei, S. A., S. S. Mohtasebi, R. Massudi, S. Rafiee, and A. S. Arabanian. 2010. Feasibility of near infrared spectroscopy for analysis of date fruits. International Agrophysics 24 (4): 351-356.

20. Minich, D. M. 2019. A review of the science of colorful, plant-based food and practical strategies for "eating the rainbow. Nutrition and Metabolism 2019.
21. Mouazen, A. M., W. Saeys, J. Xing, J. De Baerdemaeker, and H. Ramon. 2005. Near infrared spectroscopy for agricultural materials: an instrument comparison. Journal of Near Infrared Spectroscopy 13 (2): 87-97.
22. Nicolai, B. M., K. Beullens, E. Bobelyn, A. Peirs, W. Saeys, K. I. Theron, and J. Lammertyn. 2007. Nondestructive measurement of fruit and vegetable quality by means of NIR spectroscopy: A review. Postharvest Biology and Technology 46 (2): 99-118.
23. Nicolai, B. M., T. Defraeye, B. De Ketelaere, E. Herremans, M. L. Hertog, W. Saeys, A. Torricelli, T. Vandendriessche, and P. Verboven. 2014. Nondestructive measurement of fruit and vegetable quality. Annual Review of Food Science and Technology 5: 285-312.
24. Omid, M., A. Mahmoudi, and M. H. Omid. 2010. Development of pistachio sorting system using principal component analysis (PCA) assisted artificial neural network (ANN) of impact acoustics. Expert Systems with Applications 37 (10): 7205-7212.
25. Pan, L., Q. Zhang, W. Zhang, Y. Sun, P. Hu, and K. Tu. 2016. Detection of cold injury in peaches by hyperspectral reflectance imaging and artificial neural network. Food Chemistry 192: 134-141.
26. Purcell, D. E., M. G. O'Shea, R. A. Johnson, S. Kokot. 2009. Near-infrared spectroscopy for the prediction of disease ratings for Fiji leaf gall in sugarcane clones. Journal of Applied Spectroscopy 63 (4): 450-457.
27. Rotem, J. 1994. The genus Alternaria: biology, epidemiology, and pathogenicity. American Phytopathological Society Press, St. Paul, Minnesota.
28. Salchenberger, L. M., E. M. Cinar, and N. A. Lash. 1992. Neural networks: A new tool for predicting thrift failures. Decision Sciences 23 (4): 899-916.
29. Sankaran, S., A. Mishra, J. M. Maja, and R. Ehsani. 2011. Visible-near infrared spectroscopy for detection of Huanglongbing in citrus orchards. Computers and Electronics in Agriculture 77 (2): 127-134.
30. Sigmund, R., and E. Gustav. 1991. The cultivated plants of the tropics and subtropics. Institute of Agronomy in the Tropics, University of Gottingen, Germany, p. 552.
31. Sankaran, S., R. Ehsani, S. A. Inch, and R. C. Ploetz. 2012. Evaluation of visible-near infrared reflectance spectra of avocado leaves as a non-destructive sensing tool for detection of laurel wilt. Plant Disease 96 (11): 1683-1689.
32. Sankaran, S., and R. Ehsani. 2013. Comparison of visible-near infrared and mid-infrared spectroscopy for classification of Huanglongbing and citrus canker infected leaves. Agricultural Engineering International: CIGR Journal 15 (3): 75-79.
33. Sherf, A. F., and A. A. MacNab. 1986. Vegetable diseases and their control. John Wiley and Sons, USA, 722 pp.
34. Simmons, E. G. 2000. Alternaria themes and variations (244-286) species on Solanaceae. Mycotaxon 75: 1-115.
35. Song, Y., Q. Diao, and H. Qi. 2015. Polyamine metabolism and biosynthetic genes expression in tomato (*Lycopersicon esculentum* Mill) seedlings during cold acclimation. Journal of Plant Growth Regulation 75: 21-32.
36. Teye, E., X. Y. Huang, and N. Afoakwa. 2013. Review on the potential use of near infrared spectroscopy (NIRS) for the measurement of chemical residues in food. American Journal of Food Science and Technology 1: 1-8.
37. Taiz, L., and E. Zeiger. 2002. Plant Physiology. 3rd ed Sinauer Associates Inc Publishers. Sunderland, MA, 690pp.
38. Thomma, B. P. 2003. *Alternaria* spp.: from general saprophyte to specific parasite. Molecular Plant Pathology 4 (4): 225-236.

39. Wold, S., M. Sjöström, and L. Eriksson. 2001. PLS-regression: a basic tool of chemometrics. Chemometrics and Intelligent Laboratory Systems 58 (2): 109-130.
40. Xie, C., Y. Shao, X. Li, and Y. He. 2015. Detection of early blight and late blight diseases on tomato leaves using hyperspectral imaging. Scientific Reports 5: 16564.
41. Xie, C., and Y. He. 2016. Spectrum and image texture features analysis for early blight disease detection on eggplant leaves. Sensors 16 (5): 676.
42. Yin, X., and S. Zhao. 2013. Hyperspectral recognition of processing tomato early blight based on GA and SVM. In Fifth International Conference on Machine Vision (ICMV 2012): Computer Vision, Image Analysis and Processing (Vol. 8783, p. 87831D). International Society for Optics and Photonics.
43. Yoplac, I., H. Avila-George, L. Vargas, P. Robert, and W. Castro. 2019. Determination of the superficial citral content on microparticles: An application of NIR spectroscopy coupled with chemometric tools. Heliyon 5 (7): e02122.
44. Zhang, D., J. Y. He, P. Haddadi, J. H. Zhu, Z. H. Yang, and L. Ma. 2018. Genome sequence of the potato pathogenic fungus *Alternaria solani* HWC-168 reveals clues for its conidiation and virulence. BMC Microbiology 18 (1): 1-13.
45. Zitter, T. A., J. L. Drennan, M. A. Mutschler, and M. J. Kim. 2004. Control of early blight of tomato with genetic resistance and conventional and biological sprays. In I International Symposium on Tomato Diseases 695 (pp. 181-190).

نشریه ماشین‌های کشاورزی
https://jame.um.ac.ir/

مقاله پژوهشی

جلد ۱۲، شماره ۱، بهار ۱۴۰۱، ص ۹۴-۸۱

تشخیص بیماری لکه‌موجی گیاه گوجه‌فرنگی بر پایه طیف‌سنجی مرئی/ فروسرخ نزدیک و تجزیه مؤلفه‌های اصلی- شبکه عصبی مصنوعی قبل از ظهور علائم بیماری

فرزاد آزادشهرکی[۱*]، کسری شریفی[۲]، بهاره جمشیدی[۳]، روح الله کریم‌زاده[۴]، هانیه نادری[۵]

تاریخ دریافت: ۱۳۹۹/۰۹/۲۳
تاریخ پذیرش: ۱۳۹۹/۱۱/۲۷

چکیده

تشخیص زودهنگام بیماری گیاهان قبل از وقوع علائم، می‌تواند افت عملکرد را محصول را کاهش داده و کیفیت آن را افزایش دهد. این امر همچنین مصرف سموم شیمیایی، مشکلات زیست‌محیطی و هزینه تولید را کاهش می‌دهد. هدف از انجام این تحقیق، تشخیص غیر تخریبی بیماری لکه‌موجی گیاه گوجه‌فرنگی و همچنین تشخیص مهم‌ترین عوامل بیماری‌زای آن (*A. solani*, *A. alternate*) از یکدیگر در مراحل اولیه بیماری، قبل از بروز علائم ظاهری، با استفاده از طیف‌سنجی مرئی/ فروسرخ نزدیک (۴۰۰-۹۰۰ نانومتر) بود. داده‌های طیفی از برگ‌های گیاهان آلوده به *A. alternate* و *A. solani* در ۴۸، ۷۲، ۹۶ و ۱۲۰ ساعت بعد از تلقیح بیماری استخراج شدند. به‌منظور توسعه مدل‌های تشخیص بر اساس داده‌های طیفی، از تجزیه مؤلفه‌های اصلی (PCA) همراه با شبکه عصبی مصنوعی (ANN) استفاده شد. نتایج نشان داد که مدل PCA-ANN توانست گیاهان آلوده و نوع پاتوژن را با دقت ۹۳-۱۰۰ درصد در نمونه‌های تست شناسایی کند. در ۹۶ ساعت بعد از تلقیح، علاوه بر به‌دست آمدن مدل ساده‌تر پیش‌بینی (۸ مؤلفه اصلی و ۳ نرون در لایه مخفی)، دقت ۱۰۰ درصد تشخیص حاصل شد. مدل‌های تدوین شده، در تمامی زمان‌های بعد از تلقیح، در تشخیص گیاهان آلوده با *A. solani* که دارای قدرت بیماری‌زایی بالایی می‌باشد نسبت به گیاهان سالم، هیچ خطایی نداشتند. استفاده از طیف‌سنجی مرئی/ فروسرخ نزدیک (۴۰۰-۹۰۰ نانومتر) همراه با PCA-ANN توانست بیماری لکه‌موجی گوجه‌فرنگی و نوع پاتوژن آن را قبل از بروز علائم ظاهری (با دقت ۱۰۰-۹۳ درصد) بدون هیچ آماده‌سازی گیاه، به‌صورت غیر مخرب تشخیص دهد. نتایج این پژوهش نشان داد که این تکنیک می‌تواند برای تشخیص سریع، کم‌هزینه و زودهنگام این بیماری گوجه‌فرنگی به‌جای روش‌های آزمایشگاهی زمان‌بر، گران و مخرب به‌کار رود.

واژه‌های کلیدی: تجزیه مؤلفه‌های اصلی، طیف‌سنجی فروسرخ نزدیک، گوجه‌فرنگی، لکه‌موجی

۱- مؤسسه تحقیقات فنی و مهندسی کشاورزی، سازمان تحقیقات، آموزش و ترویج کشاورزی، کرج، ایران
۲- بخش تحقیقات بیماری‌های گیاهان، مؤسسه تحقیقات گیاهپزشکی کشور، سازمان تحقیقات، آموزش و ترویج کشاورزی، تهران، ایران
۳- مؤسسه تحقیقات فنی و مهندسی کشاورزی، سازمان تحقیقات، آموزش و ترویج کشاورزی، کرج، ایران
۴- دانشکده فیزیک، دانشگاه شهید بهشتی، تهران، ایران
۵- شرکت واندا اطلس، کرج، ایران
(*- نویسنده مسئول: Email: farzad_shahrekian@yahoo.com)

DOI: 10.22067/jam.2021.67436.1001

Journal of Agricultural Machinery

Homepage: https://jame.um.ac.ir/

Full Research Paper
Vol. 12, No. 1, Spring 2022, p. 95-106

Investigation on the Capability of GreenSeeker Sensor in Predicting Nitrogen Status and Fractional Vegetation Cover of Spinach Crop

M. Hashemi Jozani[1], H. Bagherpour[2*], J. Hamzei[3]

1- MSc graduated student, Department of Biosystems Engineering, Bu-Ali Sina University, Hamedan, Iran
2- Assistant Professor, Department of Biosystems Engineering, Bu-Ali Sina University, Hamedan, Iran
3- Associate Professor, Department of Agronomy and Plant Breeding, Faculty of Agriculture, Bu-Ali Sina University, Hamedan, Iran

Received: 24-01-2021
Revised: 16-05-2021
Accepted: 02-06-2021
Available Online: 28-09-2021

How to cite this article:
Hashemi Jozani, M., H. Bagherpour, and J. Hamzei. 2022. Investigation on the Capability of GreenSeeker Sensor in Predicting Nitrogen Status and Fractional Vegetation Cover of Spinach Crop. Journal of Agricultural Machinery 12 (1): 95-106.
DOI: 10.22067/jam.2021.68387.1013

Abstract

Fractional vegetation cover (FVC) and normalized difference vegetation index (NDVI) are the most important indicators of greenness and have a strong correlation with green biomass. The objective of this study was to evaluate a hand-held GreesnSeeker (GS) active remote sensing instrument to estimate NDVI and FVC in the spinach plant. In this study, the color indices of the G-B index and Excess Green (ExG) were used as color vegetation indices to discriminate leaves from soil background. During 28 to 44 days after emergence (DAG), the results showed good correlations between chlorophyll yield and NDVI (R = 0.61 to 0.91), and the correlation between NDVI of GS and biomass was significant. In addition, in this growth stage, the results showed a good coefficient of correlation between NDVI of GS and FVC (R = 0.67 to 0.82). In assessing the nitrogen rate on the NDVI of GS, the results showed significant differences only at the short period of growth stage (28 to 36 DAG). The results revealed that GreenSeeker performed well for estimation both chlorophyll and biomass yield of spinach crop and it could be used as a suitable instrument for estimation of leaf area index in the middle of the plant growth period.

Keywords: Canopy, Chlorophyll, Optical sensor, Segmentation

Introduction

The main challenges for global food security and sustainable development are how to increase food production whereas improving resource use efficiencies and reducing risks of environmental contamination (Guo *et al.*, 2010; Chen *et al.*, 2014). Blanket fertilizer nitrogen (N) recommendations lead to low N use efficiency (NUE) due to field-to-field variability in soil N supply (Cao *et al.*, 2016). Traditionally, pre-plant nitrogen requirements have been estimated by using soil samples and crop yield levels from previous years. The estimated rate is then applied uniformly to the field (Sawyer, 1994). Many farmers often apply fertilizer N in doses higher than the blanket recommendations to ensure that there is no yield loss because of N deficiency (Purba *et al.*, 2015). Using fertilizer over plant demand may result in surface runoff and pollution of streams. Under-application of nitrogen may diminish crop production and result in low economic returns to the producer (Miao *et al.*, 2011).

Advances in technology have led to development of active remote sensing systems that are now available commercially (Inman *et al.*, 2007). In principle, they can be mounted on a VRT fertilizer system that is used to vary the amount of fertilizer for a given area in 'real-time (Williams, 2006).

(* - Corresponding Author Email: h.bagherpour@basu.ac.ir)

Recently, farmers using precision agriculture tools and technologies such as leaf color chart (LCC), chlorophyll meter (SPAD), GreenSeeker, and real-time on-the-go optical sensing measurements (OPM) based variable rate (VRT) fertilizer application. These tools and technologies can reduce under or over-application of N (Boyer *et al.,* 2011; Bagherpour *et al.,* 2017). Raun *et al.* (2002) analyzed optical sensing and VRT for Oklahoma, USA winter wheat production. They showed that the extra income owning to an increase in NUE (N use efficiency) can cover the expected costs of the technology and that OPM-based VRT would be most profitable in areas of high spatial variability.

Leaf color chart has been used successfully to optimize fertilizer N application in wheat and rice (Ladha *et al.,* 2007). SPAD chlorophyll meter was confirmed to provide a quick, simple, and nondestructive estimation of leaf chlorophyll content (Chapman and Barreto, 1997). The use of SPAD with grain (Ramesh *et al.,* 2002) and vegetables (cabbage and carrot) has recently been tried (Westerveld *et al.,* 2004). Normalized difference vegetation index (NDVI) as a spectral vegetation index is useful for acquiring crop information indirectly, such as productivity potential, photosynthetic efficiency, and potential yield (Raun *et al.,* 2001; Inman *et al.,* 2007, Thind *et al.,* 2017).

Both NIR and red irradiance are strongly influenced by plant cover. NIR irradiance increases and red irradiance decreases with increasing plant cover. Given these relationships, NDVI from vegetated surfaces is heavily influenced by chlorophyll content in the vegetation. A deficiency in nutrients such as nitrogen decreases pigment formation, which subsequently increases red reflectance (Jones *et al.,* 2007).

NDVI is a broadband index that has a good correlation with green biomass and leaf area index (Pen˜uelas *et al.,* 1994). Raun *et al.* (2001) showed that the expected yield determined from NDVI had a strong relation with actual grain yield in winter wheat. Bausch and Diker (2001) investigated the remote sensing techniques to increase the nitrogen use efficiency of corn. Their results showed that the NIR could well predict the plant N at the 9-leaf to 12-leaf crop growth stages. However, the effects of the soil background on reflectance had a negative effect on these relations.

Site-specific N management strategy using GreenSeeker™ optical sensor (GS) was evaluated in dry direct-seeded rice (DDSR) in north-western India. N use efficiency was improved by more than 12% when N fertilizer management was guided by GS as compared to when the general N fertilizer recommendation was followed (Ali *et al.,* 2014).

Sharma *et al.* (2011) observed that high N use efficiency in irrigated wheat grown in Northwest India can be achieved by replacing general fertilizer recommendation with an optical sensor-based N management strategy. Enciso *et al.* (2017) evaluated current commercially available sensor technology for use in a ground-based platform for plant phenol typing and crop management decisions. Results showed that the Normalized Difference Vegetation Index (NDVI) data collected using the GreenSeeker sensors were more consistent and presented less variability when compared to the Decagon SRS sensor.

Currently, most of the methods available for measuring leaf area index are based on manual measurements, which are time-consuming, laborious, and destructive (Fuentes *et al.,* 2014). Aerial and ground-based remote sensors have emerged as an important source of information on vegetative canopy through vegetation indices. The NDVI is related to the quantitative biomass and can be used to monitor vegetative growth and to determine biophysical variables such as leaf area (Junges *et al.,* 2019). Ter-Mikaelian and Parker (2000) estimated the biomass of white spruce seedlings with vertical photo imagery. The accuracy of this technique was comparable to the traditional methods using seedling basal diameter. Lukina *et al.* (1999) evaluated the use of a digital image to estimate vegetation coverage and a multispectral radiometer to

measure NDVI index in winter wheat. The results of this study showed a strong correlation between NDVI and vegetation coverage (r^2 = 0.66 to 0.96). In addition, NDVI have a strong correlation with dry biomass (r^2 = 0.52) and with nitrogen content (r^2 = 0.66).

Spinach (*Spinacia oleracea*) is a leafy green flowering plant native to central and western Asia. Its leaves are a common edible vegetable consumed either fresh, or after storage using preservation techniques by canning, freezing, or dehydration. Spinach is rich with vitamins such as vitamin C, vitamin A, vitamin E, minerals like magnesium, manganese, iron, calcium, and folic acid. Spinach is also a good source of chlorophyll, which is known to aid in digestion (FAO, 2020). Along with these advantages, to increase crop yield, it needs high N fertilizer and in the commercial production of this plant, the recovery of N is poor, which may result in environmental contamination. To increase spinach yield and decrease its environmental consequence, there is a need to optimize nitrogen consumption (Navarrete *et al.*, 2016). Therefore, this study aimed to investigate the relationship of nitrogen rate, leaf area index, and biomass with NDVI to find an effective, fast and non-destructive way to estimate leaf N in spinach plants and to test the potential linkage between FVC and biomass with NDVI of GS.

Materials and Methods

Plant material and experimental setup

This study was conducted at the agricultural research station, faculty of agriculture, university of Bu-Ali Sina (35°1’ N, 48°31’ E, 1690 m alt) during the 2019 growing season. This site has a semi-arid and cold climate, an average annual rainfall of 333 mm and an average temperature of 24° C in the warmest month (Hamzei *et al.*, 2012).

Spinach seeds ‘native cultivar of Nahavand’ was planted on March 10th with 20 plants per m^2 density. The experiment was laid out as Randomized Complete Block Design with three replications including four levels of nitrogen (0, 75, 150, and 300 kg ha^{-1}). Each experimental unit contained six lines a distance of 30 cm and a length of 6 m, and the distance between each block was 1 m. Three random soil sample cores were obtained from each plot prior to fieldwork using a 3 cm diameter hand probe to a depth of 0-15 cm for potassium (K), phosphorus (P), pH, and organic matter and 0-30 cm in depth for nitrate. Soil samples were air-dried, ground to pass through a 2 mm screen, and were mixed before analysis for soil pH, available P, K, and organic matter. Soil pH was measured in a 1:1 ratio of soil to deionized H_2O solution (Watson and Brown, 1998), P by the Olsen method (Olsen *et al.*, 1954), K was analyzed using the 1-N ammonium acetate method (Thomas, 1982), soil nitrogen was determined using O'Brain and Flore (1962) method and organic matter was measured using the loss following ignition method (Schulte and Hopkins, 1996). Plots in all experiments were irrigated with flood irrigation. The result of soil analysis was presented in Table 1.

Table 1- The result of soil analysis in the research site

Soil characteristic	Quantity	Unit
Texture	sandy clay loam	-
pH	7.15	-
Organic carbon	2.38	%
Organic matter	4.10	%
Total N	0.20	%
Available P	57.84	mg kg^{-1}
Available K	703.30	mg kg^{-1}

NDVI and SPAD Value Measurements

Canopy reflectance was measured during 20 to 56 days after emergence with a

GreenSeeker hand-held optical sensor unit (Trimble Navigation Ltd., Sunnyvale, California, USA) over 12 plots of field. According to the Instructions for Use (Figure 1), the GreenSeeker was held at 65 cm above the crop canopy using an adjustable shoulder harness. Readings were taken for the defined area of each plot every four days throughout the experimental period. Spectral measurements were collected from each plot by moving the sensor across the center of each plot with an area of 1.8×2 m^2. To analyze the chlorophyll content of leaves, leaf samples were taken from areas located at both sides of each plot with a length of 1.5 m along the length. The SPAD readings were taken as an average of three different leaf readings located in the middle to the upper level of the plant excluding the midrib. In this study, a portable chlorophyll meter SPAD-502 (Minolta Co., LTD. Japan) was used to assess the nitrogen status of spinach leaves at various growth stages.

Fig.1. The Handheld Greemseeker and height of the sensor

Determination of Chlorophylls and total Carotenoids in Leaves

After reading the NDVI of the central section of each plot with the GreenSeeker sensor and imaging with the visual imaging system, one leaf located in the middle to the upper level of the four plants at the inside of the two side sections were hand-harvested. The spinach samples were placed in plastic bags, weighed, labeled, carefully closed, and then refrigerated for later processing in the laboratory. In the laboratory, samples were washed, frozen, and dried. The chlorophyll and carotenoid pigments were extracted in 99% acetone by macerating the leaves with a mortar and pestle. The absorption of the extracts at wavelengths of 470 nm, 645 nm, and 664 nm was measured by spectrophotometer UV/visible (Varian-carry 100) according to the spectrophotometric method of Inskeep and Bloom (1985).

Measuring crop biomass

The main objective of this measuring was to estimate final crop biomass by NDVI of GS in the period of growth stages. At each sampling location, spinach biomass was measured by cutting all plants at ground level from within a 1-m^2 quadrat at the end of growth stages. Biomass samples were transported to the laboratory where fresh weight was recorded.

Acquiring visual images

After reading, the NDVI of the sample area using the GreenSeeker sensor, a corresponding visual image was acquired using a Samsung digital camera with a resolution of 8 Mpixels (3264×2248). The imaging system was mounted to a pole on a platform held horizontally 1.5 m above the ground. For each plot, three photographs were taken and the area photographed was approx. 1.8×2 m^2. All the images were taken between

at cloudy conditions or on areas shaded with a sheet to eliminate the effect of sunlight on image quality. All images were saved in JPEG-Format. The images were processed by LabView 2014 (National Instruments Corporation, Austin, TX, USA) and MatLab 2016a (MathWorks, Inc., Natick, Massachusetts, US).

Image segmentation

This section aims to separate the soil background from the canopy representing green plant parts. This allowed determining the ground cover of living plant leaves. Several methods have been developed for segmenting crop canopy images. The common segmentation technologies used for this purpose are color index-based segmentation, threshold-based segmentation, and learning-based segmentation (Hamuda *et al.,* 2016). Most researchers have used color to separate soil from a plant (Meyer and Camargo-Neto, 2008; Kirk *et al.,* 2009). In a recent study at the early stage of growing, according to Woebbecke *et al.* (1995), the G-B (green-blue) index was used as a color index-based segmentation to discriminate leaves from soil background. Nevertheless, in the flowering period, the Excess Green (ExG), according to Equation 1, the index showed good results than G-B (Soontranon *et al.,* 2014). Because of unreliable results in the auto threshold, fixed threshold values were used for each series of images, which were taken under similar light conditions. After segmentation of images, the fractional vegetation cover (FVC) was calculated as the ratio of the number of pixels of all vegetation to the total number of pixels in the image (Song *et al.,* 2015). The temporal segmentation results of the crops were shown in Figure 2. In this Figure, it can be observed that the color indices of G-B and ExG perform well in segregating this crop from its background.

a (G-B) b (G-B) c (ExG) d (ExG)

Fig.2. The segmentation results of the crop at a different stage of growth. a and b are early stage, c and d are the late stages of growing

$$\mathrm{ExG} = 2\mathrm{G} - (\mathrm{R} + \mathrm{B}) \qquad (1)$$

Results and Discussion

Changing NDVI during growing stages

The change of GS readings in the canopy of spinach was shown in Figure 3. The GS readings for all treatments (N0 to N300) increased until 44 DAG and then decreased. With increasing the length of growth period, spinach leaves with a high concentration of N fertilizer always had higher GS values than those with a low concentration of N fertilizer. For all days of growth period value of

treatment, N300 was higher than that of other N treatments. These changes indicated that it is possible to predict the nitrogen level of the canopy for all days of the growth stage. This Figure also shows that for all nitrogen levels, the GS reading peaking at 44 DAG. After 44 days, for all treatment, GS readings were dramatically declined due to the maturation of plants. Changes in SPAD readings in leaves of spinach were shown in Figure 3. Similar to GS readings, the SPAD readings have high variance at the early stage of plant growth, whereas at the late stage of growing, these data have low variance. Data collection overlapped with plants' anthesis, which interfered with the GreenSeeker™ NDVI values and decreased readings in the later phases of growing (Basyouni *et al.*, 2015). Additionally, the flowering progress might have consumed leaf N, which decreased sensor readings at later stages (Lawrie and Wheeler, 1974).

Liu *et al.* (2006) reported similar results for the SPAD reading changes during the growth stage of 25 to 35 days after sowing. However, they did not investigate the SPAD reading changes at the late stage of growth. Junges *et al.* (2019) studied a vineyard in Brazil using the GreenSeeker remote sensor and reported similar results for the GS readings. The index increases rapidly at first (September to November), followed by a relative stabilization (December to February), and decreases in the final stage (March to May).

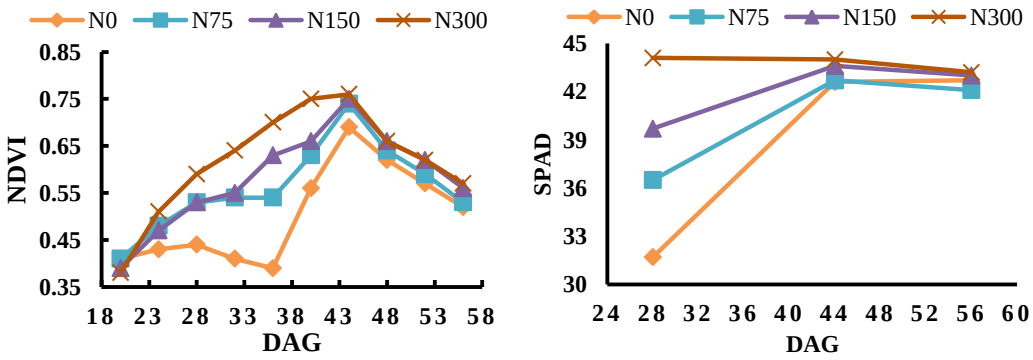

Fig.3. Effects of N levels on GreenSeeker and SPAD values at different days after emergence

Table 2 demonstrates the Pearson's correlation coefficients between GreenSeeker NDVI and the other variables. These results showed that NDVI has a good correlation with chlorophyll yield and biomass with correlation coefficients (R) ranging from 0.61 to 0.91 and from 0.69 to 0.87, respectively. The highest correlation between these variables was obtained at the growth period of 32-40 days. After 44 days, nutrition deficiency in the plant leads to yellowing leaves. These changes in leaves color and preliminary mature of spinach plants can be the main reason for the decreasing of correlation coefficients between NDVI and these variables. This relationship concurs with work done by Raun *et al.* (1998) and Basyouni *et al.* (2016).

As Table 2 shows, NDVI correlations with leaf N and fertilizer rate were not significant ($P < 0.05$) at 20 and 24 DAG. This can be related to the small size of plants at the early stages of growth, which results in background noise interfering with the NDVI readings (Basyouni *et al.*, 2015). As plants grew and filled the plots with time, these correlations were strong. This corresponds with the results of Wang *et al.* (2012), Dunn and Goad (2015), and Ali *et al.* (2020) showed a strong correlation between GreenSeeker NDVI readings and chlorophyll yield in geranium and ornamental cabbage and wheat.

Table 2- Mean correlation coefficient of plots between GS NDVI- chlorophyll yield, NDVI - Biomass, and NDVI - FVC during the growth period

Day After Emergence	NDVI vs. chlorophyll yield	NDVI vs. biomass
20	0.47	0.51
24	0.74**	0.53
28	0.88**	0.73**
32	0.90**	0.76**
36	0.91**	0.85**
40	0.86**	0.87**
44	0.61*	0.69*
48	0.41	0.45
52	0.42	0.46
56	0.42	0.46

*, **, representing correlation coefficient (r), significant at $P \leq 0.05$, $P \leq 0.01$, respectively.

NDVI correlations with biomass were also not significant at the early stage of establishment. In addition, there was no significant correlation between these variables at the last stage of plant growth. The decreasing NDVI values at the end of the cycle were expected due to the senescence and yellowing of the plant leaves. This result was similar to previous literature findings in dianthus (Basyouni *et al.*, 2016) and grape (Junges *et al.*, 2017).

Effects of fertilizer rate on NDVI

Table 3 shows GS readings during the growth followed linear trends as fertilizer rates increased. With increasing N rate, the linear trends of NDVI and leaf N rates were significant. Comparing the mean value of the GreenSeeker™ NDVI indicated that there are significant differences among N rates. However, after 44 DAG there are no significant differences between N treatments. For the early growth stage, the result of this study was similar to the result of Basyouni *et al.* (2016) that investigated the use of non-destructive sensors to assess nitrogen status in potted dianthus production. However, during the late growth stage, these results are in contrast to their finding.

Table 3- GreenSeeker™ NDVI means, and trend analysis at six dates of days after emergence (DAG) and five N fertilizer rates

Total N applied (kg ha^{-1})	DAG						
	20	24	28	36	44	52	56
0	0.415	0.430^{a}	0.441^{a}	0.390^{a}	0.690	0.575	0.525
75	0.415	0.481^{ab}	0.530^{b}	0.540^{b}	0.745	0.591	0.535
150	0.39	0.475^{ab}	0.535^{b}	0.635^{c}	0.752	0.620	0.565
300	0.385	0.515^{b}	0.595^{c}	0.710^{d}	0.761	0.625	0.575
	N.S	L*	L**	L**	N.S	N.S	N.S

*, **, linear (L) response across treatments at $P \leq 0.05$, $P \leq 0.01$, respectively. N.S: Non-Significant difference

Estimate FVC using NDVI of GS

The traditional method of estimating FVC is to harvest vegetation and measure all the one-sided leaf areas directly. In this study, the relation between FVC and GS NDVI was done to investigate the capability of GS to measure FVC in spinach. As Figure 4 shows, at the early stage of the growing period from 28 to 40 DAG, there were significant correlations between GS-NDVI and FVC extracted by the low-cost camera. However, before 28 and after 44 DAG there were no significant correlations between these variables. Figure 5 showed GS NDVI and FVC regression at 28, 40, and 52 DAG. As this figure showed, although the FVC was higher at the late growth stage, because of N deficiency in leaves the GS NDVI and FVC correlation was low. Results indicated that at the early stage of growth, the GS NDVI was a good index for the estimation

of canopy leaf area. Whereas at the late period of growing, it is not a good estimator of canopy leaf area. This result was similar to the previous study that investigated the relationship between NDVI and FVC in semiarid grassland (Fan *et al.*, 2009; Tang *et al.*, 2020). Also at the late stage of growth and at the higher ranges of FVC, when the vegetation canopy tends to be closed, NDVI saturates and can no longer be used to detect any differences in FVC (Pontailler *et al.*, 2003). The findings of Lukina *et al.* (1999) and Sembiring *et al.* (1998) on estimating vegetation coverage in wheat using digital images and spectral radiance, respectively, were also supported the results in his work.

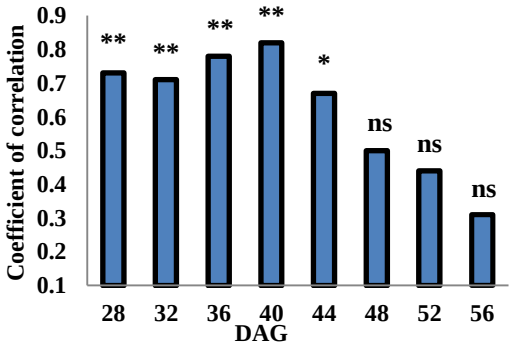

Fig.4. Coefficient of correlations between GS-NDVI and FVC at a different growing stage. (**: significant at P ≤ 0.01, ns: non-significant)

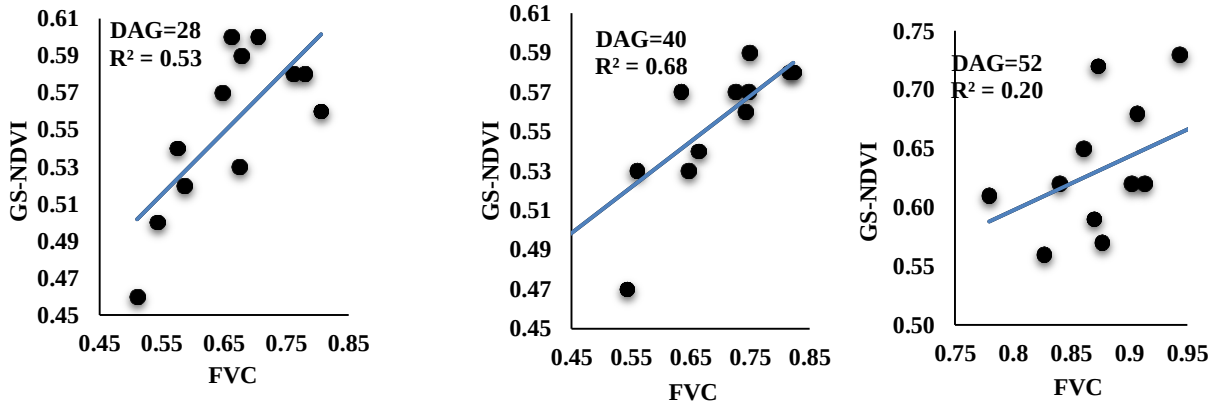

Fig.5. NDVI from sensor vs. FVC measured by the visual camera at three growth stages (22, 40, and 52 DAG)

Conclusion

The NDVI data acquired using the GS sensor and the visual imaging system were sensitive to changes in plant chlorophyll yield and plant biomass in row crop spinach. Correlations between NDVI and biomass were approximately the same as the correlation of NDVI and chlorophyll yield in the period of growth. Each growing stage demonstrated a different response relationship between sensor response and plant characteristics. At the early and late stages of growth, there were no significant correlations among NDVI with biomass, chlorophyll yield, and FVC. The best growth stage for investigating and estimating the chlorophyll yield and biomass using GS was the period of 28 to 40 DAG, in this period the high values of coefficient of correlation were obtained between NDVI of GS with chlorophyll yield and biomass. To estimate the FVC of spinach, the period of 36 to 40 DAG was considered as a recommended period for

measuring FVC using GS. Results of this study showed that the GreenSeeker has high reliability and capability for the estimation of chlorophyll yield, biomass, and FVC in the middle of the plant growth period.

References

1. Ali, A. M., and S. M. Ibrahim. 2020. Wheat grain yield and nitrogen uptake prediction using atLeaf and GreenSeeker portable optical sensors at jointing growth stage. Information Processing in Agriculture 7 (3): 375-383.
2. Ali, A. M., H. S. Thind, and S. Sharma. 2014. Prediction of dry direct-seeded rice yields using chlorophyll meter, leaf colour chart and GreenSeeker optical sensor in northwestern India. Field Crops Research 161: 11-15.
3. Bausch, W. C., and K. Diker. 2001. Innovative remote sensing techniques to increase nitrogen use efficiency of corn. Communications in Soil Science and Plant Analysis 32 (7): 1371-1390.
4. Basyouni, R., B. L. Dunn, and C. Goad. 2015. Use of nondestructive sensors to assess nitrogen status in potted poinsettia (*Euphorbia pulcherrima* L. (Willd. ex Klotzsch)) production. Scientia Horticulture 192: 47-53.
5. Basyouni, R., B. L. Dunn, and C. Goad. 2016. The use of nondestructive sensors to assess nitrogen status in potted dianthus (*Dianthus chinensis* L.) production. Canadian Journal of Plant Science 97 (1): 44-52.
6. Boyer, C. N., B. W. Brorsen, J. B. Solie, and W. R. Raun. 2011. Profitability of variable rate nitrogen application in wheat production. Precision Agriculture 12: 473-487.
7. Cao, Q., Y. Miao, J. Shen, W. Yu, F. Yuan, S. Cheng, S. Huang, H. Wang, W. Yang, and F. Liu. 2016. Improving in-season estimation of rice yield potential and responsiveness to topdressing nitrogen application with Crop Circle active crop canopy sensor. Precision Agriculture 17 (2): 136-154.
8. Chapman, S. C., and H. J. Barreto. 1997. Using a chlorophyll meter to estimate specific leaf nitrogen of tropical maize during vegetative growth. Agronomy Journal 89 (4): 557-562.
9. Chen, X., Z. CuiFan, M., Vitousek, and P. Zhao. 2014. Producing more grain with lower environmental costs. Nature 514: 486-489.
10. Dunn B., and C. Goad. 2015. Effect of foliar nitrogen and optical sensor sampling method and location for determining ornamental cabbage fertility status. HortScience 50 (1): 74-77.
11. Enciso, J., M. Maeda, J. Landivar, J. Jung, and A. Chang. 2017. A ground based platform for high throughput phenotyping. Computers and Electronics in Agriculture 141: 286-291.
12. Fabbri, C., M. Napoli, L. Verdi, M. Mancini, S. Orlandini and A. Dalla Marta, 2020. A Sustainability Assessment of the Greenseeker N Management Tool: A Lysimetric Experiment on Barley. Sustainability 12 (18): p.7303.
13. Fan, L. Y., Y. Z. Gao, H. E. B. C. Brück, and C. Bernhofer. 2009. Investigating the relationship between NDVI and FVC in semi-arid grassland in Inner Mongolia using in-situ measurements. Theoretical and Applied Climatology 95 (1-2): 151-156.
14. Fuentes, S., C. Poblete-Echeverría, S. Ortega-Farias, S. Tyerman, and R. De Bei. 2014. Automated estimation of leaf area index from grapevine canopies using cover photography, video and computational analysis methods. Australian Journal of Grape and Wine Research 20 (3): 465-473.
15. Guo, J. H., X. J. Liu, Y. Zhang, J. L. Shen, W. X. Han, W. F. Zhang, *et al*. 2010. Significant acidification in major Chinese croplands. Science 327: 1008-1010.
16. Good, A. G., and P. H. Beatty. 2011. Fertilizing nature: a tragedy of excess in the commons. PLoS Biology 9 (8): e1001124.
17. Hamuda, E., M. Glavin, and E. Jones. 2016. A survey of image processing techniques for plant extraction and segmentation in the field. Computers and Electronics in Agriculture 125: 184-199.
18. Hamzei, J., M. Seyedi, G. Ahmadvand and M. A. Abutalebian. 2012. The effect of additive intercropping on weed suppression, yield and yield component of chickpea and barley. Isfahan University of Technology-Journal of Crop Production and Processing 2 (3): 43-56.

19. Inman, D., R. Khosla, R. M. Reich, and D. G. Westfall. 2007. Active remote sensing and grain yield in irrigated maize. Precision Agriculture 8 (4-5): 241-252.
20. Bagherpour, H. and H.M. Monavar. 2017. Implementation of the GreenSeeker sensor for measuring canopy leaf area index of corn. Journal of Researches in Mechanics of Agricultural Machinery, 6(2).
21. Inskeep, W. P., and P. R. Bloom. 1985. Extinction coefficients of chlorophyll a and b in N, N-dimethylformamide and 80% acetone. Plant Physiology 77 (2): 483-485.
22. Jones, C. L., P. R. Weckler, N. O. Maness, R. Jayasekara, M. L. Stone, and D. Chrz. 2007. Remote sensing to estimate chlorophyll concentration in spinach using multi-spectral plant reflectance. Transactions of the ASABE 50 (6): pp.2267-2273.
23. Junges, A. H., D. Fontana, R. Anzanello, and C. Bremm. 2017. Normalized difference vegetation index obtained by ground-based remote sensing to characterize vine cycle in RioGrande do Sul, Brazil. Ciência e Agrotecnologia 41: 543-553.
24. Junges, A. H., D. C. Fontana, and C. S. Lampugnani. 2019. Relationship between the normalized difference vegetation index and leaf area in vineyards. Bragantia 78 (2): 297-305.
25. Kirk, K., H. J. Andersen, A. G. Thomsen, and J. R. Jørgensen. 2009. Estimation of leaf area index in cereal crops using red–green images. Biosystem Engineering 104: 308-317.
26. Ladha, J. K., J. S. Bains, and R. K. Gupta. 2007. On-farm evaluation of leaf color chart for need-based nitrogen management in irrigated transplanted rice in northwestern India. Nutrient cycling in agroecosystems 78 (2): 167-176.
27. Lawrie, A. C., and C. T. Wheeler. 1974. The effects of flowering and fruit formation on the supply of photosynthetic assimilates to the nodules of *Pisum sativum* L. in relation to the fixation of nitrogen. New Phytol 73: 1119-1127.
28. Liu, Y. J., Y. P. Tong, Y. G. Zhu, H. Ding, and F. A. Smith. 2006. Leaf chlorophyll readings as an indicator for spinach yield and nutritional quality with different nitrogen fertilizer applications. Journal of Plant Nutrition 29 (7): 1207-1217.
29. Lukina, E. V., M. L. Stone, and W. R. Raun. 1999. Estimating vegetation coverage in wheat using digital images. Journal of Plant Nutrition 22 (2): 341-350.
30. Meyer, G. E., and J. Camargo-Neto. 2008. Verification of color vegetation indices for automated crop imaging applications. Computer and Electronics in Agriculture 63: 282-293.
31. Miao, Y., B. A. Stewart, and F. Zhang. 2011. Long-term experiments for sustainable nutrient management in China. A review. Agronomy for Sustainable Development 31 (2): 397-414.
32. Navarrete, J. C. 2016. Development of a breeding strategy for nitrogen use efficiency in spinach. Doctoral dissertation, Wageningen University.
33. O'Brain, J. E., and J. Flore. 1962. Ammonia determination by automatic analysis. Wastes Engineering 33: 352-355.
34. Pen˜uelas, J., J. A. Gamon, A. L. Fredeen, J. Merino, and C. B. Field. 1994. Reflectance indices associated with physiological changes in nitrogen- and water-limited sunflower leaves. Remote Sensing of Environment 48: 135-146.
35. Pontailler J. Y., G. J. Hymus, and B. G. Drake. 2003. Estimation of leaf area index using ground-basedremote sensed NDVI measurements: validation and comparison with two indirect techniques. Canadian Journal of Remote Sensing 29: 381-387.
36. Purba, J., R. K. Sharma, M. L. Jat, H. S., Thind, R. K. Gupta, *et al.* 2015. Site-specific fertilizer nitrogen management in irrigated transplanted rice (*Oryza sativa*) using an optical sensor. Precision Agriculture 16 (4): 455-475.
37. Ramesh, K., B. Chandrasekaran, T. N. Balasubramanian, U., Bangarusamy, R. Sivasamy and N. Sankaran. 2002. Chlorophyll dynamics in rice (*Oryza sativa*) before and after flowering based on SPAD (chlorophyll) meter monitoring and its relation with grain yield. Journal of Agronomy and Crop Science 188 (2): 102-105.

38. Raun W. R., G. V. Johnson, H. Sembiring, E. V. Lukina, J. M. LaRuffa, W. E. Thomason, S. B. Phillips, J. B. Solie, M. L. Stone, and R. W. Whitney. 1998. Indirect measure of plant nutrients. Communications in Soil Science and Plant Analysis 29 (11): 1571-1581.
39. Raun, W. R., J. B. Soile, G. V. Johnson, M. L. Stone, E. V. Lukina, W. E. Thomason, and J. S. Schepers. 2001. In-season prediction of potential grain yield in winter wheat using canopy reflectance. Agronomy Journal 93: 131-138.
40. Raun, W. R., J. B. Solie, G. V. Johnson, M. L. Stone, R. W. Mullen, K. W. Freeman, *et al.* 2002. Improving nitrogen use efficiency in cereal grain production with optical sensing and variable rate application. Agronomy Journal 94: 815-820.
41. Sawyer, J. E. 1994. Concepts of variable rate technology with considerations for fertilizer application. Journal of Production Agriculture 7 (2): 195-201.
42. Sembiring, H., W. R. Raun, G. V. Johnson, M. L. Stone, J. B. Solie, and S. B. Phillips. 1998. Detection of nitrogen and phosphorus nutrient status in winter wheat using spectral radiance. Journal of Plant Nutrition 21 (6): 1207-1233.
43. Schulte, E. E., and B. G. Hopkins. 1996. Estimation of soil organic matter by weight-loss-on ignition. SSSA Special Publication 46. Madison, WI: SSSA.
44. Sharma, R. K., M. L. Jat, K. L. Martin, P. Chandna, and *et al.* 2011. Assessment of the nitrogen management strategy using an optical sensor for irrigated wheat. Agronomy for Sustainable Development 31 (3): 589-603.
45. Song, W., X. Mu, G. Yan, and S. Huang. 2015. Extracting the green fractional vegetation cover from digital images using a shadow-resistant algorithm. Remote Sensing 7: 10425-10443.
46. Soontranon, N. P. Srestasathiern, and P. Rakwatin. 2014. Rice growing stage monitoring in small-scale region using ExG vegetation index. In: International Conference on Electrical Engineering/ Electronics, Computer, Telecommunications and Information Technology 1-5.
47. Tang, L., M. He, and X. Li, 2020. Verification of Fractional Vegetation Coverage and NDVI of Desert Vegetation via UAVRS Technology. Remote Sensing 12 (11): 1742.
48. Ter-Mikaelian, M. T., and W. C. Parker. 2000. Estimating biomass of white spruce seedlings with vertical photo imagery. New Forests 20 (2): 145-162.
49. Thind, H. S., A. Kumar, O. P. Choudhary, R. K. Gupta, and M. V. Ashistha. 2017. Site-specific fertilizer nitrogen management using optical sensor in irrigated wheat in the Northwestern India. Agricultural Research 6 (2): 159-168.
50. Thomas, G. W. 1982. Exchangeable cations. In A. L. Page *et al.* (Eds.). Methods of soil analysis. Agronomy Monographs 9: 159-165.
51. Wang, Y. W., B. L. Dunn, D. B. Arnall, and P. Mao. 2012. Use of an active canopy sensor and SPAD chlorophyll meter to quantify geranium nitrogen status. HortScience 47: 45-50.
52. Watson, D., and J. R. Brown. 1998. PH and lime requirement. In J. R. Brown (Ed.) Recommended Chemical Soil Test Procedure for the North Central Region (p. 13). North Central Regional Res. Pub. No. 221 (revised). Missouri Agric. Exp. Stat. SB 1001, Univ. of Missouri, Columbia.
53. Westerveld, S. M., A. W. McKeown, M. R. McDonald, and C. D. Scott-Dupree 2004. Assessment of chlorophyll and nitrate meters as field tissue nitrogen tests for cabbage, onions, and carrots. HortTechnology 14 (2): 179-188.
54. Williams, J. R., 2006. High clearance fertilizer application system. U.S. Patent 7,077,070.
55. Woebbecke, D. M., G. E. Meyer, K. Von Bargen, and D. A. Mortensen. 1995. Color indices for weed identification under various soil, residue, and lighting conditions. Trans. ASAE 38: 259-269.

نشریه ماشین‌های کشاورزی
https://jame.um.ac.ir/

مقاله پژوهشی
جلد ۱۲، شماره ۱، بهار ۱۴۰۱، ص ۱۰۶-۹۵

ارزیابی قابلیت حسگر Greenseeker در برآورد وضعیت نیتروژن و تخمین مقدار شاخص FVC گیاه اسفناج

مهران هاشمی جوزانی[۱]، حسین باقرپور[۲*]، جواد حمزه‌ای[۳]

تاریخ دریافت: ۱۳۹۹/۱۱/۰۵
تاریخ پذیرش: ۱۴۰۰/۰۳/۱۲

چکیده

شاخص پوشش گیاهی سبز کسری (FVC) و شاخص نرمال شده تفاضل پوشش گیاهی (NDVI) از شاخص بسیار مهم سبزینگی می‌باشند و ارتباط بسیار قوی با زیست‌توده سبز دارند. هدف اصلی این پژوهش، ارزیابی شاخص NDVI حاصل از حسگر دستی Greesnseeker (GS) در تخمین مقدار زیست‌توده، کلروفیل و شاخص FVC در گیاه اسفناج می‌باشد. در این پژوهش برای جداسازی مناسب زمینه خاک از گیاه از شاخص‌های رنگی G-B و ExG استفاده شد. در طول دوره رشد ۲۸ تا ۴۴ روز بعد از جوانه‌زنی گیاه، نتایج تحقیق نشان داد که NDVI حاصل از GS ارتباط خوبی با کلروفیل داشته (R = 0.61 to 0.91) و ارتباط بین این شاخص با زیست‌توده نیز معنی‌دار بود. علاوه بر این، نتایج نشان داد که در این دوره رشد ارتباط خوبی بین شاخص NDVI حاصل از GS با شاخص FVC وجود دارد (R = 0.67 to 0.82). در حسگر در ارزیابی تاثیر نرخ نیتروژن بر شاخص NDVI، مشخص شد که تنها در دوره کوتاه ۲۸ تا ۳۶ روز پس از جوانه‌زنی ارتباط خطی معنی‌داری بین این دو متغیر وجود دارد. نتایج نشان داد که حسگر Greenseedke توانایی خوبی در تخمین کلروفیل و مقدار زیست‌توده گیاه دارد و از آن می‌توان در میانه رشد گیاه، مقدار شاخص پوشش گیاهی سبز کسری را به‌خوبی برآورد کرد.

واژه‌های کلیدی: پوشش گیاهی، حسگر نوری، قطعه‌بندی، کلروفیل

۱- دانشجوی کارشناسی ارشد، گروه مکانیک بیوسیستم، دانشکده کشاورزی، دانشگاه بوعلی سینا، همدان، ایران
۲- استادیار گروه مکانیک بیوسیستم، دانشکده کشاورزی، دانشگاه بوعلی سینا، همدان، ایران
۳- دانشیار گروه زراعت و اصلاح نباتات، دانشکده کشاورزی، دانشگاه بوعلی سینا، همدان، ایران
(*- نویسنده مسئول: Email: h.bagherpour@basu.ac.ir)

DOI: 10.22067/jam.2021.68387.1013

FORMAT OF MANUSCRIPT PREPARATION FOR JOURNAL OF AGRICULTURAL MACHINERY

It is important that the manuscript be written according to the Journal format. Submission to this journal proceeds totally online and you will be guided stepwise through the creation and uploading of your files through the web site of the Journal as: http://jame.um.ac.ir

Essential title page information

The title page MUST be prepared and uploaded separately from the main text with the following information:

• Title. Concise and informative and not more than 15 words.

• Author names and affiliations. Present the authors' affiliation addresses (where the work was actually done) below the names. Indicate all affiliations with a superscript number immediately after the author's name and also in front of the appropriate address. Provide the full postal address of each affiliation and if available, the e-mail address of each author.

• Corresponding author. Clearly indicate who will handle correspondence at all stages of refereeing and publication, also post-publication. Ensure that phone numbers (with country and area code) are provided in addition to the e-mail address and the complete postal address. Contact details must be kept up to date by the corresponding author.

• Present/permanent address. If an author has moved since the work described in the article was done, or was visiting at the time, a 'Present address' (or 'Permanent address') may be indicated as a footnote to that author's name. The address at which the author actually did the work must be retained as the main, affiliation address. Superscript numerals are used for such footnotes.

Paper configuration

Each paper should have the following distinct sections: Title, Abstract and up to five Keywords, Introduction, Material and methods, Results and discussion, Conclusion, and References. The Acknowledgment (briefly), Recommendations and Nomenclature can also be added. Each section should be prepared as follow:

Abstract: A concise and factual abstract is required. The abstract should state briefly the purpose of the research, the principal results and major conclusions. It should not exceed 250 words. The abstract is presented separately from the article in a single paragraph, so it must be able to stand alone. For this reason, References should be avoided. Also, non-standard or uncommon abbreviations should be avoided, but if essential they must be defined at their first mention in the abstract itself.

Keywords: Up to five keywords appear immediately after the abstract with alphabetical order.

Introduction: Clearly state the research problem and the necessity of research, the objectives of the work and provide an adequate background, avoiding a detailed literature survey or a summary of the results.

Material and methods: Provide sufficient detail to allow the work to be reproduced. Methods already published should be indicated by a reference: only relevant modifications should be described. For the analytical and modeling works a section may be added as "Theory".

Results and discussion: Results should be clear and concise. The discussion should explore the significance of the results of the work, not repeat them. A combined Results and Discussion section is often appropriate. Avoid extensive citations and discussion of published literature.

Conclusion: The main conclusions of the study is presented in a short Conclusions section, which should be stand alone.

Paper layout

The main text should be prepared in A4 paper size, with 1.5 line spacing and all margins of 3 cm. All pages should be numbered sequentially and not more than 15 pages. All lines should be numbered continuously by applying the "Line numbering" command of MS Word.

Fonts

- All writings should be written using Times New Roman font. Both American and British English format are accepted, but not their mixture!
- The font size for title is 14 point and for the main text is 12 point.
- The subtitles should be written in Bold and font size of 12 point.

Units

Please use SI units only. It is not necessary to give the SI unit and (say) its Imperial equivalent. Engineering Notation, where units are in multiples of 1,000, should be used. Thus, we wish to see the use of mm and m and not cm. Use exponent form instead of conventional format (e.g. m s^{-1} and NOT m/s).

Math formulae

Present simple formulae in the line of normal text where possible. In principle, variables are to be presented in italics. Number consecutively any equations that have to be displayed separately from the text in the right margin (if referred to explicitly in the text).

Tables

Number tables consecutively in accordance with their appearance in the text. Place footnotes to tables below the table body and indicate them with superscript lowercase letters. Avoid vertical rules. Be sparing in the use of tables and ensure that the data presented in tables do not duplicate results described elsewhere in the article. The Table caption appears above the Table with font size of 10. Use no border for the Tables.

Figures

Ensure that each illustration has a caption. Supply captions separately, not attached to the figure. A caption should comprise a brief title (not on the figure itself) and a description of the illustration. Keep text in the illustrations themselves to a minimum but explain all symbols and abbreviations used (preferably in the caption). The caption should allow the reader to understand the main elements of what is being shown without needing to refer to the main text. The Figure caption appears below the Figure and written with font size of 10 points. Use no border for the Figures. The font size within the Figure should not smaller than 8 point and bigger than 10 point. Try to present the Figures in gray scale instead of color illustration. The followings are a sample of Table and Figure.

Table 1- Consumption of inputs during the first year of saffron cultivation

Type of inputs	Consumption (kg ha^{-1})
Consumed corms	3000
Urea	100
Ammonium phosphate	100
Animal manure	32000
Consumed irrigation water	3000 (m^3)*

* The annual water consumption for saffron cultivation was considered equal to 3000 m^3 (Mahdavi, 1999).

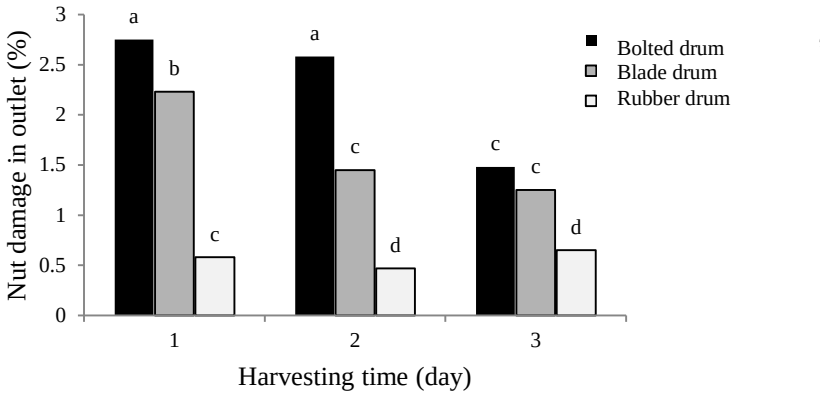

Fig. 3. The effects of harvesting time and machine type on the percentage of cracked shells in the outlet

References

Citation in text

Please ensure that every reference cited in the text is also present in the reference list (and vice versa). Unpublished results and personal communications are not recommended in the reference list, but may be mentioned in the text. If these references are included in the reference list they should follow the standard reference style of the journal and should include a substitution of the publication date with either 'Unpublished results' or 'Personal communication'. Avoid anonymous references. Citation of a reference as 'in press' implies that the item has been accepted for publication.

Reference style

Use "Author, Date" style for list of references and citations all in English language using Times New Roman font size of 10 point as follow:

Citations

Single author: (Loghavi, 2008).

Two authors: (Aghkhani and Abbaspour-Fard, 2009).

Three authors and more: (Abbaspour-Fard *et al.*, 2008).

Multiple citations: (Smith, 1999; Samuel *et al*., 2008; Smith and Samuel, 2009)

Use the complete name of the journals instead of their abbreviations. For those authors using EndNote software for list of References and citations, please use the following style which can be downloaded from Journal of Agricultural Machinery:

Style Name: Jame Endnote Style

List of References

Journal article

Aghkhani, M. H., and M. H. Abbaspour-Fard. 2009. Automatic off-road vehicle steering system with a surface laid cable: Concept and preliminary tests. Biosystems Engineering 103: 265-270. DOI: 10.1016/j.biosystemseng.2009.04.013

Special issue

Rice, K. 1992. Theory and conceptual issues. In: Gall, G.A.E., Staton, M. (Eds.), Integrating Conservation Biology and Agricultural Production. Agricultural Ecosystems Environment: 9-26.

Reference to a Book

Gaugh, H. G. 1992. Statistical Analysis of Regional Yield Trials. Elsevier. Amsterdam.

Reference to a chapter in an edited book

Mettam, G. R., and L. B. Adams. 1999. How to prepare an electronic version of your article. PP 281-304 in B. S. Jones and R. Z. Smith eds. Introduction to the Electronic Age. E-Publishing Inc., New York.

Reference to a thesis or dissertation (if you can, avoid this type of reference)

Abbaspour-Fard, M. H. 2001. The dynamic behavior of particulate biomaterials using discrete element method (DEM). Faculty of Agriculture. Newcastle University, Newcastle upon Tyne.

Reference to a conference proceeding

Hemmat, A., V. I. Adamchuk, and P. Jasa. 2007. On-the-go soil strength sensing using an instrumented disc coulter. International Agricultural Engineering Conference (IAEC). Asian Association for Agricultural Engineering, Bangkok, Thailand.

Web references

As a minimum, the full URL should be given and the date when the reference was last accessed. Any further information, if known (DOI, author names, dates, reference to a source publication, etc.), should also be given. Web references can be included in the reference list e.g.:

Brittion, A. 2006. How much and how often should we drink British Medical Journal, 332: 1224-1225. Available from: http://bmj.bjjournals.com/cgi/content/full/332/7552/1224. Accessed 2 June 2006.

Miscellaneous

- All submitted papers will be peer reviewed by some accredited referees under the supervision of the editorial board and if accepted will be put in queue for publication based on the date of acceptance and other journal's rules and regulations.
- The editorial board of the Journal keeps their right to accept or reject any of the submitted papers.
- No change can be made on a paper which has been proof read by the authors.

Persian abstract

The title, abstract, and Persian keywords should be at the bottom of the article.

مندرجات

مقالات پژوهشی

نشریه ماشین های کشاورزی

با شماره پروانه ۸۹/۱۲۶۳۹ و درجه علمی – پژوهشی شماره ۳/۱۱/۳۷۸۱ از وزارت علوم، تحقیقات و فناوری
۸۹/۶/۱۳ ۸۹/۳/۱۷

"بر اساس مصوبه وزارت عتف از سال ۱۳۹۸، کلیه نشریات دارای درجه "علمی-پژوهشی" به نشریه "علمی" تغییر نام یافتند."

جلد ۱۲ شماره ۱ بهار ۱۴۰۱

صاحب امتیاز: دانشگاه فردوسی مشهد

مدیر مسئول: سید محمدرضا مدرس رضوی — استاد- گروه مکانیک دانشکده مهندسی (دانشگاه فردوسی مشهد)

سردبیر: محمدحسین عباسپور فرد — استاد- گروه مهندسی مکانیک بیوسیستم (دانشگاه فردوسی مشهد)

ناشر: انتشارات دانشگاه فردوسی مشهد

نشانی: مشهد- کد پستی ۹۱۷۷۵ صندوق پستی ۱۱۶۳
دانشکده کشاورزی- دبیرخانه نشریات علمی - نشریه ماشین‌های کشاورزی - نمابر:۰۵۱۳۸۷۸۷۴۳۰

این نشریه در پایگاه‌های زیر نمایه شده است:
AGRIS، CABI، DOAJ، Google scholar،پایگاه استنادی جهان اسلام (ISC)، **سامانه نشریات علمی پایگاه اطلاعات علمی جهاد دانشگاهی** (SID)، **بانک اطلاعات نشریات کشور** (MAGIRAN)
مرجع دانش (CIVILICA)

پست الکترونیک: jame@um.ac.ir

مقالات این شماره در سایت http://jame.um.ac.ir **به‌صورت مقاله کامل نمایه شده است.**

این نشریه به تعداد ۴ شماره در سال و به‌صورت آنلاین منتشر می‌شود.

انجمن مهندسان مکانیک ایران

نشریه علمی
ماشین های کشاورزی

دانشگاه فردوسی مشهد

جلد ۱۲ شماره ۱
سال ۱۴۰۱
(شماره پیاپی: ۲۳)

شاپا: ۶۸۲۹-۲۲۲۸

عنوان مقالات

مقالات علمی-پژوهشی